9-12-2014

Development of Novel Small Molecules for Imaging and Drug Release

Yanting Cao

Yanting Cao

Candidate

Department of Chemistry and Chemical Biology

Department

This dissertation is approved, and it is acceptable in quality and form for publication:

Approved by the Dissertation Committee:

Prof. Wei Wang, Chairperson

Prof. Yang Qin

Prof. Charles E. (Chad) Melançon III

Prof. Changjian Feng

DEVELOPMENT OF NOVEL SMALL MOLECULES FOR IMAGING AND DRUG RELEASE

by

YANTING CAO

B.E., Pharmaceutical Engineering,
East China University of Science and Technology, 2008

DISSERTATION

Submitted in Partial Fulfillment of the
Requirements for the Degree of

Doctor of Philosophy
Chemistry

The University of New Mexico
Albuquerque, New Mexico

July, 2014

Acknowledgements

First and foremost, I would like to express my sincere gratitude to my advisor Prof. Wei Wang for his continuous encouragement, guidance and support. It is my honor to be his student. His intelligence, diligence, and personality inspire me to finish my PhD study with confidence. I am sure I will benefit a lot from his guidance not only for the current, but also for my future work and life.

Also, I would like to thank all my committee members, Prof. Yang Qin, and Prof. Charles E. (Chad) Melançon III, and Prof. Changjian Feng for their continuous support, valuable comments, and precious time.

During the past several years, I spent lots of time with the members in Prof. Wang's group. We are like a big family. I would like to offer my best regards to all the ex-members and current members in Prof. Wang's group, especially Dr. Shilei Zhang, Dr. Yinan Zhang, Dr. Wei Jiang, Dr. Yafei Ji, Dr. Xingshuai Zhang, Dr. Xixi Song, Dr. Weimin Xuan, Aiguo Song, Xiaobei Chen, Chenguang Yu, He Huang, Gen Li, Dr. Jiahong Zhou, Dr. Fang Zhang, Dr. Huijuan Jiang, Yongyi Wei, and Yuxian He. I wish them a great future.

Also, I am really grateful to all our collaborators. I would like to thank Prof. Ke Jian (Jim) Liu and his group members, Dr. Rong Pan, and Dr. Xixi Zhou at UNM College of Pharmacy for their help, support and collaboration on the fluorescence imaging studies, cell viability studies and part of the DNA cross-links tests. Also, I would like to thank Prof. Debra Dunaway-Mariano and her group, especially Chunliang Liu for help and collaborations on the DNA cross-links tests as well as his insightful suggestions. I would also like to thank Prof. Charles E. (Chad) Melançon III and his group and Prof. Fusen Liang and his group for their help and support.

Last but not least, I would like to express special thanks to my family for their unconditional love and support. My hard working parents have instilled in me many good qualities that are so essential in completing my PhD studies. No words can fully express my thanks to them. I am so proud of them and love them so much. During the past five years, I was so lucky that I met my best friend, my husband, Chenguang Yu. He is always here to share my happiness and sorrow. His encouragement and optimism walk me through the difficult times. He has made my life more enjoyable. Without his help and support, I would never gone this far.

DEVELOPMENT OF NOVEL SMALL MOLECULES FOR IMAGING AND DRUG RELEASE

by

YANTING CAO

B.E., Pharmaceutical Engineering,
East China University of Science and Technology, 2008

Ph.D., Chemistry, University of New Mexico, 2014

Abstract

Small organic molecules, including small molecule based fluorescent probes, small molecule based drugs or prodrugs, and smart multifunctional fluorescent drug delivery systems play important roles in biological research, drug discovery, and clinical practices. Despite the significant progress made in these fields, the development of novel and diverse small molecules is needed to meet various demands for research and clinical applications. My Ph.D study focuses on the development of novel functional molecules for recognition, imaging and drug release.

In the first part, a turn-on fluorescent probe is developed for the detection of intracellular adenosine-5'-triphosphate (ATP) levels based on multiplexing recognitions. Considering the unique and complicated structure of ATP molecules, a fluorescent probe has been implemented with improved sensitivity and selectivity due to two synergistic binding recognitions by incorporating of 2, 2'-dipicolylamine (Dpa)-Zn(II) for targeting of phospho anions and

phenylboronic acid group for cis-diol moiety. The novel probe is able to detect intracellular ATP levels in SH-SY5Y cells. Meanwhile, the advantages of multiplexing recognition design concept have been demonstrated using two control molecules.

In the second part, a prodrug system is developed to deliver multiple drugs within one small molecule entity. The prodrug is designed by using 1-(2-nitrophenyl)ethyl (NPE) as phototrigger, and biphenol biquaternary ammonium as the prodrug. With controlled photo activation, both DNA cross-linking agents mechlorethamine and o-quinone methide are delivered and released at the preferred site, leading to efficient DNA cross-links formation and cell death. The prodrug shows negligible cytotoxicity towards normal skin cells (Hekn cells) with and without UV activation, but displays potent activity towards cancer cells (HeLa cells) upon UV activation. The multiple drug release system may hold a great potential for practical application.

In the last part, a new photo-initiated fluorescent anticancer prodrug for DNA alkylating agent mechlorethamine releasing and monitoring has been developed. The theranostic prodrug consists a photolabile NPE group, an inactive form of mechlorethamine and a nonfluorescent coumarin in one small molecule. It is demonstrated that the prodrug shows negligible cytotoxicity towards normal skin cells (Hekn cells) with and without UV activation, while the original parent drug mechlorethamine can be photocontrol-released and induces effective DNA cross-linking activity. Importantly, the drug release progress can be conveniently monitored by the 'off-on' fluorescence enhancement in cells. Moreover, the selective prodrug is not only cell permeable but also nuclear permeable. Therefore, the prodrug serves as a promising drug delivery system for spatiotemporal control release and monitoring of an anticancer drug to obtain the optimal treatment efficacy.

Contents

List of Abbreviations

Acetone-d_6	deuterated acetone
ADME	absorption, distribution, metabolism, excretion
ADP	adenosine-5'-diphosphate
AIBN	azobisisobutyronitrile
AMP	adenosine-5'-monophosphate
ATP	adenosine-5'-triphosphate
Boc	t-butoxycarbonyl
°C	degrees Celsius
calcd.	calculated
CCK-8	cell counting kit-8
$CDCl_3$	deuterated chloroform
cm	centimeter
CPA	cyclophosphamide
CPT	camptothecin
δ	chemical shift
DAPI	4',6-diamidino-2-phenylindole
DCM	dichloromethane
DDC	diethyldithiocarbamate
DDSs	drug delivery systems
DMEM	Dulbecco's Modified Eagle medium
DMSO	dimethyl sulfoxide

DMSO-d_6	deuterated dimethyl sulfoxide
DNA	deoxyribonucleic acid
Dpa	dipicolylamine
EDG	electron-donating group
EPR	electronic paramagnetic resonance
ESI	electrospray ionization
EWG	electron-withdrawing group
EVE	ethyl vinyl ether
FBS	fetal bovine serum
FRET	Fluorescence resonance energy transfer
g	gram(s)
GMC	gemcitabine
GSH	glutathione
h	hour(s)
HEPES	4-(2 -Hydroxyethyl)piperazine-1-ethanesulfonic acid
HOMO	highest occupied molecular orbital
HPLC	high performance liquid chromatography
Hz	hertz
ICT	intramolecular charge transfer
ICLs	interstrand cross-links
IFA	ifosfamide
J	coupling constant
J1	L-melphalanyl-p-L-fluorophenylalanine ethyl ester

λ_{em}	emission wavelength
λ_{ex}	excitation wavelength
LUMO	lowest unoccupied molecular orbital
MDDSs	multidrug delivery systems
MeCN	acetonitrile
MeOD	deuterated methanol
mg	milligram
MHz	megahertz
min	minute(s)
mL	milliliter
mM	millimolar
mmol	millimole
m.p.	melting point
MsCl	methanesulfonyl chloride
MW	microwave
NBS	N-Bromosuccinimide
nm	nanometer
nM	nanomolar
NMR	nuclear magnetic resonance
NPE	(2-nitrophenyl)ethyl
o	ortho
PBS	phosphate buffer solution
PCT	Photoinduced Charge Transfer

PET	Photoinduced Electron Transfer
Ph	phenyl
ppm	parts per million
(RP)HPLC	reverse phase high performance liquid chromatography
RGD peptide	arginylglycylaspartic acid
rt	room temperature
S_0	ground state
S_1	excited singlet state
T_1	excited triplet state
TBAF	tetra-n-butylammonium fluoride
TBS	tert-butyldimethylsilyl
TEA	triethylamine
TFA	trifluoroacetic acid
THF	tetrahydrofuran
TLC	thin layer chromatography
QM	quinone methide
µM	micromolar
µL	milliliter
W	watt(s)

Chapter 1

Introduction

1.1 Background

During the past several decades, vast progress has been achieved in the field of fluorescent imaging which has significant impact on biomedical research, drug discovery, and clinical practices. Fluorescent imaging allows the *in vivo* visualization of function molecules (amino acids, coenzyme, carbohydrates, nucleosides, nucleotides, etc.) in their intact and native psychological state with high sensitivity, selectivity, fast response time, flexibility, biocompatibility and high spatial and temporal resolution [1-9]. It also provides information about the structure and/or dynamics of living systems at a molecular level to fully elucidate the roles of molecule of interest [1].

Despite the wide clinical applications of chemotherapeutic agents, their high reactivity often accompanies high systemic toxicity and poor tumor selectivity, leading to severe adverse effects which greatly hinder their therapeutic efficiency. In order to alleviate or even overcome these limitations, various strategies have been developed such as targeted therapies [10], antibody-drug conjugates [11], nano-particle drugs [10, 12], and electrochemotherapy [13-19], etc. Among these therapies, prodrug strategy has provided an alternative to redesign the drug molecule through a chemical approach to improve multiple properties of the parent agents including bioavailability, duration of pharmacological effects, stability, solubility, selectivity and to decrease toxicity [20].

An emerging area arises based on the integration of anticancer prodrug and fluorescent reporter to achieve multi-functions [21]. The theranostic molecule is not only a

prodrug but also a fluorescent reporter that enables simultaneous monitoring and delivering of the active drug to the target. These features are highly desirable for reaching the optimal therapeutic efficiency in chemotherapy. Also, they emit fluorescence signals that have potential applications for researchers to study the drug delivery process, to control drug dosage, etc.

1.2 Fluorescent Probes

To explore and study the biological activities in the living system, the first step is to visualize the dynamic processes of molecules involved. Therefore, various detection methods have been utilized to transform biological information into other detectable signals, examples includes radioactive tracers, EPR (electronic paramagnetic resonance) probes, ion electrodes, etc[1]. Among them, fluorescent probes have received considerable attention as they can provide dynamic information about the quantity and localization of the molecule of interest with high sensitivity, selectivity, biocompatibility, sub-nanometer spatial resolution (e.g., by fluorescence imaging microscopy), and sub-millisecond temporal resolution, etc. [1-9, 22].

As the photophysical properties of fluorescent molecules are strongly affected by their surrounding medium, they are generally applied for the investigation of physicochemical, biochemical, and biological systems, thus known as fluorescent probes. Fluorescent probe/sensor development was initially promoted by the blooming of supramolecular chemistry and the advancement of photochemistry. Supramolecular chemistry provides the basis of selective recognition between synthetic host molecules and guest molecules using noncovalent interactions [23-24], and photochemistry offers the

basic design principles how structure modification is related to photophysical properties. Since then, a large number of fluorescent probes have been developed for targeting various molecules and ions [25-26], especially to meet the demand of biological and life science.

Nowadays, an increasing number of versatile fluorescent molecules have been developed to enable the noninvasive study of various biological processes [27-30], at the same time, advanced visualization methods have been utilized to give high quality detection with a moderate cost. These achievements make fluorescent imaging as a new exciting tool with great potential in basic research, drug discovery and clinical applications.

1.2.1 Common Features of Fluorescent Probes

A typical fluorescent probe [31-32] consists of a fluorophore (signaling moiety) for fluorescent signal generation, a receptor (recognition moiety) for analyte recognition, and a spacer, linking them together. The recognition event, which takes place at the receptor, and accordingly affects its topology and characters, is transduced through spacer to the signaling moiety and consequently changes its photophysical characteristics. Based on the differences in analyte recognition, fluorescent probes fall in two categories. Conventional analyte recognition is based on noncovalent interactions, including hydrogen bonding, π-π, donor-acceptor, electrostatic, hydrophobic, hydrophilic, and coordination based interactions. When analyte recognition takes place where a covalent bond is formed, it is reaction-based fluorescent probe (Figure 1.1). Both types of fluorescent probes are essential for the detection of different types of analytes.

Figure 1.1. Conventional sensory systems and reaction-based sensory systems.

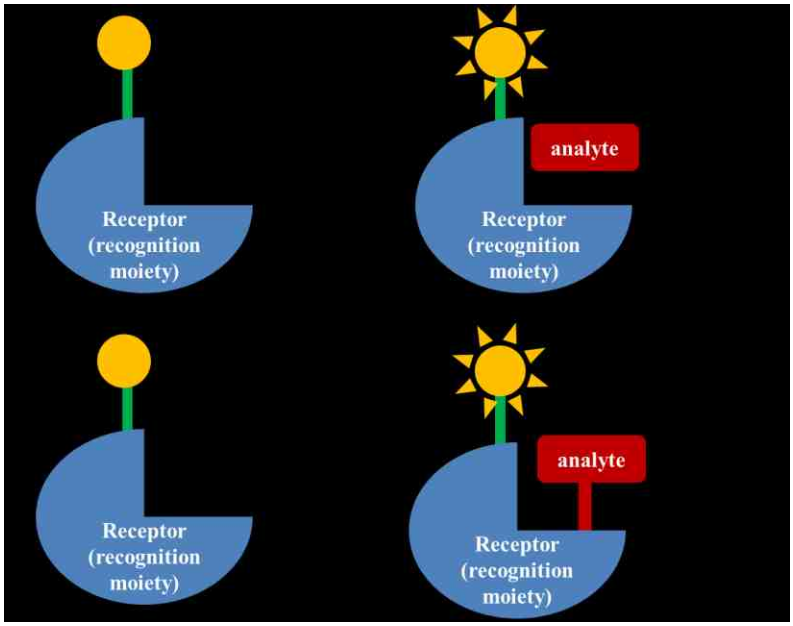

1.2.1.1 Fluorophore (Signaling Moiety)

Organic dyes are commonly used fluorophores which cause fluorescent emission ranging from the ultraviolet to the near-infrared in the electromagnetic spectrum. Upon excitation, a molecule undergoes fast energy absorption ($\approx 10^{-15}$s) and is excited from the ground state S_0 (the most common state at room temperature for most organic species) to the excited singlet state (S_1). Upon relaxation from S_1 to S_0, fluorescence is generated in the form of light (Figure 1.2). When the receptor interacts with its surroundings, information is transduced by the linker to the fluorophore and alters its fluorescence properties (such as absorption and emission spectra, quantum yield, lifetime, etc.). By measuring the differences in the fluorescence properties, spatial and temporal information of the microenvironment (such as ion and molecular concentration, polarity, etc.) can be monitored.

Figure 1.2. Jablonski diagram.

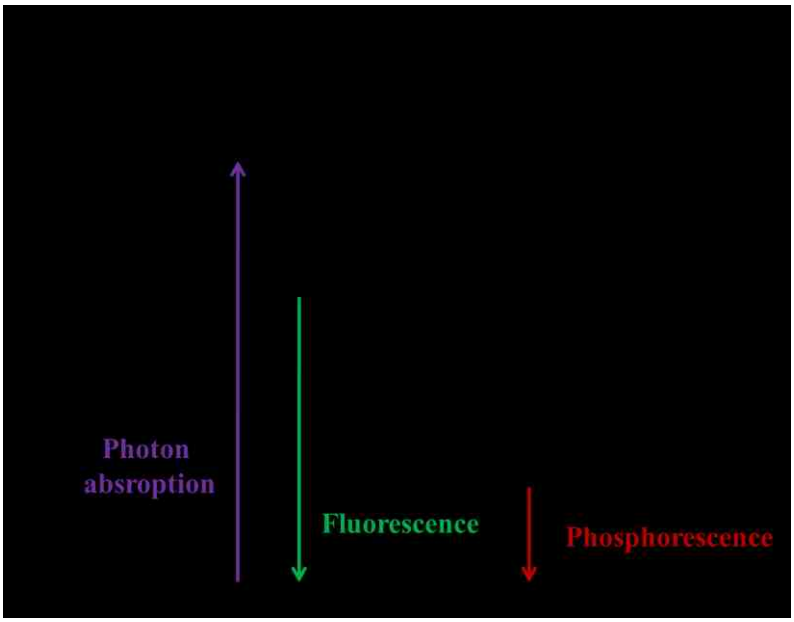

1.2.1.2 Receptor (Recognition Moiety)

For practical applications, a fluorescent probe should be able to detect a small amount of a particular analyte among various other species existing in the surrounding, therefore, specificity and sensitivity become two important parameters for fluorescent probe design. The specificity and sensitivity of a probe are designed based on the specific interactions or reaction between the receptor and the analyte.

1.2.1.3 Spacer (Linker)

Depending on the underlying photophysical mechanism, the spacer can be saturated to disconnect the electronic systems of chromophore and binding unit or unsaturated to couple these electronic subsystems.

1.2.2 Design Principles of Fluorescent Probes

A fluorescent probe converts non-optical information into optical signals based on the alterations in the photophysical properties of the fluorophore. Different fluorophores have different energy transfer mechanisms to affect fluorescence properties. Listed in the followings are some of the most commonly used photoinduced processes that lead to photophysical changes.

1.2.2.1 Photoinduced Electron Transfer (PET)

One of the most extensively employed mechanisms in the design of fluorescent probes is based on photoinduced electron transfer (PET) process (Figure 1.3) [33-36]. In a fluorescent molecule, an electron is promoted from HOMO to LUMO upon light absorption. Subsequent decay back to HOMO produces fluorescence emission. However, the fluorescence emission process can be disrupted by introducing a quencher to the system. The quencher works by either reductive electron transfer or oxidative electron transfer. In the unbounded state, a fast electron transfer (from HOMO of reductive quencher to the HOMO of the excited fluorophore, known as reductive quench; from LUMO of the fluorophore to the LUMO of the excited fluorophore, known as oxidative quench) quenches the fluorescence of the system. The fluorescence emission can be regained by slowing down or switching off the electron transfer process. It is usually realized by analyte binding at the receptor to modulate the redox potential of the quencher.

Figure 1.3. PET mechanism. (a) reductive PET; (b) oxidative PET.

(a)

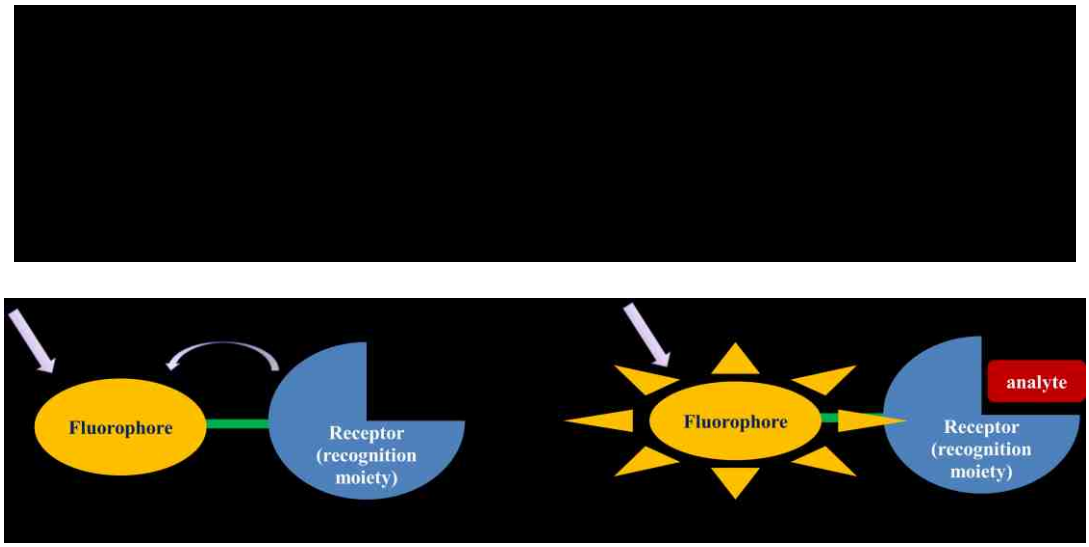

(b)

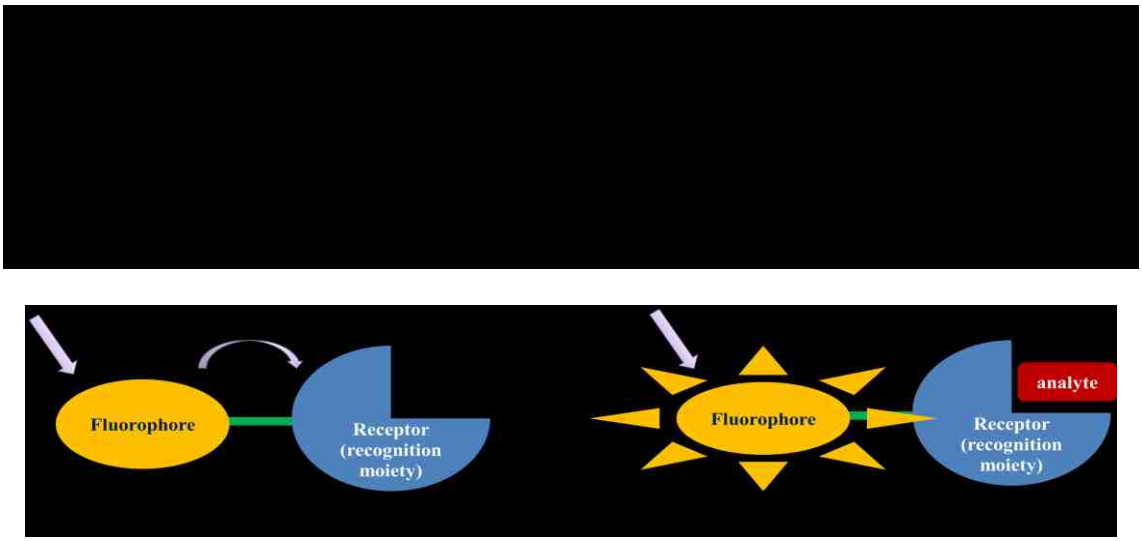

1.2.2.2 Photoinduced Charge Transfer (PCT)

Photoinduced charge transfer is another widely applied process in the design of fluorescent probes [37-38]. When a fluorophore contains an electron-donating group (EDG)

conjugated to an electron-withdrawing group (EWG), it undergoes intramolecular charge transfer (ICT) from the donor to the acceptor upon light absorption. The consequent change in dipole moment results in a Stokes shift which depends on the microenvironment of the fluorophore. When an analyte binds to an electron-donating group, the electron-donating ability is reduced, the decrease in conjugation leads to a blue shift of the absorption spectrum and a decrease in extinction coefficient. Conversely, the binding between an analyte and an electron-withdrawing group leads to an increase in conjugation, i.e. a red shift of the absorption spectrum and an increase in extinction coefficient. In addition to all these shifts, changes in quantum yields and lifetimes are often observed.

1.2.2.3 Fluorescence Resonance Energy Transfer (FRET)

Fluorescence resonance energy transfer is one kind of "Förster resonance energy transfer" (FRET) when both the donor and the acceptor are fluorophores[39]. When there are interactions between a donor moiety and an acceptor moiety, non-radiative excitaion energy is transferred from the donor to the acceptor. It often takes place if the emission spectrum of the donor overlaps with the absorption spectrum of the acceptor, and that several vibronic transitions in the donor have practically the same energy as the corresponding transitions in the acceptor. Such transitions are dipole-dipole coupled in resonance (Figure 1.4). The surrounding environment changes the spectra properties of either donor or acceptor, or the space between donor and acceptor, thus results in a change of the spectra properties of acceptor or donor.

Figure 1.4. FRET mechanism.

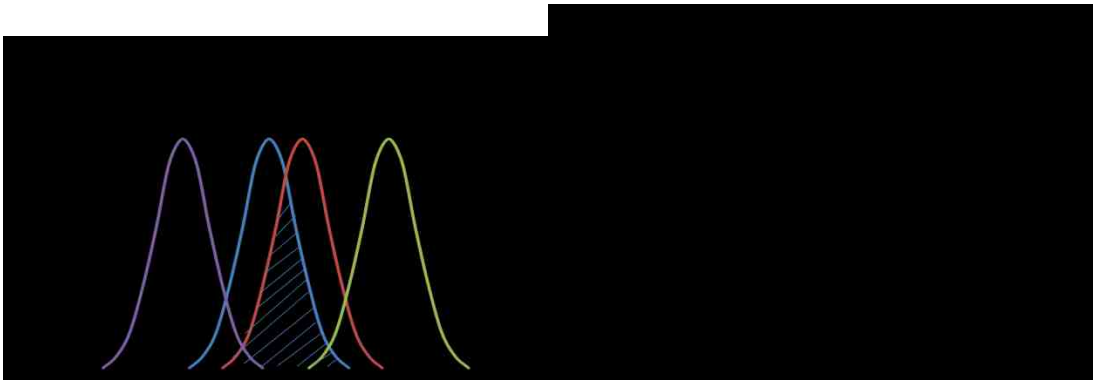

1.2.2.5 Excimers and Exciplex Formation

Excimers are dimers in the excited state. They are formed by collision between an excited molecule and an identical unexcited molecule [40-41]. Dual fluorescence is observed with a monomer band and a structureless broad band at longer wavelength due to excimer formation. When a fluorescent probe contains two fluorophores whose mutual distance is affected by analyte complexation,[39] recognition of this analyte can be monitored by the monomer/eximer fluorescence-intensity ratio.

Exciplexes are another form of excited-state complexes. They are formed by collision of an excited molecule (electron donor or acceptor) with an unlike unexcited molecule (electron acceptor or donor).

Excimer formation: $M^* + M \longleftrightarrow (MM)^*$

Exciplex formation: $D^* + A \longleftrightarrow (DA)^*$; $A^* + D \longleftrightarrow (DA)^*$

1.3 Cancer Chemotherapy

Cancer, characterized by the uncontrolled cell growth [42-43], is currently the second

most common cause of deaths in the US, accounting for nearly one in every four deaths [44]. Among the management options such as surgery, radiation therapy and palliative care, chemotherapy is currently the leading treatment option to treat many cancer types, especially for the systematic treatment of metastasis [45]. Chemotherapeutic agents are small molecule drugs that interfere with DNA replication, repair, translation or cell division, thus inhibit cancerous cell proliferation [46]. Clinical chemotherapeutic agents include DNA alkylating agents, anti-metabolites, anti-microtubule agents, topoisomerase inhibitors and cytotoxic antibiotics, among which, DNA alkylating agent is one of the most prominent class of anticancer agents due to their high degree of reactivity [47-49].

Being the first modern cancer chemotherapeutic agent in the DNA alkylating family, nitrogen mustard type anticancer drug has attracted lots of investigations and is one of the most heavily employed anticancer agents in use today [48-49]. For example, Valchlor by Ceptaris Therapeutics, is a gel formulation of mechloethamine hydrochloric salts approved by US Food and Drug Administration in August 2013 for the treatment of Stage IA and IB mycosisfungoides-type cutaneous T-cell lymphoma (Scheme 1.1a). Leukeran by GlaxoSmithKline, contains DNA alkylating agent chlorambucil is currently used for treating chronic lymphocytic leukemia (Scheme 1.1b). Both of these nitrogen mustard type anticancer drugs bear a reactive N,N-*bis*-(2-chloroethyl)amine to form interstrand cross-links (ICLs) between DNA double strands, mostly at the guanine N-7. To carry sufficient reactivity, the nitrogen mustard type drug must have enough electron density on the amine nitrogen to form the highly electrophilic aziridinium ring through intramolecular displacement of the chloride. This highly electophilic aziridinium ring is the actual reactant with DNA bases in forming covalent bonds, shutting down DNA

replications and transcriptions, and consequently leading to mutations and/or cell death (Scheme 1.2) [48].

Scheme 1.1 Nitrogen mustard type chemotherapeutic agents

(a) Valchlor (Mechloethamine hydrochloric salt)

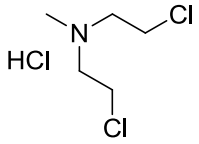

(b) Leukeran (Chlorambucil)

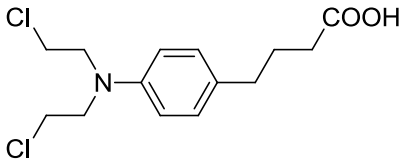

Scheme 1.2 Mechanism of action of nitrogen mustard type anticancer drug

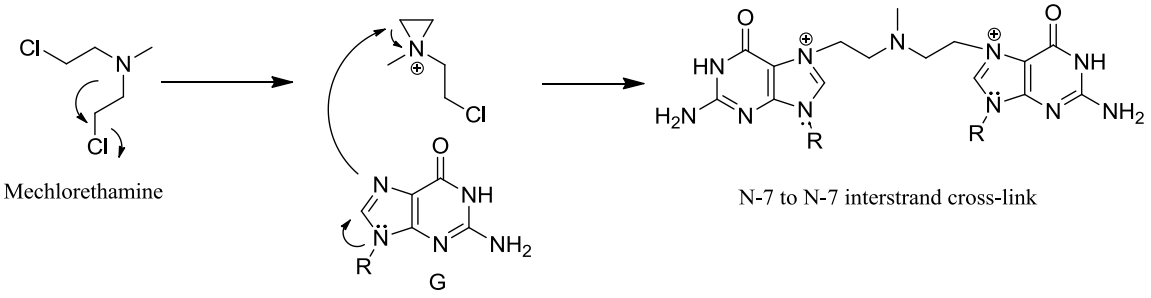

Besides the nitrogen mustard type DNA interstrand cross-links (ICLs) inducing agents, quinone methide derivatives have displayed good activities as antitumor agents or antibiotics. Its reactivity was mainly caused by its forming highly polarized structure to react with nucleophiles, especially DNA bases at the exocyclic methylene group to form benzylic adducts[50] (Scheme 1.4). Various quinone methide derivatives have been

developed as DNA intercross linking agents. For example, Mitozytrex or Mutamycin, containing mitomycin C, is a commercially available chemotherapeutic agent for the treatment of stomach cancer, pancreas cancer and other types of cancer [51-52] (Scheme 1.3a). Anthracycline is a class of very effective anticancer drugs that showed potent activity against a wide spectrum of cancer types [53-54]. Their antitumor activities are caused by the formation of QMs which undergo tandem reactions to form DNA cross-links [55-56], see the first example of anthracycline discovered – Daunomycin (Daunorubicin) (Scheme 1.3b).

Scheme 1.3 Quinone methide derivatives

(a) Mitozytrex or Mutamycin (Mitomycin C)

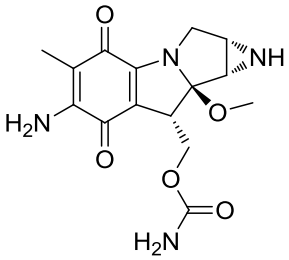

(b) Daunomycin (Daunorubicin)

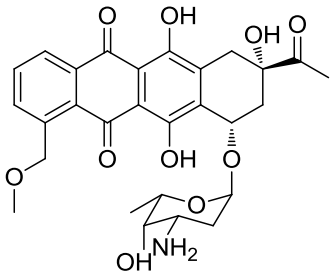

Scheme 1.4 Mechanism of action of quinone methide type anticancer drug

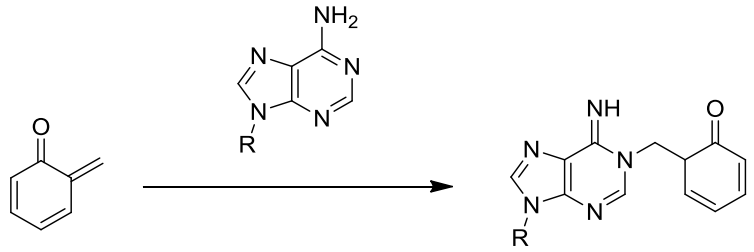

quinone methide intermediate

interstrand cross-link

Despite the wide applications of the nitrogen mustard type and quinone methide type chemotherapeutic agents, their high degree of reactivity came alone with low selectivity lead to high systematic toxicity and limited therapeutic indices [57-58], i.e. severe or even life-threatening side effect with little therapeutic effects [20]. Therefore, prodrug strategy becomes a very important option in designing less cytotoxic anticancer drugs.

1.3.1 Nitrogen Mustard Based Prodrugs

Anticancer prodrugs are the less active and less cytotoxic forms of drug derivative that has some barrier to its utility as an effective drug, after activation or metabolism, it is preferentially released at the site of action [20, 59-60]. In general, a prodrug is designed by attachment of the active moiety (parent drug) through an activatable linkage to the "promoiety" [61] (Scheme 1.5). The promoiety is designed to improve selectivity based on the differences between cancer cells and normal cells. There are generally three strategies in designing the promoiety: 1. Active targeting, promoiety is designed by taking advantage of the differences in cell surface makers such as receptor or antigen between tumor cells and normal cells. 2. Passive targeting, promoiety is designed by taking advantage of the differences in biochemical or physiological properties between tumor cells and normal cells such as pH, oxidative stress, etc. 3. External activator, promoiety is

designed based on external stimuli such as light or heat to achieve direct control of drug release in the targeted area [61].

Scheme 1.5 An illustration of the prodrug concept

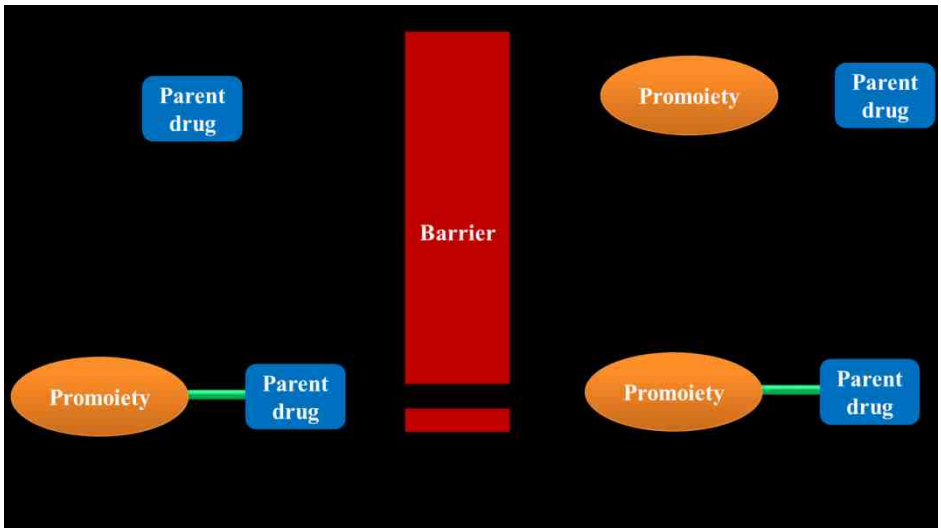

As nitrogen mustard type anticancer drugs bear very high reactivity, much effort has been devoted to making prodrugs to improve the clinical utilities of nitrogen mustard type anticancer agents. For example, cyclophosphamide (CPA) [62-64] and its isomer ifosfamide (IFA) [65] are prodrugs that can be activated *in vivo* by cytochrome P450 to release the ultimate DNA alkylating agent phosphamide mustard. Based on the parent drug chlorambucil, a number of lipophilic prodrugs have been developed. Examples include clinical approved prednimustine, the ester of prednisolone-chlorambucil conjugate, is able to selectively target tumor cells with cancer specific receptors [66-67]. Bestrabucil, the benzoate of the estradiol-chlorambucil conjugate, has been approved for the treatment of estrogen-receptor positive breast cancer [68-69]. Other examples include the dipeptide prodrug of melphalan, J1 (L-melphalanyl-p-L-fluorophenylalanine ethyl

ester, which can be activated by aminopeptidase to release melphalan. The selectivity of prodrug J1 is designed based on the elevated aminopeptidase activity in the plasma of cancer patient. It is currently in phase I clinical trial for the treatment of disseminated solid tumors in adults [70-73]. Another prominent example is hypoxia activated prodrugs for the selective treatment of solid tumors. PR-104, currently under clinical trial, works converting to PR104A, subsequently to PR-104H and PR-104A metabolites under hypoxic conditions [74]. To the best of our knowledge, no light activated nitrogen mustard type prodrug has been reported.

Scheme 1.6 Structure of nitrogen mustard type prodrugs

(a) cyclophosphamide (CPA)

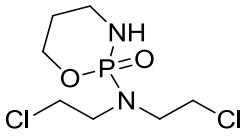

ifosfamide (IFO)

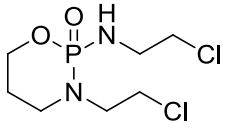

(b) Prednimustine

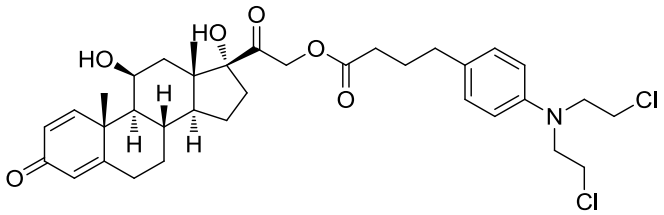

(c) Bestrabucil

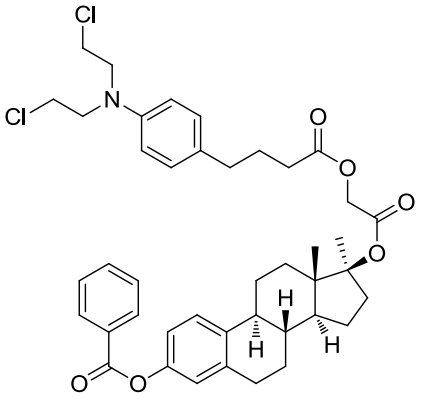

(d) J1 (L-melphalanyl-p-L-fluorophenylalanine ethyl ester

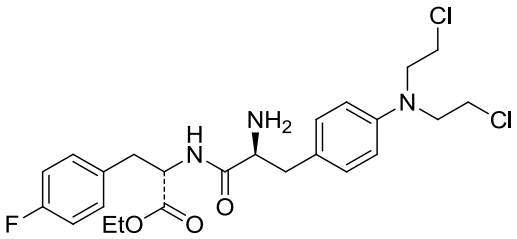

(e) PR-104

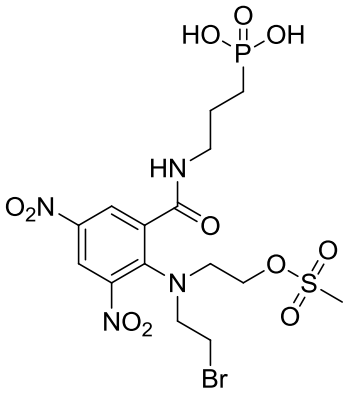

1.3.2 O-quinone Methide (o-QM) as Inducible DNA Alkylating Agent

With the fact that quinone methide derivatives are excellent DNA alkylating agents, they can be generated in different ways. As is reported, they can be generated by photo-irradiation [75-77], oxidation [78-81], or fluoride inducing [55, 82-83]. Recently, biphenyl biquaternary ammonium derivatives have been reported to have much more potent ISC

activity than the traditional phenyl biquaternary ammonium upon photochemical activation [50] (Scheme 1.7a). Its high reactivity is caused by the formation of bisquinone methide intermediate instead of monoquinone methide intermediate. Meanwhile, its structural affinity with a DNA helix improves DNA alkylating potency. Based on the previous report, Zhou group developed a phenyl selenide biphenyl compound which can be efficiently oxidized by periodate to release quinone methide for DNA bisalkylation [81] (Scheme 1.7b).

Scheme 1.7 Biphenyl biquaternary ammonium based quinone methide prodrug

(a) light activated quinone methide prodrug

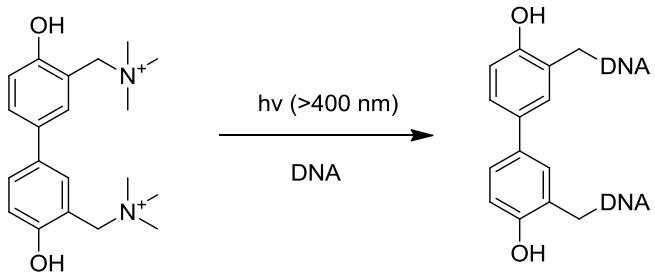

(b) oxidation mediated quinone methide prodrug

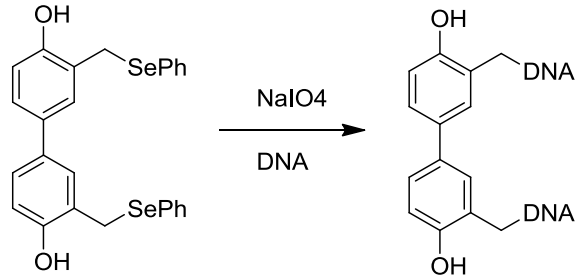

1.4 Multiple Drug Release Chemotherapy

Many diseases, especially cancer, usually cannot be fully cured by a single drug treatment due to the pathological complexity. However, multiple drug chemotherapy may

have enhanced therapeutic efficiency compared with traditional chemotherapy [84]. Compared with traditional chemotherapy, multiple drug chemotherapy is more potent so that lower dosage is administrated, leading to suppression of severe side effect. Considerable efforts have been devoted to nano-material based multidrug delivery system, but limited progress was made in small molecule based multidrug delivery system [84].

The combination of prodrug design and multiple drug release to the desired site would be potentially useful. In the field of small molecule based multiple drug delivery system, dual acting antibiotics have been developed previously [85], only very few dual acting anticancer prodrugs were developed. Back in 1999, Smyth and coworkers made a novel class of β-lactamase-dependent prodrug using cephalosporin as prodrug nucleus. Through enzyme catalyzed hydrolysis, two structural distinct components – 3' acetoxy group and the side chain sulfur-attached S-amino moiety was released [86]. Based on the same cephalosporin prodrug nucleus structure, further modification gave a prodrug that inhibits estrogen production in hormone-dependent breast cancer by the release of aminoglutethimide (an aromatase inhibitor) at the 3'-position and coumate (a sulfatase inhibitor) as the S-aminosulfenimine [87]. The synergistic effect of two drugs released at the same site may become an alternative approach for chemotherapy.

Scheme 1.8 Cephalosporin-based dual-release prodrug

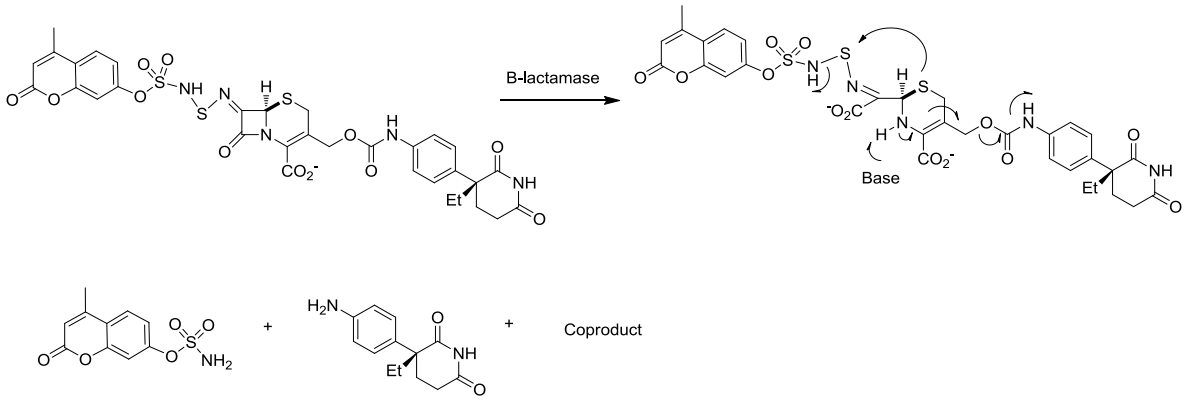

1.5 Combining Fluorescent Imaging with Prodrug Therapy

Despite the traditional role of fluorescent molecules in detecting small molecules, they have found many new applications in the field of life sciences as a versatile tool. Nowadays, with the development of drug delivery system, people have developed a novel type of fluorescent imaging agent that carries dual functions. On the one hand, it is a prodrug that can be activated by various biological stimuli to release parent drug to improve selectivity and reduce cytotoxicity. On the other hand, the prodrug itself is an imaging agent that emits fluorescence light upon drug release. These properties facilitate the monitoring of drug delivery process, help to diagnose diseases, and guide in controlling the dosage level in a spatial and temporal manner.

Among various studies in this field, a large amount of the multifunctional anticancer drug delivery systems (DDSs) to date are based on nano-materials [21, 88-93], only a few examples of small-molecule based drug delivery system have been reported[94-99]. In 2011, Perez et al. developed a cell-specific theranostic prodrug for cancer imaging and therapy. Taking advantage of the over-expressed folic acid receptors on many types of tumor cells, the authors synthesized folate doxorubicin conjugate. Both the fluorescence and

cytotoxicity are quenched by the covalently linked folic acid, through targeted cellular uptake, disulfide bond undergoes glutathione mediated dissociation and nuclear translocation to display enhanced fluorescence, meanwhile release doxorubicin [94] (Scheme 1.9a). In 2012, Kim et al. designed a theronostic prodrug using a RGD peptide as a cancer-targeting unit, a naphthalimide moiety as a fluorescent reporter to release a model anticancer agent camptothecin (CPT). Through RGD-dependent endocytosis, it is preferentially taken up by $\alpha_v\beta_3$ integrin rich U87 cells over $\alpha_v\beta_3$ integrin deficient C6 cells. Subsequently, disulfide bond cleavage takes place in the cytoplasm, resulting in CPT release and a red-shifted fluorescence emission [96](Scheme 1.9b). In 2012, Shabat et al. reported a novel molecular design of a prodrug based on a self-immolative linker attached to a pair of FRET fluorophores and chemotherapeutic agent camptothecin. The prodrug is recognized by enzyme penicillin-G-amidase to release the parent drug camptothecin, meanwhile, the disassembly of the prodrug gave off fluorescent signals which provide information about the actual location and amount of drug release [97](Scheme 1.9c). In 2013, with a similar strategy, Kim et al. made a gemcitabine-coumarin-biotin conjugate in which biotin is the cancer targeting unit, gemcitabine (GMC) is the active drug, and coumarin is the fluorescent reporter. Upon uptake into the tumor cells, abundant thiols in tumor cells lead to disulfide bond cleavage, and subsequently release gemcitabine drug and cause fluorescence enhancement [99](Scheme 1.9d). In 2013, Zhou et al. developed a fluorescent activatable anticancer prodrug. It contains a naphthalimide as fluorescent reporter and a chloroambucil as a potent anticancer drug which are linked by a disulfide link. Through intracellular thiol mediated disulfide cleavage, free active DNA alkylating agent was released, meanwhile, produced a red-

shifted fluorescent signal [98]. The combination of fluorescent imaging and prodrug therapy makes a powerful tool in enhancing therapeutic effect as well as providing fluorescent information about drug delivery.

Scheme 1.9 Examples of combing fluorescent imaging with prodrug strategy

(a) Folic acid mediated activation

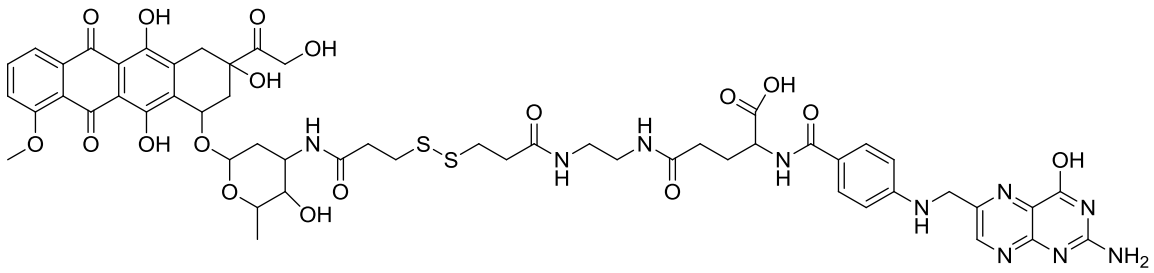

(b) RGD peptide mediated activation

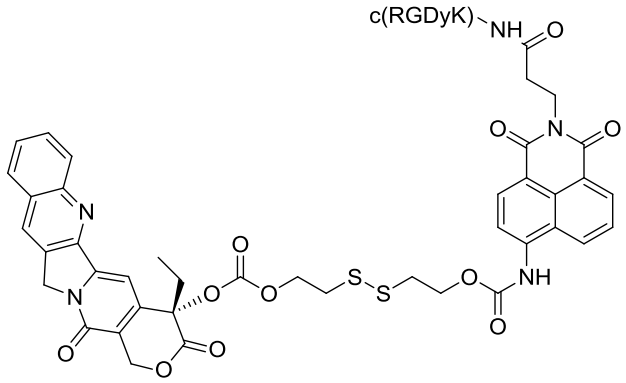

(c) Penicillin-G-amidase mediated activation

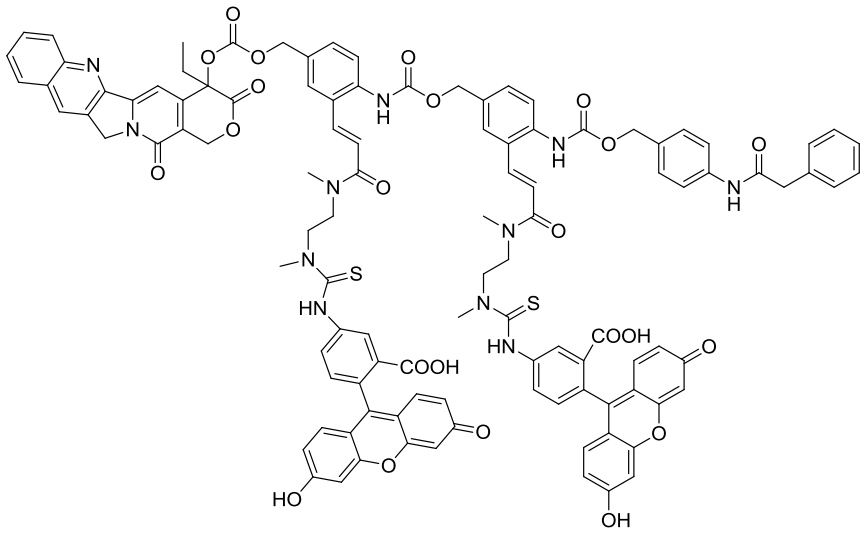

(d) Biotin mediated activation

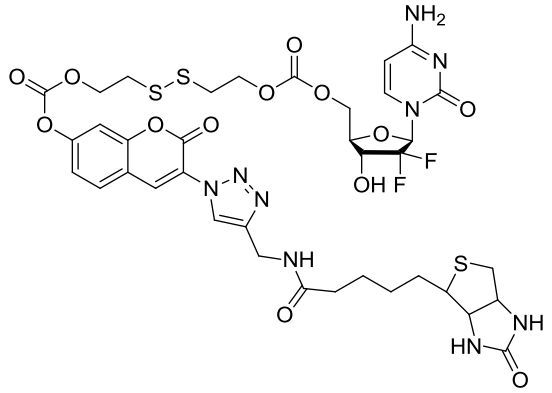

(e) Thiol mediated activation

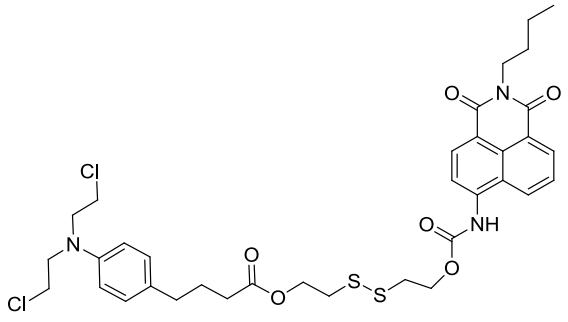

1.6 Research Summary

Despite the enormous efforts made in the field of fluorescence imaging and anticancer prodrug design, there are significant challenges facing upon us. On the one hand, novel fluorescent probes to detect function molecules in the living system with good selectivity and sensitivity are needed to meet the requirement of biochemical research. On the other hand, new anticancer prodrugs with high selectivity and low cytotoxicity are in great demand to fight against cancer. Moreover, the combination of fluorescent imaging and prodrug chemotherapy will not only be a good candidate in drug discovery but also be a versatile tool in biomedical research. Therefore, I will detail my efforts in the above mentioned areas. Chapter 2 presents a novel fluorescent probe for detection of ATP in biological system. Chapter 3 reports a photo-triggered multiple drug releasing prodrug. Chapter 4 focuses on the development of a multi-functional photo-triggered fluorescent prodrug for imaging and drug release.

1.7 References

[1] B. Valeur, *Molecular Fluorescence: Principles and Applications*, Wiley-VCH Verlag GmbH, **2001**.

[2] W. H. Tan, Z. Y. Shi, R. Kopelman, *Anal. Chem.* **1992**, *64*, 2985.

[3] W. E. Moerner, T. Basche, *Angew. Chem., Int. Ed.* **1993**, *32*, 457.

[4] W. E. Moerner, *Acc. Chem. Res.* **1996**, *29*, 563.

[5] J. M. Lehn, *Supramolecular Chemistry*, VCH: Weinheim, **1995**.

[6] P. M. Goodwin, W. P. Ambrose, R. A. Keller, *Acc. Chem. Res.* **1996**, *29*, 607.

[7] A. W. Czarnik, *Fluorescent Chemosensors for Ion and Molecule Recognition*, A. C., Washington, **1992**.

[8] V. a. S. Balzani, F. , *Supramolecular Photochemistry*, Ellis-Horwood limited, Chichester, **1991**.

[9] V. Balzani, *Supramolecular Photochemistry*, Reidel, Dordrecht, **1987**.

[10] M. Chidambaram, R. Manavalan, K. Kathiresan, *J. Pharm. Pharm. Sci.* **2011**, *14*, 67.

[11] B. A. Teicher, R. V. Chari, *Clin. Cancer Res.* **2011**, *17*, 6389.

[12] T. A. a. V. Faunce, Timothy, *J. Law Med.* **2009**, *16*, 822.

[13] R. Heller, R. Gilbert, M. J. Jaroszeski, *Adv. Drug Delivery Rev.* **1999**, *35*, 119.

[14] J. O. Larkin, C. G. Collins, S. Aarons, M. Tangney, M. Whelan, S. O'Reily, O. Breathnach, D. M. Soden, G. C. O'Sullivan, *Ann. Surg.* **2007**, *245*, 469.

[15] M. Marty, G. Sersa, J. R. Garbay, J. Gehl, C. G. Collins, M. Snoj, V. Billard, P. F. Geertsen, J. O. Larkin, D. Miklavcic, I. Pavlovic, S. M. Paulin-Kosir, M. Cemazar,

N. Morsli, D. M. Soden, Z. Rudolf, C. Robert, G. C. O'Sullivan, L. M. Mir, *European Journal of Cancer Supplements* **2006**, *4*, 3.

[16] G. Sersa, D. Miklavcic, M. Cemazar, Z. Rudolf, G. Pucihar, M. Snoj, *Eur. J. Surg. Oncol.* **2008**, *34*, 232.

[17] M. G. Moller, S. Salwa, D. M. Soden, G. C. O'Sullivan, *Expert Rev. Anticancer Ther.* **2009**, *9*, 1611.

[18] A. Testori, G. Tosti, C. Martinoli, G. Spadola, F. Cataldo, F. Verrecchia, F. Baldini, M. Mosconi, J. Soteldo, I. Tedeschi, C. Passoni, C. Pari, A. Di Pietro, P. F. Ferrucci, *Dermatol Ther* **2010**, *23*, 651.

[19] T. Hampton, *JAMA* **2011**, *305*, 549.

[20] V. B. Stella, R.; Hageman, M.; Oliyai, R.; Maag, H.; Tilley, J., *Prodrugs: Challenges and Rewards*, **2007**.

[21] P. Rai, S. Mallidi, X. Zheng, R. Rahmanzadeh, Y. Mir, S. Elrington, A. Khurshid, T. Hasan, *Adv. Drug Delivery Rev.* **2010**, *62*, 1094.

[22] X. S. Xie, *Acc. Chem. Res.* **1996**, *29*, 598.

[23] K. A. a. T. Kunitake, *Supramolecular Chemistry: Fundamentals and Applications*, Springer, Heidelberg, **2006**.

[24] D. G. Cho, J. L. Sessler, *Chem. Soc. Rev.* **2009**, *38*, 1647.

[25] P. J. Jiang, Z. J. Guo, *Coord. Chem. Rev.* **2004**, *248*, 205.

[26] L. Basabe-Desmonts, D. N. Reinhoudt, M. Crego-Calama, *Chem. Soc. Rev.* **2007**, *36*, 993.

[27] Y. Yang, Q. Zhao, W. Feng, F. Li, *Chem. Rev.* **2012**, *113*, 192.

[28] E. L. Que, D. W. Domaille, C. J. Chang, *Chem. Rev.* **2008**, *108*, 1517.

[29] M. Beija, C. A. M. Afonso, J. M. G. Martinho, *Chem. Soc. Rev.* **2009**, *38*, 2410.

[30] H. N. Kim, W. X. Ren, J. S. Kim, J. Yoon, *Chem. Soc. Rev.* **2012**, *41*, 3210.

[31] A. P. deSilva, H. Q. N. Gunaratne, T. Gunnlaugsson, A. J. M. Huxley, C. P. McCoy, J. T. Rademacher, T. E. Rice, *Chem. Rev.* **1997**, *97*, 1515.

[32] P. D. Beer, P. A. Gale, *Angew. Chem. Int. Ed.* **2001**, *40*, 486.

[33] E. U. Akkaya, M. E. Huston, A. W. Czarnik, *J. Am. Chem. Soc.* **1990**, *112*, 3590.

[34] A. P. deSilva, H. Q. N. Gunaratne, T. Gunnlaugsson, M. Nieuwenhuizen, *Chem. Commun.* **1996**, 1967.

[35] L. Fabbrizzi, M. Licchelli, P. Pallavicini, A. Perotti, D. Sacchi, *Angew. Chem. Int. Ed.* **1994**, *33*, 1975.

[36] I. Aoki, T. Sakaki, S. Shinkai, *Chem. Commun.* **1992**, 730.

[37] W. a. L. Rettig, R. , *Probe design and chemical sensing, Topics in Fluorescence Spectroscopy, Vol. 4*, Lakowicz J R, **1994**.

[38] B. B. Valeur, J. and Pouget, J., *Fluorescent Chemosensors for Ion and Molecule Recognition, ACS Symposium Series 538*, American Chemical Society, Washington, DC, **1993**.

[39] J. R. Lakowicz, *Principles of Fluorescence Spectroscopy*, 2nd ed., Plenum, **1999**.

[40] H. Bouaslaurent, A. Castellan, M. Daney, J. P. Desvergne, G. Guinand, P. Marsau, M. H. Riffaud, *J. Am. Chem. Soc.* **1986**, *108*, 315.

[41] D. Marquis, J. P. Desvergne, H. Bouaslaurent, *J. Org. Chem.* **1995**, *60*, 7984.

[42] T. Finkel, M. Serrano, M. A. Blasco, *Nature* **2007**, *448*, 767.

[43] D. Hanahan, R. A. Weinberg, *Cell* **2000**, *100*, 57.

[44] in *Cancer Facts & Figures 2013*, American Cancer Society, Atlanta, **2013**.

[45] R. T. Skeel, *Handbook of Cancer Chemotherapy*, Lippincott Williams and Wilkins, USA, **2007**.

[46] V. Malhotra, M. C. Perry, *Cancer Biol. Ther.* **2003**, *2*, S2.

[47] P. D. Lawley, *Bioessays* **1995**, *17*, 561.

[48] S. R. Rajski, R. M. Williams, *Chem. Rev.* **1998**, *98*, 2723.

[49] D. M. Noll, T. M. Mason, P. S. Miller, *Chem. Rev.* **2005**, *106*, 277.

[50] M. Freccero, C. Di Valentin, M. Sarzi-Amadè, *J. Am. Chem. Soc.* **2003**, *125*, 3544.

[51] M. Tomasz, A. Das, K. S. Tang, M. G. J. Ford, A. Minnock, S. M. Musser, M. J. Waring, *J. Am. Chem. Soc.* **1998**, *120*, 11581.

[52] I. Han, D. J. Russell, H. Kohn, *J. Org. Chem.* **1992**, *57*, 1799.

[53] S. R. Angle, J. D. Rainier, C. Woytowicz, *J. Org. Chem.* **1997**, *62*, 5884.

[54] G. Gaudiano, M. Frigerio, P. Bravo, T. H. Koch, *J. Am. Chem. Soc.* **1990**, *112*, 6704.

[55] Q. Zeng, S. E. Rokita, *J. Org. Chem.* **1996**, *61*, 9080.

[56] K. Nakatani, N. Higashida, I. Saito, *Tetrahedron Lett.* **1997**, *38*, 5005.

[57] B. A. Chabner, T. G. Roberts, *Nat. Rev. Cancer* **2005**, *5*, 65.

[58] A. Kamb, S. Wee, C. Lengauer, *Nat. Rev. Drug Discov.* **2007**, *6*, 115.

[59] F. Kratz, I. A. Müller, C. Ryppa, A. Warnecke, *Chemmedchem* **2008**, *3*, 20.

[60] Y. Singh, M. Palombo, P. J. Sinko, *Curr. Med. Chem.* **2008**, *15*, 1802.

[61] *Drug Delivery Principles and Applications* John Wiley & Sons, Inc., Hoboken, New Jersey, **2005**.

[62] M. T. McClure, I. Stupans, *Biochem. Pharmacol.* **1992**, *43*, 2655.

[63] R. F. Borch, T. R. Hoye, T. A. Swanson, *J. Med. Chem.* **1984**, *27*, 490.

[64] R. F. Borch, J. A. Millard, *J. Med. Chem.* **1987**, *30*, 427.

[65] L. Chen, D. J. Waxman, D. Chen, D. W. Kufe, *Cancer Res.* **1996**, *56*, 1331.

[66] L. Bastholt, C. J. Johansson, P. Pfeiffer, L. Svensson, S. A. Johansson, P. O. Gunnarsson, H. Mouridsen, *Cancer Chemother. Pharmacol.* **1991**, *28*, 205.

[67] M. R. Berger, M. Habs, D. Schmahl, *Arch. Geschwulstforsch.* **1985**, *55*, 429.

[68] K. Naito, K. Kubo, Y. Akao, A. Hiraiwa, T. Naoe, K. Yamada, *Gan No Rinsho* **1986**, *32*, 1443.

[69] H. Kamei, K. Takenaka, T. Goto, S. Suga, A. Fugiwara, I. Nakao, T. Agatsuma, K. Fujita, K. Isurugi, T. Kubota, et al., *Gan To Kagaku Ryoho* **1986**, *13*, 2208.

[70] J. Gullbo, S. Dhar, K. Luthman, H. Ehrsson, R. Lewensohn, P. Nygren, R. Larsson, *Anticancer. Drugs* **2003**, *14*, 617.

[71] J. Gullbo, E. Lindhagen, S. Bashir-Hassan, M. Tullberg, H. Ehrsson, R. Lewensohn, P. Nygren, M. de la Torre, K. Luthman, R. Larsson, *Invest. New Drugs* **2004**, *22*, 411.

[72] M. Wickström, K. Viktorsson, L. Lundholm, R. Aesoy, H. Nygren, L. Sooman, M. Fryknäs, L. K. Vogel, R. Lewensohn, R. Larsson, J. Gullbo, *Biochem. Pharmacol.* **2010**, *79*, 1281.

[73] S. Strese, M. Wickström, P. F. Fuchs, M. Fryknäs, P. Gerwins, T. Dale, R. Larsson, J. Gullbo, *Biochem. Pharmacol.* **2013**, *86*, 888.

[74] M. J. McKeage, Y. Gu, W. R. Wilson, A. Hill, K. Amies, T. J. Melink, M. B. Jameson, *BMC Cancer* **2011**, *11*, 432.

[75] E. Modica, R. Zanaletti, M. Freccero, M. Mella, *J. Org. Chem.* **2000**, *66*, 41.

[76] S. N. Richter, S. Maggi, S. C. Mels, M. Palumbo, M. Freccero, *J. Am. Chem. Soc.* **2004**, *126*, 13973.

[77] E. E. Weinert, R. Dondi, S. Colloredo-Melz, K. N. Frankenfield, C. H. Mitchell, M. Freccero, S. E. Rokita, *J. Am. Chem. Soc.* **2006**, *128*, 11940.

[78] J. Liu, H. Liu, R. B. van Breemen, G. R. J. Thatcher, J. L. Bolton, *Chem. Res. Toxicol.* **2005**, *18*, 174.

[79] D. C. Thompson, K. Perera, R. London, *Chem. Res. Toxicol.* **1995**, *8*, 55.

[80] S. R. Angle, W. Yang, *J. Org. Chem.* **1992**, *57*, 1092.

[81] X. Weng, L. Ren, L. Weng, J. Huang, S. Zhu, X. Zhou, L. Weng, *Angew. Chem. Int. Ed.* **2007**, *46*, 8020.

[82] P. Pande, J. Shearer, J. Yang, W. A. Greenberg, S. E. Rokita, *J. Am. Chem. Soc.* **1999**, *121*, 6773.

[83] W. F. Veldhuyzen, Y.-F. Lam, S. E. Rokita, *Chem. Res. Toxicol.* **2001**, *14*, 1345.

[84] T. O. a. S. Kidoaki, *J. Biomater. Nanobiotechnol.* **2012**, *3*, 55.

[85] S. Mobashery, S. A. Lerner, M. Johnston, *J. Am. Chem. Soc.* **1986**, *108*, 1685.

[86] T. P. Smyth, M. J. O'Connor, M. E. O'Donnell, *J. Org. Chem.* **1999**, *64*, 3132.

[87] J. W. Grant, T. P. Smyth, *J. Org. Chem.* **2004**, *69*, 7965.

[88] J. M. Bryson, K. M. Fichter, W.-J. Chu, J.-H. Lee, J. Li, L. A. Madsen, P. M. McLendon, T. M. Reineke, *Proc. Natl. Acad. Sci. U.S.A.* **2009**, *106*, 16913.

[89] Q. Lin, Q. Huang, C. Li, C. Bao, Z. Liu, F. Li, L. Zhu, *J. Am. Chem. Soc.* **2010**, *132*, 10645.

[90] Y.-P. Ho, K. W. Leong, *Nanoscale* **2010**, *2*, 60.

[91] A. Jana, K. S. P. Devi, T. K. Maiti, N. D. P. Singh, *J. Am. Chem. Soc.* **2012**, *134*, 7656.

[92] S. Karthik, N. Puvvada, B. N. P. Kumar, S. Rajput, A. Pathak, M. Mandal, N. D. P. Singh, *ACS Appl. Mater. Interfaces* **2013**, *5*, 5232.

[93] Q. Lin, C. Bao, Y. Yang, Q. Liang, D. Zhang, S. Cheng, L. Zhu, *Adv. Mater.* **2013**, *25*, 1981.

[94] S. Santra, C. Kaittanis, O. J. Santiesteban, J. M. Perez, *J. Am. Chem. Soc.* **2011**, *133*, 16680.

[95] M. H. Lee, J. Y. Kim, J. H. Han, S. Bhuniya, J. L. Sessler, C. Kang, J. S. Kim, *J. Am. Chem. Soc.* **2012**, *134*, 12668.

[96] K. Ock, W. I. Jeon, E. O. Ganbold, M. Kim, J. Park, J. H. Seo, K. Cho, S.-W. Joo, S. Y. Lee, *Anal. Chem.* **2012**, *84*, 2172.

[97] O. Redy, D. Shabat, *J. Control. Release* **2012**, *164*, 276.

[98] J. Wu, R. Huang, C. Wang, W. Liu, J. Wang, X. Weng, T. Tian, X. Zhou, *Org. Biomol. Chem.* **2013**, *11*, 580.

[99] S. Maiti, N. Park, J. H. Han, H. M. Jeon, J. H. Lee, S. Bhuniya, C. Kang, J. S. Kim, *J. Am. Chem. Soc.* **2013**, *135*, 4567.

Chapter 2

Development of Fluorescent Probe for ATP

2.1 Background

Adenosine-5'-triphosphate (ATP) is a multifunctional nucleoside widely existing in biological systems. Being a universal energy source for various cellular functions in almost all living systems, it is also involved in many other biological processes [1]. For example, ATP acts as a phosphate donor in kinase-catalyzed protein phosphorylation. It plays an important role as signaling substances in periphery as well as in central nervous systems [2]. Recently, it was found that ATP plays a vital role in mediating distinct forms of sensory transduction within the central nervous system [3]. Furthermore, ATP released from human neutrophils helps to amplify chemotactic signals and direct cell orientation [2]. The ability to significantly detect the local or dynamic ATP concentrations in biological environment is critical for fully elucidating its roles in living systems.

In recent years, much effort has been devoted to the development of fluorescent probes for ATP detection [4-21]. The ATP structure contains a tri-phospho anion connected by a ribose with an adenine base (Figure 2.1). However, most of ATP probes focused on the recognition of tri-phospho anion. In 2002, it was first discovered by the Hamachi group that anthracene derivatives bearing Zn(II)-dipicolylamine selectively binds to phosphorylated chemical species, and causes fluorescence change [22]. Later, they published a turn-on fluorescent probe for ATP based on the previous discovery [21]. It contains fluorescein as fluorophore with two Zn(II)-dipicolylamine moieties for binding with tri-phospho anion on ATP (Scheme 2.1).

Figure 2.1 ATP structure

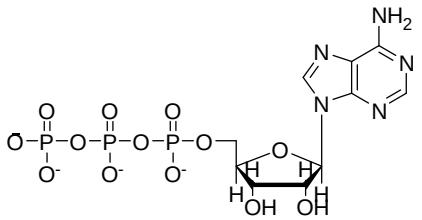

Scheme 2.1 ATP probe developed by the Hamachi group

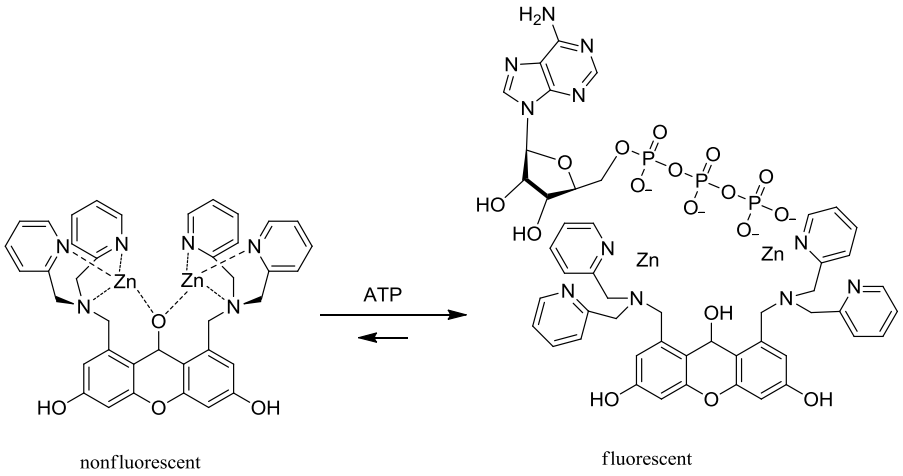

To achieve better sensitivity and selectivity, we have developed a turn-on fluorescent probe with multiplexing recognitions towards ATP - 2, 2'-dipicolylamine (Dpa)-Zn(II) strongly binds to phospho anions, and phenylboronic acid binds to a *cis*-diol on the ribose. Firstly, we demonstrated that the probe was able to response to ATP with good sensitivity and selectivity in aqueous buffer at physiological pH. Furthermore, the probe was applied for the monitoring of intracellular ATP levels in SH-SY5Y cells. In the end, we compared the probe with two control compounds and showed the advantages of

multiplexing recognitions over traditional fluorescent probe bearing a single recognition group.

2.2 Design Strategy

The unique structure of ATP promoted us to apply multiplexing recognitions to detect ATP aimed at enhancing selectivity and sensitivity. Unlike most of the simple analytes, ATP has a relatively complicated structure with three parts. A purine base (adenine) attached to the 1' carbon atom and three phosphate groups attached to the 5' carbon atom of pentose sugar (ribose). In aqueous solution at physiological pH, the triphosphate residue exists as a tetra-charged anion [23]. We proposed that a fluorescent probe having dual interactions with both tetra-charged triphosphate ion and ribose would exhibit stronger and more specific binding than single interaction with either phospho ion or ribose. Taking advantage of the previous discovery that 2, 2'-dipicolylamine (Dpa)-Zn(II) binds strongly to phospho ions [22], and the relatively strong and specific binding affinity between phenylboronic acid and a *cis*-diol which is an essential component in monosaccharide [24-29], we incorporated into the fluorescent probe a 2, 2'-dipicolylamine (Dpa)-Zn(II) moiety for tri-phospho ion recognition and a phenylboronic acid moiety for ribose binding. As is shown in Scheme 2.2, probe **2-1** was composed of a polyamine appended anthracene as the fluorophore with two receptors connected to the amine groups at both end of the anthracene. The lone pair electrons on both of the unbounded amines are expected to quench the fluorescence of anthracene by PET pathway, resulting in non-fluorescence. Upon binding of phospho ion to 2, 2'-dipicolylamine (Dpa)-Zn (II) moiety, PET pathway from one of the amine was blocked, resulting in weak fluorescence.

Upon binding of *cis*-diol to phenylboronic acid, PET pathway of the other free amine was blocked, also resulting in weak fluorescence. The fluorescence can be turned on only if both PET pathways of the amines were blocked by binding with phospho ion and ribose, respectively. Thus, ATP is expected to turn on the fluorescence with its structure bearing both a triphosphate moiety and a ribose moiety (Scheme 2.2). In order to achieve good selectivity with ATP against ADP and AMP, the proper length between phospho ion and ribose diol should be considered. From the structure of these molecules, ATP could interact with the probe better than ADP and AMP with a longer distance between phospho ion and ribose diol, as well as stronger binding between 2, 2'-dipicolylamine (Dpa)-Zn (II) and triphosphate than monophosphate and diphosphate.

Scheme 2.2 Proposed ATP binding mechanism

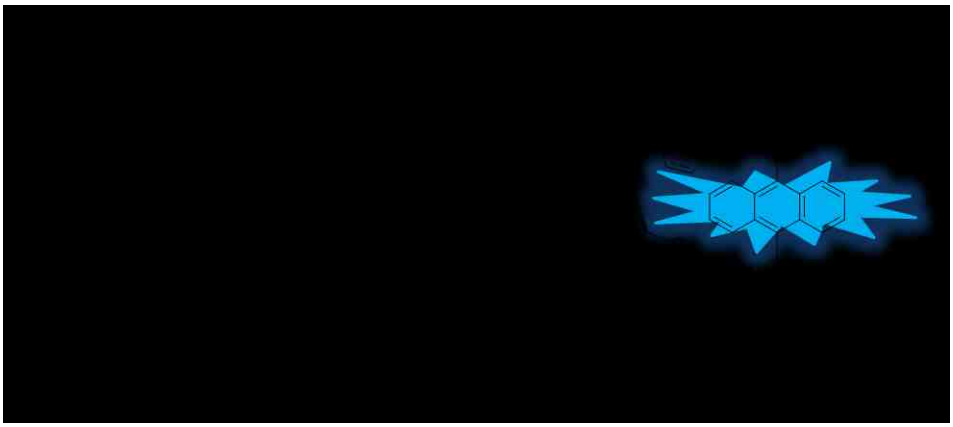

To verify the hypothesis that both the 2, 2'-dipicolylamine (Dpa)-Zn (II) moiety and the phenylboronic acid group contribute to ATP binding, we designed control compounds **2-2** and **2-3** (Figure 2.2). Control **2-2** has the similar structure as probe **2-1** except it contains a phenyl group instead of a phenylboronic receptor. Control **2-3** has the similar

structure as probe **2-1** except it contains a hydroxyl methyl group instead of the 2, 2'-dipicolylamine (Dpa)-Zn(II) moiety. Based on our hypothesis, upon the addition of ATP, we expect to see strong fluorescence of probe **2-1**, compared with no or weak fluorescence with control compounds **2-2** and **2-3**.

Figure 2.2 Structure of probe **2-1**, control compound **2-2** and control compound **2-3**.

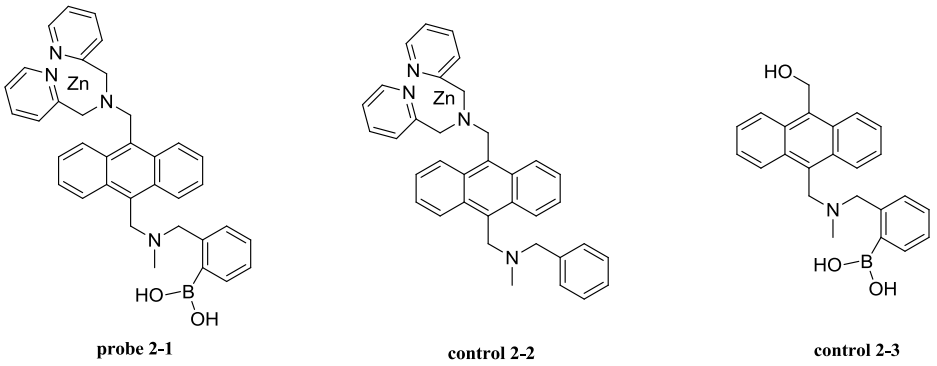

2.3 Synthesis

The synthesis of probe **2-1** was outlined in Scheme 2.3. Using the typical procedure for making compound **2-4** 10-(hydroxymethyl)anthracene-9-carbaldehyde through two steps, the hydroxyl group was subsequently protected as silyl ether. Reductive amination gave **2-7** in good yield, followed by Boc protection of the secondary amine. The introduction of 2, 2'-dipicolylamine (DPA) was conducted by making methyl sulfate as a good leaving group. After deprotection of Boc, phenylboronic acid moiety was successfully incorporated into the anthracene backbone. In the end, Zn(II) was coordinated to DPA by stirring with zinc nitrate THF solution for 30 min.

Scheme 2.3 Synthesis of probe 1

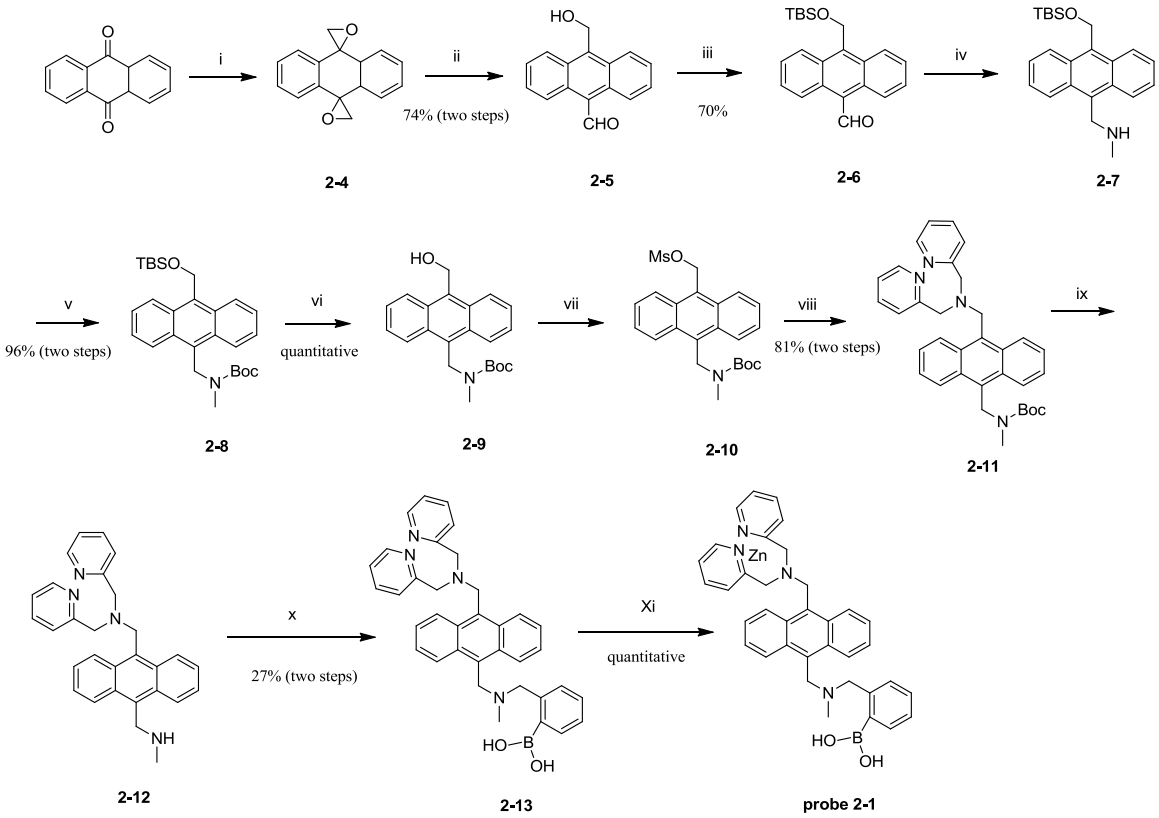

Reaction conditions: (i). NaH, $(CH_3)_3SI$, dry DMSO, r.t., under dark environment, 1.5 h. (ii). LiBr, dry MeCN, 60 ºC, under dark environment, 16 h. (iii). TBSCl, imidazole, dry DMF, r.t., 14 h. (iv). CH_3NH_2 in methanol, $NaBH_4$, 6h. (v). Boc_2O, anhydrous ethanol, 5 h. (vi). TBAF, THF, r.t. 3 h. (vii). MsCl, dry CH_2Cl_2, TEA, 0 ºC to r.t. (viii). 2,2'-dicopicolylamine, MeCN, reflux, 36 h. (ix). TFA, CH_2Cl_2, r.t. 2h. (x). 2-(2-(bromomethyl)phenyl)-5,5-dimethyl-1,3,2-dioxaborinane, K_2CO_3, THF, reflux, 39 h. (xi). $Zn(NO_3)_2$ solution, THF, r.t. 0.5 h.

The synthesis of control compound **2-2** was similar to that of probe **2-1** except the coupling reaction was conducted with (bromomethyl)benzene instead of 2-(2-(bromomethyl)phenyl)-5,5-dimethyl-1,3,2-dioxaborinane (Scheme 2.4). The synthesis of control compound **2-3** was outlined in Scheme 2.5, starting from compound **3**, reductive

amination afforded compound **13** which was further converted to control compound **2-3** by reaction with 2-(2-(bromomethyl)phenyl)-5,5-dimethyl-1,3,2-dioxaborinane.

Scheme 2.4 Synthesis of control **2-2**

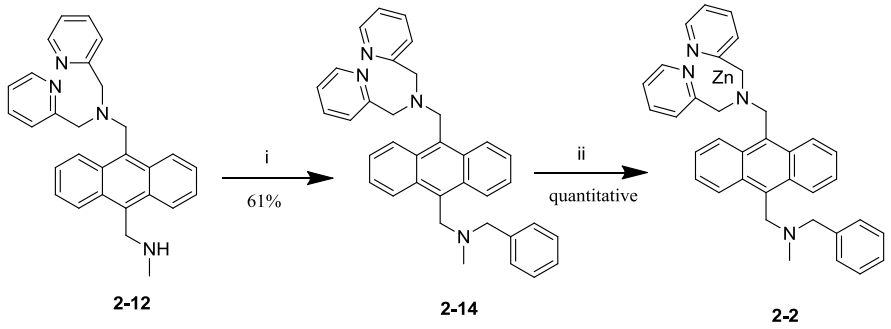

Reaction conditions: (i). (bromomethyl)benzene, K_2CO_3, THF, reflux, 24 h, separated by reverse phase HPLC. (ii). $Zn(NO_3)_2$, THF, r.t. 0.5 h.

Scheme 2.5 Synthesis of control **2-3**

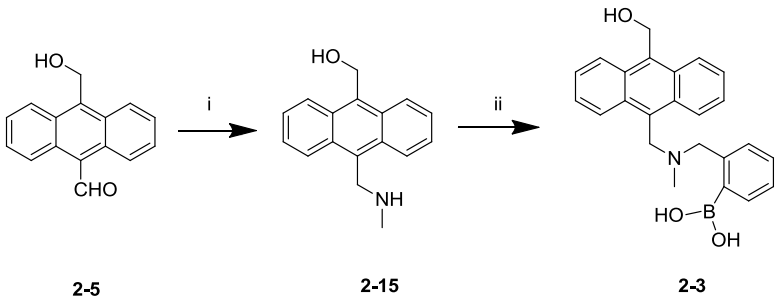

Reaction conditions: (i). CH_3NH_2, $NaBH_4$, ethanol, r.t. 6 h. (ii). 2-(2-(bromomethyl)phenyl)-5,5-dimethyl-1,3,2-dioxaborinane, K_2CO_3, THF, reflux, 39 h.

2.4 Results and Discussions

2.4.1 Evaluation of Probe 2-1 in HEPES Buffer

With probe **2-1** in hand, we first tested its fluorescence properties and established the optimal test conditions. Notably, probe **2-1** showed good solubility in water. Accordingly, all the experiments were performed in HEPES buffer (10mM, pH = 7.2). As designed, probe **2-1** exhibited weak fluorescence in the absence of ATP which can be explained as the lone pair electrons from the two amine atoms (amine attached to 2, 2'-dipicolylamine (DPA)-Zn(II) and phenyl boronic acid, respectively) quenched the fluorescence by PET pathway. The fluorescence intensity enhancement was observed with as low as 0.01 μM ATP. The characteristic peaks of anthracene fluorophore between 410nm and 480nm continued to increase with increasing amount of ATP, maximum fluorescence emission was reached with 30 μM of ATP. Meanwhile, the relationship between ATP concentration and fluorescence intensity was investigated. The fluorescence intensity at 415 nm was proportional to ATP concentration (Figure 2.1).

(a) (b)

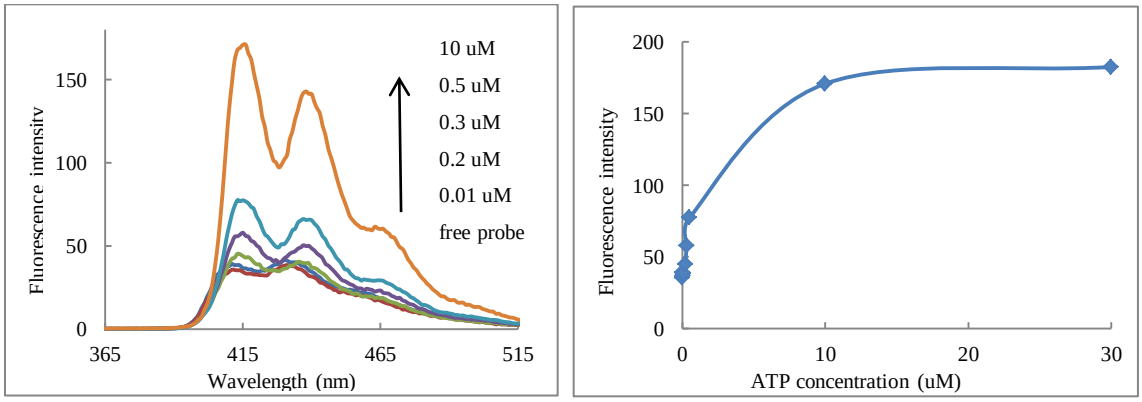

Figure 2.1 Effect of ATP concentrations on the fluorescence emission of probe **2-1**. Probe **2-1** (10 μM) was studied in a HEPES buffer (pH = 7.2, 0.01 M) at room temperature in the absence and presence of ATP at different concentrations (10 nM~30 μM). After 3 min, the reaction

solution was immediately sampled for fluorescence measurement. (a). fluorescence spectra. (b). fluorescence intensity at 415 nm was plotted vs. ATP concentrations.

Based on the results above, we subsequently conducted the selectivity test of probe **2-1** towards ADP, AMP, other phosphates and sugar in aqueous solution. The fluorescence intensity increased moderately upon the addition of ADP. Very weak fluorescence intensity was observed upon the addition of AMP and other compounds (Figure 2.2). These results demonstrated that probe **2-1** showed a certain level of selectivity for discriminating ATP from ADP, AMP, phosphates, and mannose.

(a) (b)

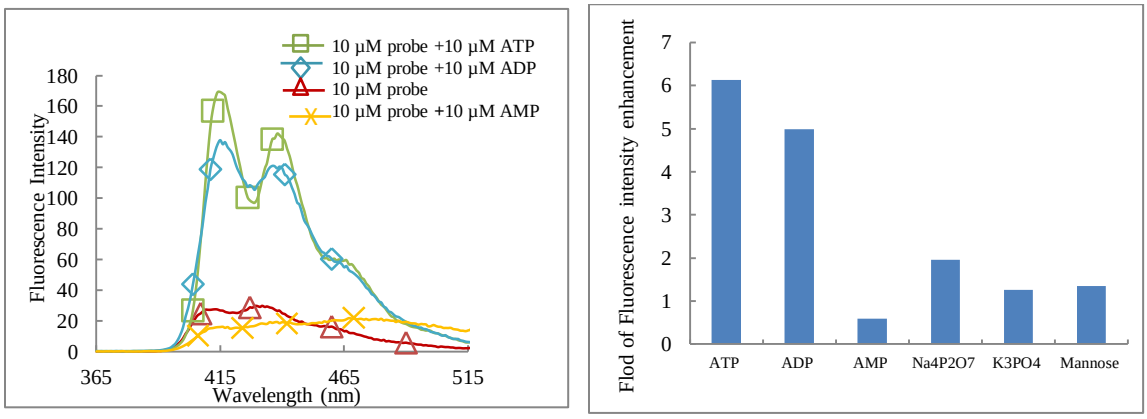

Figure 2.2. The selectivity of probe **2-1** towards ATP and other species. 10 μM probe **2-1**, prepared from a stock solution of MeCN, was studied in a HEPES buffer (pH = 7.2, 0.01 M) at room temperature in the presence of 10 μM various analytes (1 equiv.). After 3 min, reaction solution was sampled for fluorescence measurement. (a). fluorescence spectra. (b). Fold of fluorescence enhancement for various species at λ_{em} = 415 nm.

2.4.2 Fluorescent Detection of Intracellular ATP Levels

We further investigated the biological applications of probe **2-1** in living cells. Probe **2-1** was incubated with neural cancer cells SH-SY5Y cells, 30 min after the extracellular addition of ATP, fluorescence imaging was conducted. Results showed that stronger fluorescence signals were observed with increased ATP concentrations from no ATP, 50 μM ATP, to 100 μM ATP addition (Figure 2.3a-c). Furthermore, the ATP deficient condition was created when SH-SY5Y cells were treated with KCN (0.1mM), an inhibitor for glycolysis under glucose starvation conditions, a substantial decrease in fluorescence was observed (Figure 2.3 d). All the results demonstrated that intracellular ATP level was reflected by the fluorescence signals of probe **2-1** in live cells.

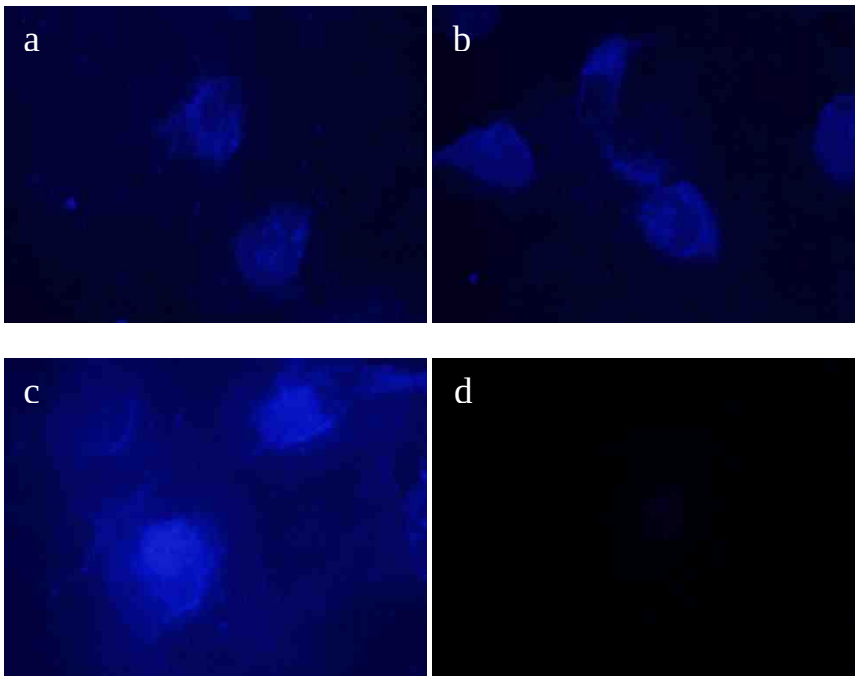

Figure 2.3. (a) Fluorescence images of SH-SY5Y cells stained with 10μM probe **2-1**. (b) Fluorescence images of SH-SY5Y cells stained with 10μM probe **2-1** upon addition of 50μM ATP. (c) Fluorescence images of SH-SY5Y cells stained with 10μM probe **2-1** upon addition of

100μM ATP. (d) Fluorescence images of SH-SY5Y cells stained with 10μM probe **2-1** after treatment of 0.1 mM KCN in the absence of glucose.

2.4.3 Mechanism Study of Probe 2-1 Comparing with Control Compounds 2-2 and 2-3

To verify our hypothesis that multiplexing recognition gave better fluorescence responses compared with traditional fluorescent probes with only a single recognition group, we tested the fluorescence responses of control **2-2** and control **2-3** towards ATP in comparison with probe **2-1**. Both the control compound **2-2** and control **2-3** were tested in the same condition as of probe **2-1**. Compound **2-2** showed weaker fluorescence enhancement upon the addition of ATP in the buffer as well as poor resolution in cell imaging, both of which proved that the phenylboronic acid moiety is playing a role in ATP binding (Figure 2.4 and Figure 2.6a). Compound **2-3** showed no fluorescence enhancement upon the addition of ATP in buffer and no fluorescence signal in the cell imaging (Figure 2.5 and Figure 2.6b), which proved our design strategy that 2,2'-dicopicoylamine Zn(II) moiety was also essential for ATP binding. On the other hand, probe **2-1** showed higher sensitivity both in buffer and cellular imaging. The results above proved that with two recognition groups binding phospho ion and cis-diol, respectively, probe **2-1** exceeds control compound **2-2** and **2-3** in its sensitivities for the detection of ATP molecules.

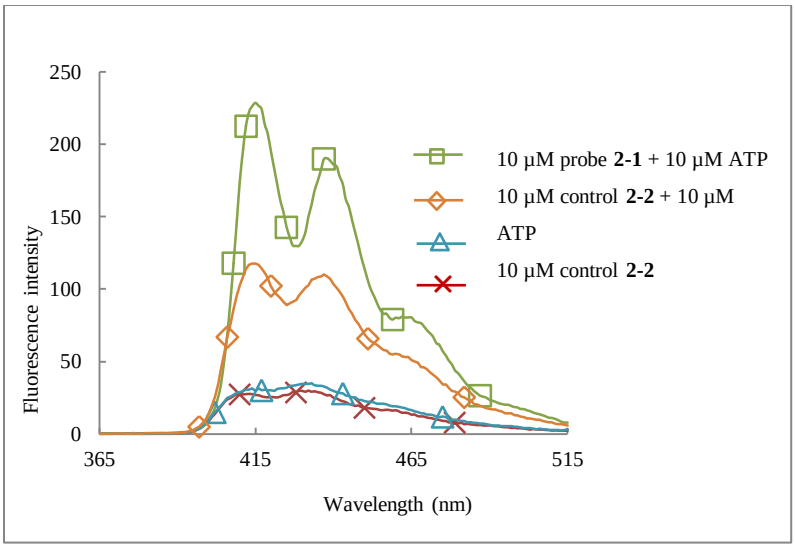

Figure 2.4. Emission spectra of probe **2-1** and control compound **2-2** (10 μM) towards ATP. Both probe **2-1** and control compound **2-2** were prepared from a stock solution of MeCN, and were studied in a HEPES buffer (pH = 7.2, 0.01 M) at room temperature in the absence and presence of 10μM ATP. After 3 min, the reaction solution was sampled for fluorescence measurement. Dashed blue line: control compound **2-2**; dashed orange line: control compound **2-2** after addition of ATP; solid red line: probe **2-1**; solid green line: probe **2-1** after addition of ATP.

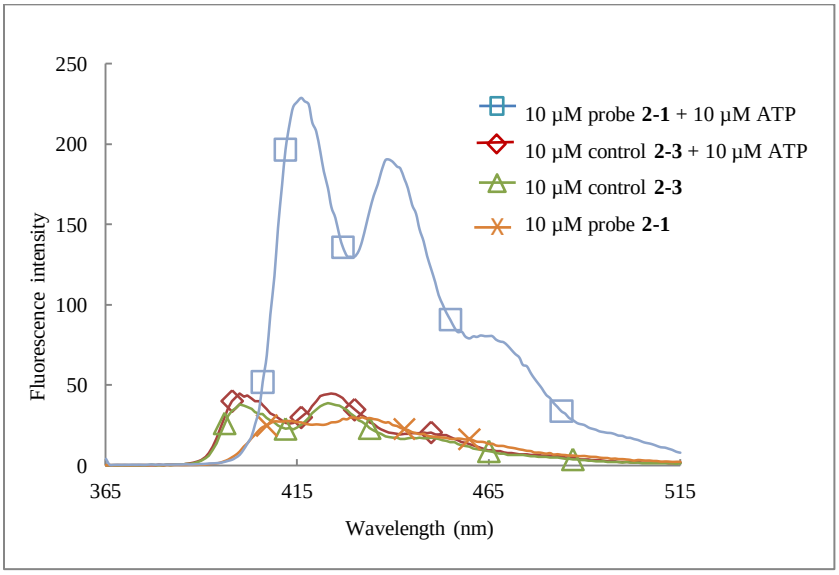

Figure 2.5. Emission spectra of probe **2-1** and control compound **2-3** (10 μM) towards ATP. Both probe **2-1** and control compound **2-3** were prepared from a stock solution of MeCN, and were studied in a HEPES buffer (pH = 7.2, 0.01 M) at room temperature in the absence and presence of 10 μM ATP. After 3 min, the reaction solution was sampled for fluorescence measurement. Dashed green line: control compound **2-3**; dashed red line: control compound **2-3** after addition of ATP; solid orange line: probe **2-1**; solid blue line: probe **2-1** after addition of ATP.

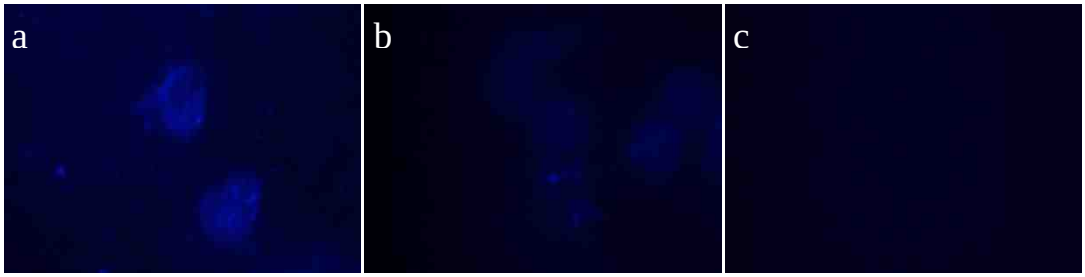

Figure 2.6. (a). Fluorescence images of SH-SY5Y cells stained with 10μM probe **2-1**. (b). Fluorescence images of SH-SY5Y cells stained with 10μM control compound **2-2**. (c). Fluorescence images of SH-SY5Y cells stained with 10uM control compound **2-3**.

2.5 Summary

In conclusion, we developed a fluorescent probe **2-1** for monitoring ATP based on multiplexing recognition. The probe worked in a pH=7.2 aqueous buffer, and showed 6.13 fold fluorescence enhancement upon ATP binding. It also exhibited a certain degree of selectivity among other structurally similar compounds including ADP, AMP, pyrophosphate ion, phosphate ion and mannose. It has been successfully applied in detecting intracellular ATP levels. Meanwhile, we made two control compounds which were tested in the same condition as probe **2-1**. Comparing with control compounds,

probe **2-1**, designed with multiplexing recognition, showed stronger fluorescence turn-on effect in buffer and gave better resolution in cell imaging. All the results demonstrated that multipoint recognition strategy may act as an effective approach in designing probes with higher resolution and better selectivity.

2.6 Experimental Section

General Information

Commercial reagents were used as received, unless otherwise stated. Merck 60 silica gel was used for chromatography, and Whatman silica gel plates with fluorescence F254 were used for thin-layer chromatography (TLC) analysis. ^{1}H and ^{13}C NMR spectra were recorded on Bruker tardis 300 or Bruker Avance 500. Data for ^{1}H are reported as follows: chemical shift (ppm), and multiplicity (s = singlet, d = doublet, t = triplet, q = quartet, m = multiplet). Data for ^{13}C NMR are reported as ppm. Mass Spectra were obtained from University of New Mexico Mass Spectral facility.

Synthesis of Probe 2-1, Control Compounds 2-2 and 2-3:

Compound 2-1 was synthesized following the procedures in Scheme 2.3.

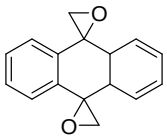

Trans-dispiro[oxirane-2,9'(10'H)-anthracene-10',2"-oxirane] (2-4).

To a stirred mixture of 60% NaH (900 mg, 22.5mmol), and anthraquinone (2080mg, 10mmol) in 60mL dry DMSO ar r.t. was added dropwise a solution of

trimethylsulfonium iodide (4590mg, 22.5mmol) in 40mL of dry DMSO over a period of 1 hour. The reaction was conducted in dark and under nitrogen protection. The reaction mixture was stirred for 5 hours until no anthraquinone remained monitored by TLC. The mixture was poured into 170mL of ice water, and filtered after standing for 0.5 hour. The residue was collected and washed with water to give the product as light yellow solids, which were used in the following reactions without further purification.

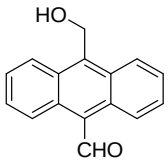

10-(hydroxymethyl)anthracene-9-carbaldehyde (2-5).

To a solution of lithium bromide (1203mg, 46.2mmol) in 150 mL of dry acetonitrile was added compound **2-4** (2360mg, 10mmol). The reaction mixture was stirred at 60 °C for 16 hours in the dark and cooled to r.t. Then, the solvent was removed and extracted with dichloromethane, washed with brine. The crude solid was purified by column chromatograph to give the product as yellow solid (1746mg, 74% two-step yield). ^{1}H NMR ($CDCl_3$, 500 MHz): δ 11.52 (s, 1H), 8.91 (d, J = 8.5 Hz, 2H), 8.54 (d, J = 8.5 Hz, 2H), 7.70~7.64 (m, 4H), 5.73 (s, 2H).

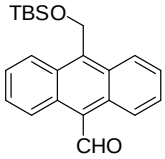

10-((tert-butyldimethylsilyloxy)methyl)anthracene-9-carbaldehyde (2-6).

Compound **2-5** (120 mg, 0.51mmol), TBSCl (100 mg, 0.66mmol), and imidazole (50 mg, 0.74mmol) were dissolved in 5mL of anhydrous DMF and stirred at r.t. for 14 hours. After solvent removal under reduced pressure, the residue was dissolved in 20 mL of ethyl acetate. It was then washed with 7 mL of water, 7 mL of 0.5N of hydrochloric acid, and 7 mL of saturated brine. The organic layer was separated, dried over anhydrous $MgSO_4$, and then evaporated to give a yellow solid. The crude product was purified by silica gel chromatography using ethyl acetate to hexane 1/50 as the eluent to give **2-6** as a yellow solid (125mg, 70% yield). ^{1}H NMR ($CDCl_3$, 500 MHz): δ 11.51 (s, 1H), 8.91 (d, J = 9 Hz, 2H), 8.50 (d, J = 9 Hz, 2H), 7.68~7.59 (m, 4H), 5.67 (s, 2H), 0.90 (s, 9H), 0.14 (s, 6H).

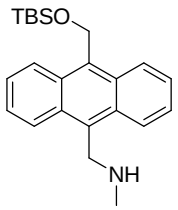

1-(10-((tert-butyldimethylsilyloxy)methyl)anthracen-9-yl)-N-methylmethanamine (2-7).

Compound **2-6** (200 mg, 0.57mmol) was dissolved in 10mL of 2.0 M solution of methylamine in methanol and the resulting mixture was stirred at r.t. for 6 hours. Then, $NaBH_4$ (65 mg, 1.71mmol) was added and the reaction mixture was stirred at r.t. for another 2 hours. The solvent was removed under reduced pressure and the residue was dissolved in ethyl acetate, the organic layer was washed with saturated $NaHCO_3$ solution and dried over anhydrous Na_2SO_4, Solvent evaporation gave a yellow solid which was used in the following reaction without further purification.

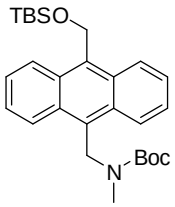

tert-Butyl(10-((tert-butyldimethylsilyloxy)methyl)anthracen-9-yl)methyl(methyl)carbamate (2-8).

To a solution of compound **2-7** (208 mg, 0.57 mmol) in 15 mL of anhydrous ethanol at r.t was added di-tert-butyl dicarbonate (224 mg, 1.0 mmol). After stirring for 5 hours, the solvent was removed under reduced pressure. Then, the reaction mixture was diluted with dichloromethane, washed with brine and the organic layer was dried over Na_2SO_4. The solvent was removed to give yellow solids which were purified on the silica gel column to afford compound **2-8** as yellow solids (265 mg, 96% two-step yield). ^{1}H NMR ($CDCl_3$, 500 MHz): δ 8.48~8.44 (m, 4H), 7.58~7.54 (m, 4H), 5.67 (s, 2H), 5.54 (s, 2H), 2.49 (s, 3H), 1.56 (s, 9H), 0.93 (s, 9H), 0.14 (s, 6H).

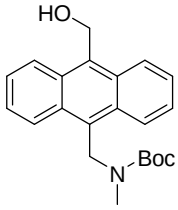

***Tert*-Butyl (10-(hydroxymethyl)anthracen-9-yl)methyl(methyl)carbamate (2-9).**

Compound **2-8** (540mg, 1.16mmol) was dissolved in THF, TBAF (450 mg, 1.72mmol) was added to the solution in one portion. The mixture turned red immediately and then became lighter. It was stirred for 1 hour and then the solvent was removed under reduced pressure. The residue was dissolved in ethyl acetate, and washed with brine. The organic

layer was evaporated under reduced pressure and dried over anhydrous Na_2SO_4 to give off a red liquid which was purified by silica gel chromatography using ethyl acetate to hexane 1 to 20 as eluent to give compound **2-9** as yellow liquid (407mg, quantitative yield). ^{1}H NMR ($CDCl_3$, 300 MHz): δ 8.48~8.45 (m, 2H), 8.34 (m, 2H), 7.57 ~ 7.48 (m, 4H), 5.65 (s, 2H), 5.31 (s, 2H), 2.41 (s, 3H), 1.54 (s, 9H).

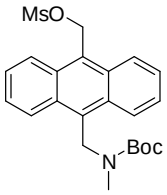

(10-((*tert*-butoxycarbonyl(methyl)amino) methyl) anthracen-9-yl) methyl methanesulfonate (2-10).

To a stirred mixture of compound **2-9** (180 mg, 0.51mmol) in 60 mL of dichloromethane, methanesulfonyl chloride (114 mg, 1.0mmol) was added at 0 °C. Then, triethylamine (126 mg, 1.25 mmol) was added and the resulting mixture was stirred at r.t. for 90 min. After the reaction was complete, the solvent was removed under reduced pressure and dissolved in dichloromethane. The organic layer was washed with brine and dried over anhydrous Na_2SO_4. After solvent evaporation, the residue was collected and used in the following step without further purification.

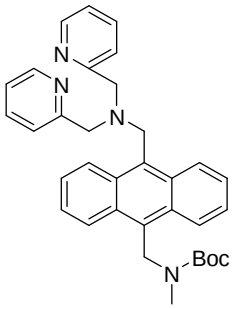

***Tert*-butyl(10-((bis(pyridin-2-ylmethyl)amino)methyl)anthracen-9-yl) methyl(methyl)carbamate(2-11).**

To a solution of compound **2-10** (220 mg, 0.51 mmol) in 17 mL of acetonitrile was added 2,2'-dicopicolyamine (111 mg, 0.56 mmol). It was refluxed for 40 hours. Then, the solvent was removed under reduced pressure, residue was dissolved in dichloromethane. The organic layer was washed with brine, dried over anhydrous Na_2SO_4. After solvent evaporation, the residue was purified by silica gel chromatograph using dicholoromethane to methanol 50 to 1 as eluent to give compound **2-11** (220mg, 81% two-step yield) as yellow solid. ^{1}H NMR ($CDCl_3$, 300 MHz): δ 8.50~8.39 (m, 4H), 8.39~8.36 (m, 2H), 7.60~7.44 (m, 6H), 7.30~7.33 (m, 2H), 7.13~7.11 (m, 2H), 5.47 (s, 2H), 4.70 (s, 2H), 3.90 (s, 4H), 2.44 (s, 3H), 1.55 (s, 9H).

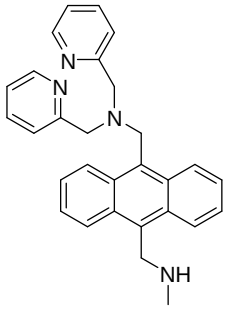

1-(10-((methylamino)methyl)anthracen-9-yl)-N,N-bis(pyridin-2-ylmethyl)methanamine (2-12).

Compound **2-11** (220 mg, 0.41mmol) was dissolved in a solution of 2.5 mL of dichloromethane and 0.6 mL of TFA. After stirred at r.t. for 0.5 hour until no compound **2-11** remained monitored by TLC, the solvent was removed under reduced pressure, and the residue was dissolved in dichloromethane, extracted with dichloromethane/saturated $NaHCO_3$, and washed with brine. The solvent was then removed to produce a yellow

liquid which was used in the next step without further purification. ^{1}H NMR ($CDCl_3$, 300 MHz): δ 8.49~8.45 (m, 4H), 8.34~8.31 (m, 2H), 7.60~7.43 (m, 6H), 7.31~7.29 (m, 2H), 7.11~7.08(m, 2H), 4.68 (s, 2H), 4.65 (s, 2H), 3.87 (s, 4H), 2.66 (s, 3H).

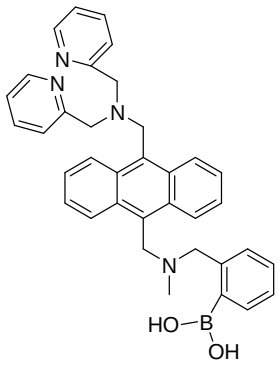

2-((((10-((bis(pyridin-2-ylmethyl)amino)methyl)anthracen-9-yl)methyl) (methyl) amino) methyl) phenylboronic acid (2-13).

To a solution of compound **2-12** (60 mg, 0.138 mmol) in 2 mL of THF was added K_2CO_3 (19 mg, 0.138 mmol) and 2,2-dimethylpropane-1,3-diyl(o-(bromomethyl)phenyl)boronate (44mg, 0.156mmol). The reaction mixture was refluxed for 39 hours. After solvent removal under reduced pressure, it was dissolved in CH_2Cl_2 and washed with brine. The organic layer was then collected. After solvent evaporation, the residue was purified on silica gel chromatograph to give compound **2-13** (24mg, 27% two-step yield) as yellow solid. ^{1}H NMR (CD_3OD-d^4, 500 MHz): δ 8.46 (d, J=8.5 Hz, 2H), 8.31 (d, J=4 Hz, 2H), 8.09 (d, J=7.5 Hz, 2H), 7.66 (d, J= 7 Hz, 1H), 7.60~7.57 (m, 2H), 7.53~7.50 (m, 4H), 7.36~7.24 (m, 5H), 7.16 (m, 2H). ^{13}C NMR (CD_3OD-d^4, 500 MHz): δ 160.25, 149.13, 138.26, 135.34, 134.27, 132.43, 132.28, 131.78, 128.98, 127.84, 127.06, 126.70, 125.40, 125.17, 123.70, 64.21, 61.48, 52.21, 50.08, 40.14.

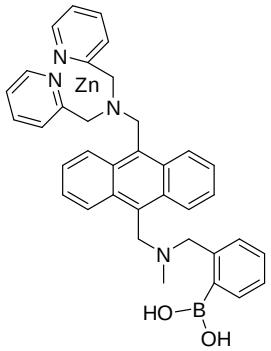

2-((((10-((Bis(pyridin-2-ylmethyl)amino)methyl)anthracen-9-yl)methyl) (methyl) amino) methyl) phenylboronic acid Zn complex (2-1).

To a solution of compound **2-13** (21 mg, 0.038 mmol) in 1mL of THF was added $Zn(NO_3)_2$ (7 mg, 0.038 mmol), and the mixture was stirred for 30 min at r.t. After concentration in vacuo, the residue was dissolved in HPLC acetonitrile and purified by reverse phase HPLC to get compound **2-1** as yellow solid (24 mg, quantitative yield). ESI-MS: [M+H-Zn] Calculated for $C_{36}H_{35}BN_4O_2$: 567.29, found 567.29.

Control 2-2 was synthesized following the procedures in Scheme 2.4.

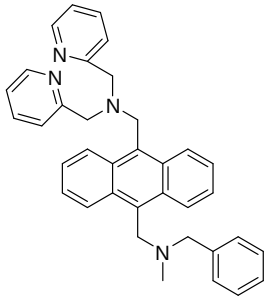

***N*-Benzyl-1-(10-((bis(pyridin-2-ylmethyl)amino)methyl)anthracen-9-yl)-N-methylmethanamine (2-14).**

To a solution of compound **2-12** (19 mg, 0.044mmol) in 1.5 mL of THF was added K_2CO_3 (10 mg, 0.072mmol). The reaction mixture was refluxed for 39 hours. After solvent removal under reduced pressure, it was dissolved in CH_2Cl_2 and washed with

brine. The organic layer was then collected. After solvent evaporation, the residue was purified on silica gel chromatograph using CH_2Cl_2 to methanol 20 to 1 as eluent to give compound **2-14** (14mg, 61% yield) as yellow solid. ^{1}H NMR ($CDCl_3$, 300 MHz): δ 8.49~8.41 (m, 5H), 7.59~7.53 (m, 2H), 7.48~7.42 (m, 4H), 7.33~7.25 (m, 8H), 7.11~7.07 (m, 2H), 4.68 (s, 2H), 4.46 (s, 2H), 3.66 (s, 4H), 3.67(s, 2H), 2.21 (s, 3H). ^{13}C NMR ($CDCl_3$, 300 MHz): δ 159.68, 148.67, 139.39, 136.15, 131.22, 129.16, 128.11, 126.98, 125.62, 125.52, 124.97, 123.56, 121.93, 62.40, 60.57, 53.66, 51.07, 42.15.

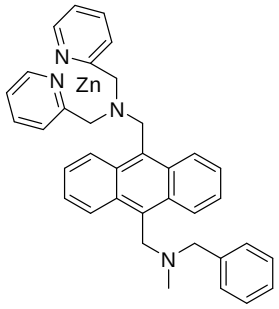

N-benzyl-1-(10-((bis(pyridin-2-ylmethyl)amino)methyl)anthracen-9-yl)-N-methylmethanamine Zn complex (2-2).

To a solution of compound **2-14** (14 mg, 0.027mmol) in 1 mL of THF was added $Zn(NO_3)_2$ (5 mg, 0.027 mmol), and the mixture was stirred for 30 min at r.t. After concentration in vacuo, the residue was dissolved in HPLC acetonitrile and purified by reverse phase HPLC to get compound **2-2** (16 mg, quantitative yield) as yellow solid. ESI-MS: [M+H-Zn] Calculated for $C_{36}H_{34}N_4$: 523.28, found 523.28.

Control Compound 2-3 was synthesized following the procedures in Scheme 2.5.

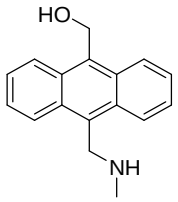

(10-((methylamino) methyl) anthracen-9-yl) methanol (2-15).

Compound **2-5** (53 mg, 0.22 mmol) was dissolved in 2mL of 33% wt methylamine in ethanol, and the resulting mixture was stirred at r.t. for 6 hours. Then, $NaBH_4$ (73 mg, 1.92 mmol) was added and the reaction mixture was stirred at r.t. for another 2 hours. The solvent was removed under reduced pressure and the residue was dissolved in ethyl acetate, the organic layer was washed with water and dried over anhydrous Na_2SO_4, Solvent evaporation gave a yellow solid which was used in the following steps without further purification.

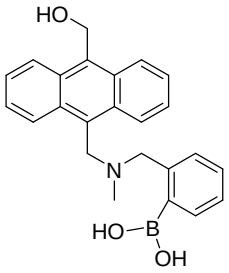

2-((((10-(hydroxymethyl) anthracene-9-yl) methyl) (methyl) amino) methyl) phenylboronic acid (2-3).

To a solution of compound **2-15** (60 mg, 0.239mmol) in 7 mL of THF was added K_2CO_3 (52 mg, 0.377 mmol) and 2,2-dimethylpropane-1,3-diyl (*o*-(bromomethyl)phenyl)boronate (44 mg, 0.155 mmol). The reaction mixture was refluxed for 39 hours. After solvent removal under reduced pressure, it was dissolved in CH_2Cl_2 and washed with brine. The organic layer was then collected. After solvent evaporation,

the residue was purified on silica gel chromatograph to give compound **2-3** as yellow solid (35% two-step yield). ^{1}H NMR (CD_3OD-*d4*, 500 MHz): δ 8.57 (d, J=9 Hz, 2H), 8.24 (d, J=8.5 Hz, 2H), 7.70 (d, J= 7.5 Hz, 1H), 7.63~7.56 (m, 4H), 7.41~7.35 (m, 2H), 7.28~7.25 (m, 1H), 5.62 (s,2H), 5.14 (s,2H), 4.46 (s, 2H), 2.43 (s, 3H). ^{13}C NMR (CD_3OD-d4, 500 MHz): δ 135.39, 132.87, 131.83, 131.46, 131.06, 129.04, 128.03, 127.62, 126.99, 126.58, 125.44, 114.06, 64.26, 57.19, 50.02, 40.01. ESI-MS: [M+H-H_2O] Calculated for $C_{24}H_{23}BNO_2$: 368.18, found 368.18.

Spectroscopic materials and methods:

Millipore water was used to prepare all aqueous solutions. The pH was recorded by a Beckman ΦTM 240 pH meter. Fluorescence emission spectra were obtained on a Shimadzu RF-5301PC spectrofluorophotometer. 10 mM probe **2-1** in MeCN was prepared as the stock solution, 5 μL of the stock solution was added to 4995 μL 10mM PH=7.2 HEPES buffer to make the final concentration of 10 μM. All the analytes (ATP, ADP, AMP, $Na_4P_2O_7$, K_3PO_4 and mannose) were prepared by dissolving the respective amount in water to make the final concentration of 10 μM. Fluorescence spectra were measured 3 min after the addition of each analyte.

Preparation of cell cultures

SH-SY5Y cell line was purchased from American Type Culture Collection. The cells were cultured in DMEM containing 10% FBS and 1% (v/v) antibiotic-antimycotic solution at 37°C with 95% air/5% CO_2 in an incubator.

Intracellular fluorescence imaging

Grow SH-SY5Y cells on coverslips inside a dish filled with DMEM culture medium. When cells reached the 70 % confluency, removed the media from the dish and added pre-warmed (37°C) staining solution containing ATP probe **2-1** (10 μM) and incubated for 30 min under growth conditions. Following a through wash, the coverslips were placed onto Olympus IX71 fluorescence microscopy and imaged with DAPI dichroic mirrors. Cells pretreated with 0.1mM KCN (inhibitor of ATP) before probe addition was used as a negative control. The images of control compound **2-2** and **2-3** stained cells were collected as another negative control.

2.7 References

[1] G. Burnstock, *Pharmacol. Rev.* **2006**, *58*, 58.

[2] P. Bodin, G. Burnstock, *Neurochem. Res.* **2001**, *26*, 959.

[3] A. V. Gourine, E. Llaudet, N. Dale, K. M. Spyer, *Nature* **2005**, *436*, 108.

[4] A. Sreenivasa Rao, D. Kim, H. Nam, H. Jo, K. H. Kim, C. Ban, K. H. Ahn, *Chem. Commun.* **2012**, *48*, 3206.

[5] P. Mahato, A. Ghosh, S. K. Mishra, A. Shrivastav, S. Mishra, A. Das, *Inorg. Chem.* **2011**, *50*, 4162.

[6] Z. Xu, D. R. Spring, J. Yoon, *Chemistry – An Asian Journal* **2011**, *6*, 2114.

[7] A. J. Moro, P. J. Cywinski, S. Korsten, G. J. Mohr, *Chem. Commun.* **2010**, *46*, 1085.

[8] H.-W. Rhee, S. J. Choi, S. H. Yoo, Y. O. Jang, H. H. Park, R. M. a. Pinto, J. C. Cameselle, F. J. Sandoval, S. Roje, K. Han, D. S. Chung, J. Suh, J.-I. Hong, *J. Am. Chem. Soc.* **2009**, *131*, 10107.

[9] Z. Xu, N. J. Singh, J. Lim, J. Pan, H. N. Kim, S. Park, K. S. Kim, J. Yoon, *J. Am. Chem. Soc.* **2009**, *131*, 15528.

[10] M. Schäferling, O. S. Wolfbeis, *Chem. Eur. J.* **2007**, *13*, 4342.

[11] P. P. Neelakandan, M. Hariharan, D. Ramaiah, *J. Am. Chem. Soc.* **2006**, *128*, 11334.

[12] J. Y. Kwon, N. J. Singh, H. N. Kim, S. K. Kim, K. S. Kim, J. Yoon, *J. Am. Chem. Soc.* **2004**, *126*, 8892.

[13] H. Abe, Y. Mawatari, H. Teraoka, K. Fujimoto, M. Inouye, *J. Org. Chem.* **2003**, *69*, 495.

[14] D. H. Lee, S. Y. Kim, J.-I. Hong, *Angew. Chem. Int. Ed.* **2004**, *43*, 4777.

[15] S. E. Schneider, S. N. O'Nei, E. V. Anslyn, *J. Am. Chem. Soc.* **2000**, *122*, 542.

[16] L. Fabbrizzi, N. Marcotte, F. Stomeo, A. Taglietti, *Angew. Chem. Int. Ed.* **2002**, *41*, 3811.

[17] F. Sancenón, A. B. Descalzo, R. Martínez-Máñez, M. A. Miranda, J. Soto, *Angew. Chem. Int. Ed.* **2001**, *40*, 2640.

[18] M. W. Hosseini, A. J. Blacker, J. M. Lehn, *J. Am. Chem. Soc.* **1990**, *112*, 3896.

[19] Y. Kurishita, T. Kohira, A. Ojida, I. Hamachi, *J. Am. Chem. Soc.* **2010**, *132*, 13290.

[20] Y. Kurishita, T. Kohira, A. Ojida, I. Hamachi, *J. Am. Chem. Soc.* **2012**, *134*, 18779.

[21] A. Ojida, I. Takashima, T. Kohira, H. Nonaka, I. Hamachi, *J. Am. Chem. Soc.* **2008**, *130*, 12095.

[22] A. Ojida, Y. Mito-oka, M.-a. Inoue, I. Hamachi, *J. Am. Chem. Soc.* **2002**, *124*, 6256.

[23] D. A. Yushchenko, O. B. Vadzyuk, S. O. Kosterin, G. Duportail, Y. Mely, V. G. Pivovarenko, *Anal. Biochem.* **2007**, *369*, 218.

[24] T. D. James, K. R. A. Samankumara Sandanayake, S. Shinkai, *Nature* **1995**, *374*, 345.

[25] L. A. Cabell, M.-K. Monahan, E. V. Anslyn, *Tetrahedron Lett.* **1999**, *40*, 7753.

[26] T. D. James, K. R. A. S. Sandanayake, S. Shinkai, *Angew. Chem. Int. Ed.* **1996**, *35*, 1910.

[27] J. C. Norrild, H. Eggert, *J. Am. Chem. Soc.* **1995**, *117*, 1479.

[28] A. Sugasaki, K. Sugiyasu, M. Ikeda, M. Takeuchi, S. Shinkai, *J. Am. Chem. Soc.* **2001**, *123*, 10239.

[29] W. Wang, S. Gao, B. Wang, *Org. Lett.* **1999**, *1*, 1209.

Chapter 3

Development of Photo-triggered Anticancer Prodrug to Release Multiple Drugs

3.1 Background

Prodrug strategy is an effective method in drug discovery, especially for the anticancer drugs [1]. It not only improves ADME (absorption, distribution, metabolism, excretion), but also greatly alleviates systematic toxicity and significantly enhances therapeutic index with controlled release of active drugs at the site of action [2]. Recently, multidrug delivery systems (MDDSs) have been developed with the advances in nanobiotechnology and material science. Multidrug delivery systems (MDDSs) allow multiple drug moieties to be delivered to be released at the preferred site. Compared with monochemotherapy, the combination therapy has brought about synergistic effect and lowered side effects so that they are commonly used in clinical chemotherapy [3]. Despite significant progress in this field, very few small molecule based multiple anticancer drug release systems are developed. The Smyth and coworker made a prodrug with a cephalosporin nucleus, upon hydrolysis by β-lactamase, releases aminoglutethimide (an aromatase inhibitor) and coumate (a sulfatase inhibitor) to inhibit estrogen production in hormone-dependent breast cancer[4]. With the limited achievements in this field, we hope to expand the horizon of this field by developing new strategies to release multiple drugs in cancer chemotherapy.

As well documented, DNA alkylating agents are one of the most widely used chemotherapeutic agents [5-6]. However, their high degree of reactivity accompanies high systematic toxicity that often prevents their clinical applications. To overcome severe side effect and improve therapeutic efficiency, prodrug strategy has been widely used to mask the highly reactive DNA alkylating agents [7]. Among various prodrug activation triggers, light is a highly orthogonal external stimulus, precise control of drug release at specific time and location can be realized [8-17]. Currently, no report was made on prodrugs that release multiple DNA alkylating agents upon activation. Thus, we have designed, synthesized and characterized a light activated prodrug **3-1** that releases two different types of chemotherapeutic agents – nitrogen mustard type mechlorethamine and quinone methide type o-quinone methide anticancer drug.

3.2 Design Strategy

As reported, biphenol biquaternary ammonium demonstrated very potent ISC properties upon photoactivation. Its extraordinary ISC activity is induced by its strong interaction with the backbone of double-stranded DNA, upon photoactivation, the subsequent formation of *o*-quinone methide intermediate easily forms intercross links with DNA double strand [10, 18]. Inspired by the previous report, we took biphenol biquaternary ammonium as the prodrug nucleus structure. The two phenol groups were masked by 1-(2-nitrophenyl)ethyl (NPE) photo-trigger, and DNA cross-linking agent mechlorethamine was inactivated at the phenol ortho position by converting to a charged nitrogen atom (Scheme 3.1).

The prodrug **3-1** was expected to be inactive as both the toxicity of o-quinone mthide and mechlorethamine was significantly reduced in the prodrug form. On the one hand, o-quinone methide was not formed until activated by light. On the other hand, the positive charge developed on the nitrogen decreases the electron density of mechlorethamine required for DNA alkylation. Upon photoactivation, NPE group was unmasked from the phenol, and o-quinone methide was formed subsequently, meanwhile, two molecules of mechlorethamine were released. Two types of DNA alkylating agents collectively react with DNA double strand to form ISC, inhibiting DNA separation during DNA replication and transcription, consequently leading to cell death. The photo-controlled activation is expected to control the dosage of drug released in a spatial and temperol manner.

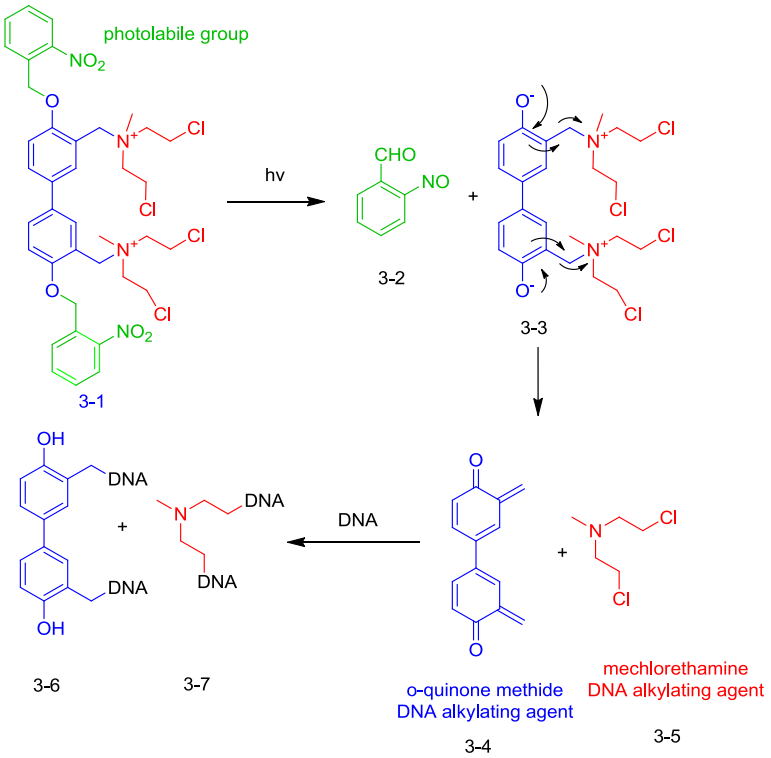

Scheme 3.1 Design of photo-triggered prodrug for multiple drug release.

3.3 Synthesis

The biphenol biquaternary ammonium prodrug **3-1** was synthesized according to the procedure shown in Scheme 3.2. Compound **3-9** was obtained by Duff Reaction. Lithium aluminum hydride reduction gave compound **3-10** in quantitative yield. Under the K_2CO_3 basic condition, the photo sensitive group 1-(bromomethyl)-2-nitrobenzene was selectively coupled at the phenolic position to yield compound **3-11** which was then converted to **3-12** using tribromophosphine. Treatment of **3-12** with excess amount of N-methyldiethanolamine under reflux condition gave compound **3-13**, which was then converted to the target product **3-1** by thionyl chloride.

Scheme 3.2 Synthetic routes for prodrug **3-1**

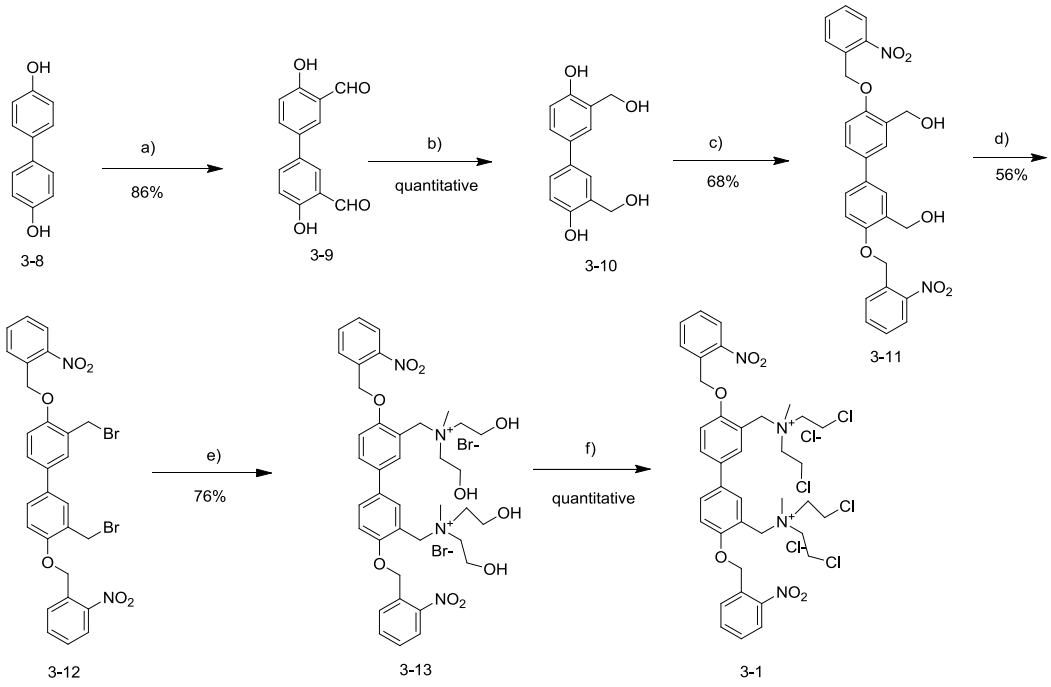

Scheme 3.2 Synthetic routes for prodrug 3-1. Reagents and conditions: (a). hexamethylenetetraamine, TFA, 80 °C, 3 h. (b). $LiAlH_4$, THF, 1.5 h. (c). 1-(bromomethyl)-2-

nitrobenzene, K_2CO_3, MeCN, 50°C, 4.5 h. (d). PBr_3, DCM, in dark, -5 °C to -3 °C, 70 min. (e). 2,2'-(methylazanediyl)diethanol, anhydrous MeCN, in dark, 85°C ,12 h. (f). $SOCl_2$, 3 d.

3.4 Photo-triggered Drug Release Studies

After obtaining prodrug **3-1**, we performed photo-triggered drug release studies. According to the proposed activation mechanism (Scheme 3.1), both the o-quinone methide **3-4** and mechlorethamine **3-5** can be released upon photoactivation.

In the presence of UV light, NPE group on prodrug **3-1** can be cleaved to form phenol biquaternary ammonium in aqueous solutions. According to Freccero and Zhou's reports [10-12, 18-19], phenol processing a quaternary ammonium group forms o-quinone methide by photoactivation in aqueous solutions. Thus, prodrug **3-1** should be able to release o-quinone methide **3-4.** However, o-quinone methide **3-4** is a very unstable intermediate that cannot be easily monitored or isolated. To prove the formation of o-QM **3-4**, DNA alkylating tests will be performed in the following section.

Meanwhile, mechlorethamine **3-3** is not easily isolated and characterized for its high reactivity and lack of UV-vis absorption. To monitor the existence of mechlorethamine **3-1**, we used diethyldithiocarbamate (DDC) to rapidly trap drug **3-5**, and monitored the UV absorption of the stable bisadduct **3-9**[20] (Scheme 3.3). Comparing with the standard compound **3-9**, the presence of **3-5** was confirmed by RP-HPLC.

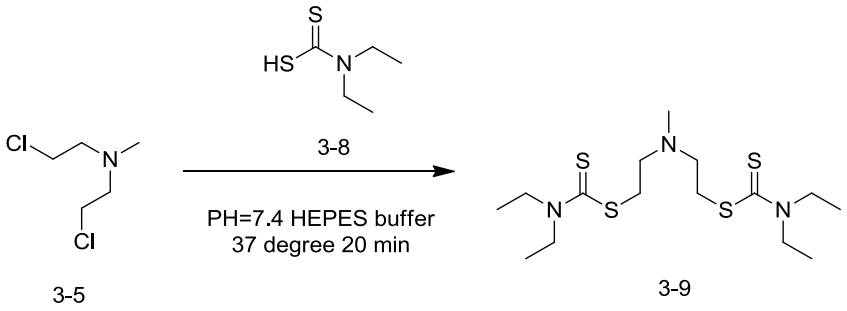

Scheme 3.3 Chemistry of detection of mechlorethamine

3.5 Kinetic Studies

Next, we conducted the more detailed kinetic studies of the photolytic reaction of prodrug **3-1** by monitoring the consumption of prodrug **3-1** as well as the formation of mechlorethamine **3-3** using RP-HPLC. An aqueous solution of 2 mM prodrug **3-1** was irradiated under UV light (2 W, 365 nm) for different time courses. We observed a decreasing peak 24.7 min corresponding to the decomposition of prodrug **3-1** (Figure 3.1a). To capture the UV-vis inactive compound **3-5**, the irradiated solution was incubated with 27.5 mM DDC at 37℃ for 20 min to complete the trapping reaction. HPLC analysis confirmed the presence of **3-5** by comparing with the standard peak of compound **3-9** at 20.3 min retention time under the same RP-HPLC condition, by monitoring the concentration of bisadduct **3-9** peak at 20.3 min, the amount of **3-5** can be calculated. Through path A: direct substitution reaction with prodrug **3-1**, there is roughly a constant concentration of **3-9** under all conditions for 20 min incubation time with DDC. The actual amount of bisadduct **3-9** released from the photolytic reaction (path B) can be obtained by subtracting **3-9** produced from path A from the total amount detected (Scheme 3.4). Using the standard curve of compound **3-9**, the conversion percentage was

plotted against time of UV irradiation. The amount of mechlorethamine released was proportional to the time of UV irradiation.

(a)

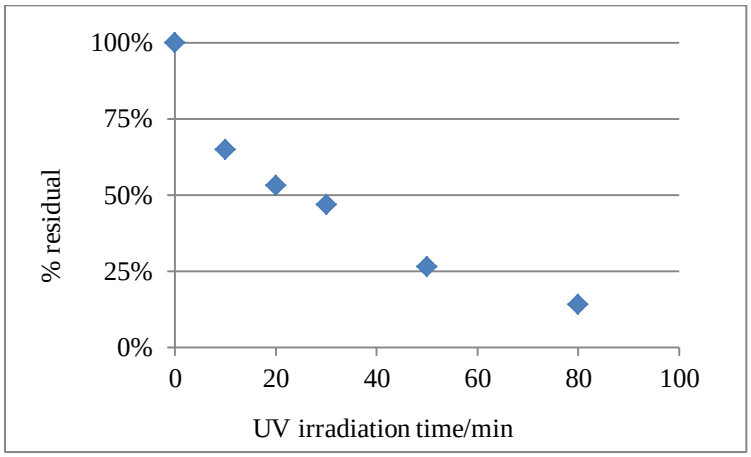

(b)

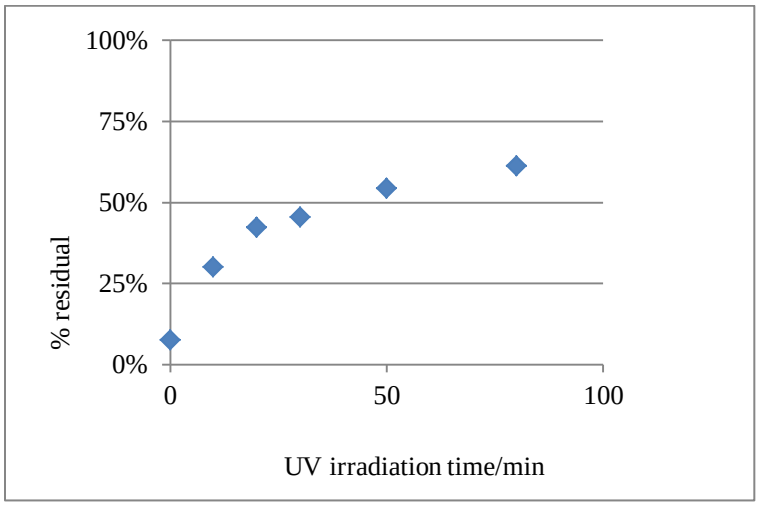

Figure 3.1. (a). Controlled decomposition of prodrug **3-1** in aqueous solution upon UV irradiation for designated time courses monitored by RP-HPLC. (b). Controlled release of mechlorethamine **3-5** in aqueous solution upon UV irradiation for designated time courses monitored by RP-HPLC.

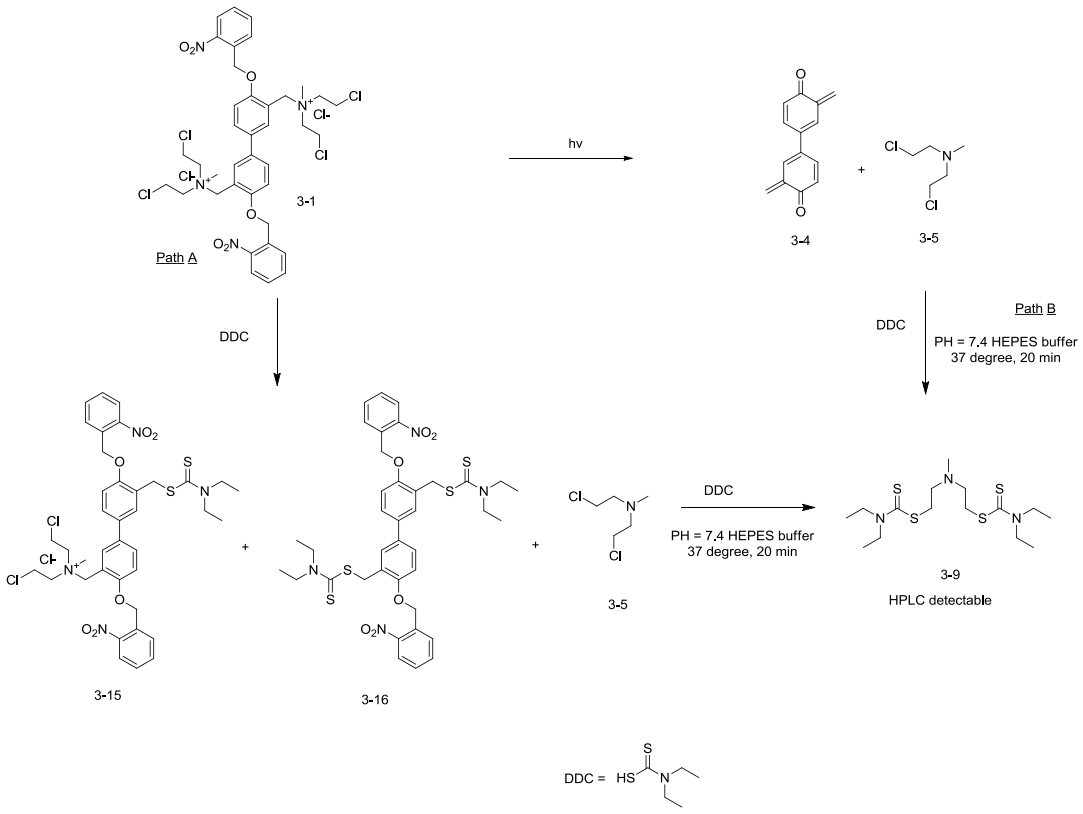

Scheme 3.4 Chemistry of detection of mechlorethamine release from prodrug **3-1** by: (path A) direct substitution with diethyldithiocarbamate (DDC) and (path B) photolytic fragmentation.

3.6 Cell Viability Test

Before conducting cellular tests, we firstly evaluated the stability and cell permeability of prodrug **3-1**. Concerning the fact that prodrug **3-1** is an electrophile, we tested its stability in a thiol rich cellular environment. As reported, GSH is present at very high levels in the cytosol, comprising about 90% of nonprotein sulfur with 1-2mM concentrations in most of cells [21]. An aqueous solution containing 10 mM prodrug **3-1** was incubated with 2 mM GSH for 6 hours at 37 ℃, DDC was incubated for 20 min to trap the released active drug **3-5**. An aliquot of solution was injected to RP-HPLC. We

have not observed decomposition of prodrug **3-1** nor increased amount of active drug **3-4**, which showed that prodrug **3-1** was very stable in a GSH rich cellular environment.

To evaluate the cell permeability of prodrug **3-1**, 0.5 mM prodrug **3-1** was incubated with HeLa cells for 2 hours, cell lysate was collected. After filtration, it was injected into RP-HPLC, a single peak on HPLC, i.e. the prodrug **3-1** peak was detected. It indicated that prodrug **3-1** was cell permeable.

Having established that prodrug **3-1** is able to release active mechlorethamine and showed high potency in inducing DNA cross-links. We evaluated its ability in inhibiting cancer cell growth as well as its cytotoxicity towards normal cells.

To begin with, cytotoxicity of prodrug **3-1** was evaluated on normal skin cells (Hekn cell lines) by using cell counting kit-8 (CCK-8). As is shown in Figure 3.2, without UV exposure on Hekn cells, inactivated prodrug **3-1** showed negligible cytotoxicity towards normal skin cells. Even with a drug concentration as high as 0.5 mM, Hekn cell viability as high as 89.2% was observed. After 30 min UV exposure, activated prodrug **3-1** showed lower cell viability than inactivated prodrug under the same concentration with majority of the cells survived. Thus, prodrug **3-1** displays low systematic toxicity towards normal cells both with and without UV activation. Its low toxicity assures its potential for further study.

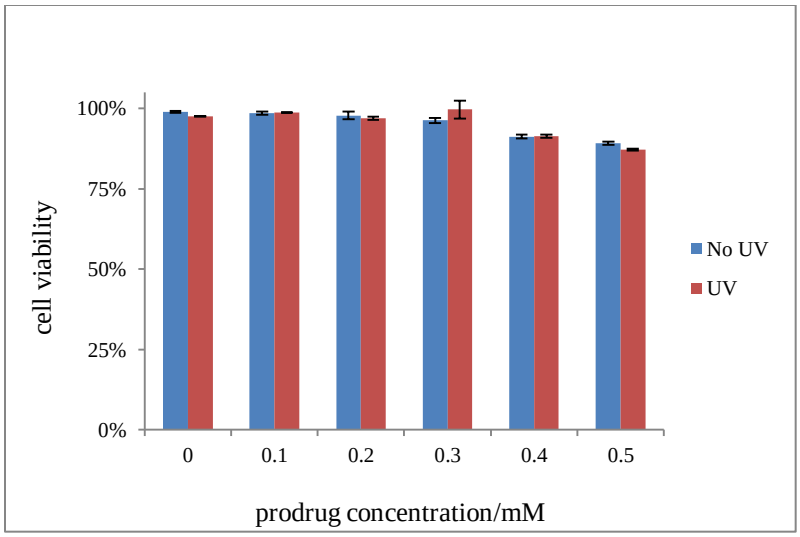

Figure 3.2. Cell viability assays of prodrug **3-1** on normal skin cells (Hekn cell lines) Prodrug **3-1** was incubated with the cells for 2 h followed by 30 min UV irradiation. The cell viability was measured after 24 h incubation using cell counting kit-8 (CCK-8).

Next, we evaluated prodrug **3-1** ability in inhibiting cancer cell growth. In the presence of 30 min mild UV irradiation (low-power UV light as light source was used and positioned 75 cm away from the reaction), with an increasing drug concentration, a larger amount of cancer cells (HeLa cells) was killed. In the absence of UV activation, prodrug 3-1 showed very limited cytotoxicity towards HeLa cells (Figure 3.3). Meanwhile, we have observed an impressive selectivity towards cancer cells. This is important in practical application. With a drug dosage of 0.5 mM and UV irradiation selectively at the tumor site, 2.1% cell viability on HeLa cells compared with 89.1% cell viability on Hekn cells. This might be explained by the selective activation of prodrug **3-1** with UV light as well as the ICL property of the inhibition mechanism. Cancer cells generally grow and divide at a much faster rate than normal cells. It is expected that much higher DNA replication and transcription activities take place in cancer cells than

those in normal cells, thus cell growth inhibition by intercross links formation is much more efficient towards cancer cells.

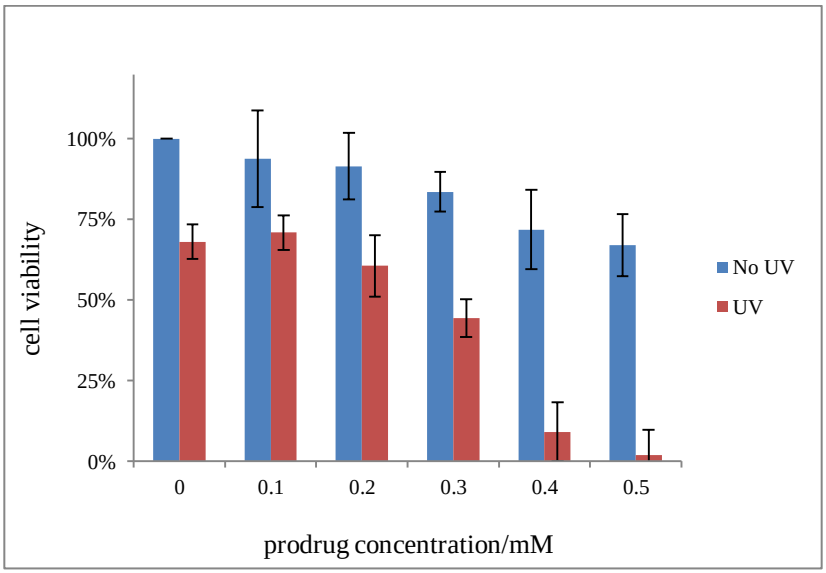

Figure 3.3. Cell viability assays of prodrug **3-1** on cancer cells (HeLa cell lines) Prodrug **3-1** was incubated with the cells for 2 h followed by 30 min UV irradiation. The cell viability was measured after 24 h incubation using cell counting kit-8 (CCK-8).

To prove that the anticancer properties of prodrug **3-1** was due to the release of both mechlorethamine **3-5** and o-quinone methide **3-4**, we made control compound **3-13** which only releases o-qionone methide **3-4** upon UV irradiation. Prodrug **3-1** exhibited much more significant potency than control compound **3-13**. At 0.5 mM concentration, prodrug **3-1** demonstrated 2.1% cell viability comparing to compound **3-13** with 60.6% cell viability. In the absence of UV, control **3-13** is less cytotoxic than prodrug **3-1**. The above results demonstrated that the incorporating mechlorethamine into the prodrug scaffold greatly improved drug potency.

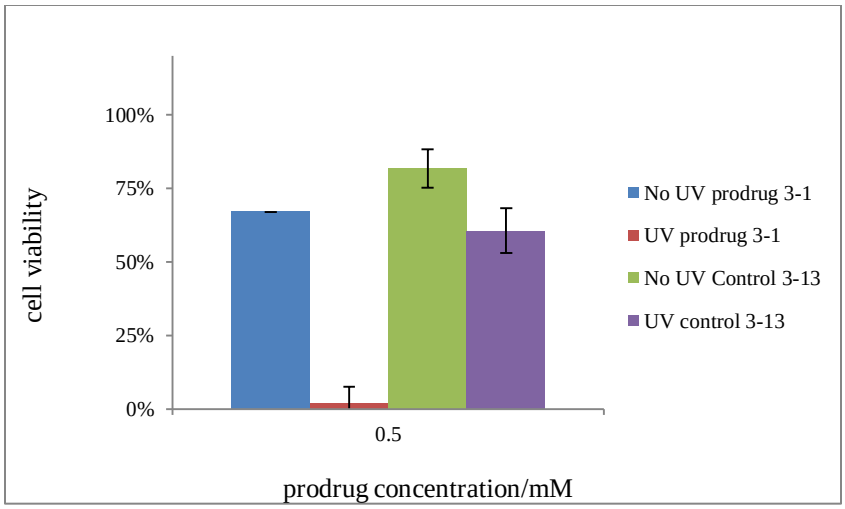

Figure 3.4. Cell viability assays of prodrug **3-1** and control compound **3-13** on cancer cells (HeLa cell lines) Prodrug **3-1** and control compound **3-13** were incubated with the cells for 2 h followed by 30 min UV irradiation. The cell viability was measured after 24 h incubation using cell counting kit-8 (CCK-8).

3.7 Summary

In conclusion, we have developed a photo-triggered multiple drug delivery system for anticancer drug releasing. The release of both of the active DNA alkylator o-quinone methide and mechlorethamine can be controlled with UV irradiation. We carried out detailed kinetic studies by monitoring the consumption of prodrug **3-1** and releasing of active mechlorethamine. From the cell viability tests, prodrug **3-1** showed negligible cytotoxicity towards normal skin cells (Hekn cells) with and without UV activation. Morever, activated prodrug **3-1** showed potent anticancer activity towards cancer cells. By comparing the results with control compound **3-13**, it showed that the anticancer activity of prodrug **3-1** was mainly contributed by the release of mechlorethamine. The preliminary results of multiple drug delivery system based on biphenol biquaternary

ammonium nucleus structure may serve as a potential prodrug candidate as chemotherapeutic agent.

3.8 Experimental Section

General Information

All reactions were carried out in dried flasks. The reactions were monitored by TLC for completion. Commercially available reagents were used as received without further purification unless otherwise specified. Merck 60 silica gel was used for column chromatography, and Whatman silica gel plates with fluorescence F254 were used for thin-layer chromatography (TLC) analysis. ^{1}H and ^{13}C NMR spectra were recorded on Bruker Avance 500 or 300. Data for ^{1}H are reported as follows: chemical shift (ppm), and multiplicity (s = singlet, d = doublet, t = triplet, q = quartet, m = multiplet). Data for ^{13}C NMR are reported as ppm. Mass Spectra were obtained from University of New Mexico Mass Spectral facility.

Synthesis of prodrug 3-1

Compound 3-1 was synthesized following the procedures in Scheme 3.2

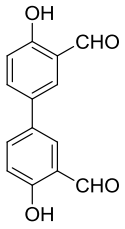

4,4'-dihydroxy-[1,1'-biphenyl]-3,3'-dicarbaldehyde (3-9)

4,4'-Biphenol (279 mg, 1.5 mmol) and hexamethylenetetraamine (472 mg, 3.37 mmol) were dissolved under argon in 5mL of anhydrous TFA, and stirred for 3 hours at 80 ℃, a

yellow solution was formed. After cooling to room temperature, the solution was poured into 4N HCl and stirred for 2 hours, during this time solids were formed. The yellow solids were collected by filtration, washed with water (2×) and cold ethanol once, and dried in vaccum. Purification by column chromatography (silica gel) gave product as yellow solids (363 mg, 86% yield). ^{1}H NMR ($CDCl_3$ with one drop of CD_3OD , 300 MHz): δ 9.97 (s, 2H), 7.71 (m, 4H), 7.07 (d, *J* = 9.3 Hz, 2H).

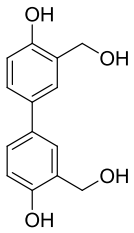

3,3'-bis(hydroxymethyl)-[1,1'-biphenyl]-4,4'-diol (3-10)

4,4'-Dihydroxy-[1,1'-biphenyl]-3,3'-dicarbaldehyde (121 mg, 0.5 mmol) was dissolved in 10 mL of dry THF, 2 eq $LiAlH_4$ (38 mg, 1 mmol) was added in portions over 30 min at 0 °C while stiring, the solution was slowly warmed up to room temperature and stirred for another 1 hour until the reaction was complete. After solvent removol, the residue was redissolved in 2N HCl, then it was extracted with ethyl acetate and 2N HCl, the organic layer was obtained. After solvent evaporation, yellow solids were obtained as desired product (123 mg, quantitative yield). ^{1}H NMR (CD_3OD, 500 MHz): δ 7.48 (s, 2H), 7.29 (d, *J* = 8.0 Hz, 2H), 6.80 (d, *J* = 8.0 Hz, 1H), 4.69 (s, 4H), ^{13}C NMR (CD_3OD, 500 MHz): δ 155.09, 133.91, 128.68, 127.35, 127.26, 166.20, 61.16.

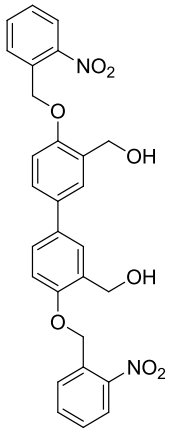

(4,4'-bis((2-nitrobenzyl)oxy)-[1,1'-biphenyl]-3,3'-diyl)dimethanol (3-11)

Potassium carbonate (22 mg, 0.161 mmol) was dissolved in 1 mL of acetonitrile, followed by the addition of 1 eq 3,3'-bis(hydroxymethyl)-[1,1'-biphenyl]-4,4'-diol (18mg, 0.073mmol) and 2.2 eq 1-(bromomethyl)-2-nitrobenzene (35mg, 0.161mmol). The reaction mixture was stirred in dark at 50 °C for 4.5 h. After solvent removal under reduced pressure, the crude product was further purified by silica column chromatography to give yellow solids as product (24 mg, 68% yield). ^{1}H NMR (acetone-d_6, 300 MHz): δ 8.16 (d, J = 8.4 Hz, 2H), 7.95 (d, J = 7.5 Hz, 2H), 7.81 (m, 4H), 7.64 (m, 2H), 7.47 (dd, J_1 = 8.4 Hz, J_1 = 2.4 Hz, 2H), 7.08 (d, J = 8.4 Hz, 2H), 5.57 (s, 4H), 4.80 (d, J = 5.7 Hz, 4H), 4.16 (t, J = 5.7 Hz, 2H). m.p.:239-240 °C.

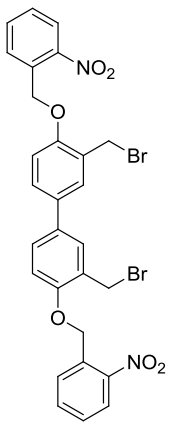

3,3'-bis(bromomethyl)-4,4'-bis((2-nitrobenzyl)oxy)-1,1'-biphenyl (3-12)

A solution of tribromophosphine (643 mg, 226 μL, 2.3 eq mmol) in 2.0 mL of anhydrous dichloromethane was added dropwise to a solution of 8(4,4'-bis((2-nitrobenzyl)oxy)-[1,1'-biphenyl]-3,3'-diyl)dimethanol (654 mg, 1 eq mmol) in 10 mL of anhydrous dichloromethane over 30 min with the temperature between -5 °C and -3 °C. The reaction mixture was stirred in dark at rt for 40 min. After the reaction is complete, it was washed with brine, concentrated and run column to give light yellow solids as product (56% yield). ^{1}H NMR (DMSO-d_6, 300 MHz): δ 8.17 (dd, J = 8.1 Hz, 2H), 7.93 (d, J = 6.6 Hz, 2H), 7.82 (m, 2H), 7.76 (d, J = 2.4 Hz, 2H), 7.62 (m, 4H), 7.16 (d, J = 9 Hz, 2H), 5.61 (s, 4H), 4.76 (s, 4H). m.p.: 216-219 °C.

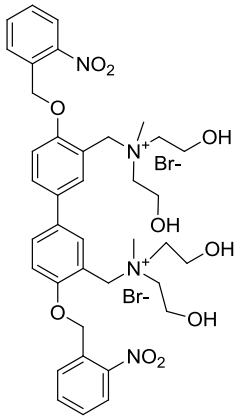

N,N'-((4,4'-bis((2-nitrobenzyl)oxy)-[1,1'-biphenyl]-3,3'-diyl)bis(methylene))bis(2-hydroxy-N-(2-hydroxyethyl)-N-methylethanaminium) bromide (3-13)

A solution of 3,3'-bis(bromomethyl)-4,4'-bis((2-nitrobenzyl)oxy)-1,1'-biphenyl (389 mg, 1.0 mmol) and 2,2'-(methylazanediyl)diethanol (357 mg, 8.0 mmol) in 10 mL of anhydrous acetonitrile was stirred in dark at 85°C for 12 h. After filtration, white solid was obtained as product (76% yield). ^{1}H NMR (DMSO-d_6, 500 MHz): 8.20 (d, J = 8.5

Hz, 2H), 7.91 (s, 2H), 7.83 (m, 6H), 7.67 (m, 2H), δ 7.32 (d, *J* = 9.0 Hz, 2H), 5.62 (s, 4H), 5.31 (m, 4H), 4.75 (s, 4H), 3.88 (m, 8H), 3.59 (m, 4H), 3.42 (m, 4H), 3.02 (m, 6H). m.p.: 212-215°C.

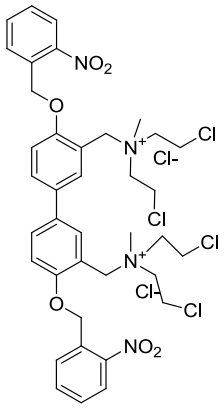

N,N'-((4,4'-bis((2-nitrobenzyl)oxy)-[1,1'-biphenyl]-3,3'-diyl)bis(methylene))bis(2-chloro-N-(2-chloroethyl)-N-methylethanaminium) chloride (3-14)

N,N'-((4,4'-bis((2-nitrobenzyl)oxy)-[1,1'-biphenyl]-3,3'-diyl)bis(methylene))bis(2-hydroxy-N-(2-hydroxyethyl)-N-methylethanaminium) bromide (43 mg, 0.05 mmol) was dissolved in 2 mL of thionyl chloride. The reaction mixture was stirred at rt for 3 d. After solvent evaporation under reduced pressure, white solid was obtained as product (quantitative yield). m.p.: 118-120 °C.

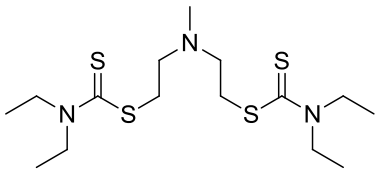

(Methylazanediyl)bis(ethane-2,1-diyl) bis(diethylcarbamodithioate) (3-9)

^{1}H NMR ($CDCl_3$, 500 MHz): δ 4.03 (m, 4H), 3.75 (m, 4H), 3.46 (t, *J* = 11.5 Hz, 4H), 2.79 (t, *J* = 12.0 Hz, 4H), 2.42 (s, 3H), 1.28 (m, 12H), ^{13}C NMR ($CDCl_3$, 500 MHz): δ 55.75, 49.47, 46.65, 34.59, 12.46, 11.58.

HPLC monitoring of drug release

Prodrug **3-1** (2 mM) was dissolved in an aqueous solution of pH 7.4 HEPES buffer (30% DMSO), a hand-held UV lamp (365 nm, 2W) was positioned 10 cm away from the reaction vial as light source. After designated reaction time, an aliquot of 200 μL solution was taken and incubated with 20 μL 27.5 mM DDC at 37 °C for 20 min to allow complete reaction. Next, an aliquot of 20 μL solution was submitted to RP-HPLC to be analyzed by a 254 nm UV detector, the amount was integrated by the area under each peak, and calculated from the standard curves under the same HPLC condition.

HPLC condition: Eclipse XDB-C8 column, flow rate is 0.8 mL/min, 0-20 min: MeCN/H_2O (10:90), 20-40 min: MeCN/H_2O (30:70).

Cell viability test

Cell viability was measured by using cell counting kit-8 (CCK-8), which quantitatively measures activities of dehydrogenases in cells. Cells (5×10^3 cells/well) were seeded into 96-well microtiter plates. Following treatment with prodrug 4-**1** and different reaction conditions (in the presence or absence of 365 nm UV light), 10 μL of CCK-8 solution was added to each well of the plate. The plate was placed into the incubator at 37 °C with 95% air/5% CO_2. After one hour incubation, the absorbance was measured at 450 nm in a Bio-Rad 3350 microplate reader. Cells without any treatment

were used as 100% cell viability. The cell viability was calculated by using the formula: Cell viability = (Experimental absorbance value – culture medium absorbance value)/(without treatment absorbance value – culture medium absorbance value).

3.9 References

[1] J. Rautio, H. Kumpulainen, T. Heimbach, R. Oliyai, D. Oh, T. Jarvinen, J. Savolainen, *Nat. Rev. Drug Discov.* **2008**, *7*, 255.

[2] *Drug Delivery Principles and Applications* John Wiley & Sons, Inc., Hoboken, New Jersey, **2005**.

[3] S. K. Tatsuya Okuda, *J. Biomater. Nanobiotechnol.* **2012**, *3*, 50.

[4] J. W. Grant, T. P. Smyth, *J. Org. Chem.* **2004**, *69*, 7965.

[5] S. R. Rajski, R. M. Williams, *Chem. Rev.* **1998**, *98*, 2723.

[6] D. M. Noll, T. M. Mason, P. S. Miller, *Chem. Rev.* **2005**, *106*, 277.

[7] V. B. Stella, R.; Hageman, M.; Oliyai, R.; Maag, H.; Tilley, J., *Prodrugs: Challenges and Rewards*, **2007**.

[8] C. Alvarez-Lorenzo, L. Bromberg, A. Concheiro, *Photochem. Photobiol.* **2009**, *85*, 848.

[9] J. J. Tepe, R. M. Williams, *J. Am. Chem. Soc.* **1999**, *121*, 2951.

[10] P. Wang, R. Liu, X. Wu, H. Ma, X. Cao, P. Zhou, J. Zhang, X. Weng, X.-L. Zhang, J. Qi, X. Zhou, L. Weng, *J. Am. Chem. Soc.* **2003**, *125*, 1116.

[11] S. N. Richter, S. Maggi, S. C. Mels, M. Palumbo, M. Freccero, *J. Am. Chem. Soc.* **2004**, *126*, 13973.

[12] E. E. Weinert, R. Dondi, S. Colloredo-Melz, K. N. Frankenfield, C. H. Mitchell, M. Freccero, S. E. Rokita, *J. Am. Chem. Soc.* **2006**, *128*, 11940.

[13] I. S. Hong, H. Ding, M. M. Greenberg, *J. Am. Chem. Soc.* **2005**, *128*, 485.

[14] M. Di Antonio, F. Doria, S. N. Richter, C. Bertipaglia, M. Mella, C. Sissi, M. Palumbo, M. Freccero, *J. Am. Chem. Soc.* **2009**, *131*, 13132.

[15] D. Verga, M. Nadai, F. Doria, C. Percivalle, M. Di Antonio, M. Palumbo, S. N. Richter, M. Freccero, *J. Am. Chem. Soc.* **2010**, *132*, 14625.

[16] A. Jana, K. S. P. Devi, T. K. Maiti, N. D. P. Singh, *J. Am. Chem. Soc.* **2012**, *134*, 7656.

[17] R. Weinstain, E. Segal, R. Satchi-Fainaro, D. Shabat, *Chem. Commun.* **2010**, *46*, 553.

[18] X. Weng, L. Ren, L. Weng, J. Huang, S. Zhu, X. Zhou, L. Weng, *Angew. Chem. Int. Ed.* **2007**, *46*, 8020.

[19] M. Freccero, C. Di Valentin, M. Sarzi-Amadè, *J. Am. Chem. Soc.* **2003**, *125*, 3544.

[20] W. A. Denny, W. R. Wilson, M. Tercel, P. Van Zijl, S. M. Pullen, *Int. J. Radiat. Oncol. Biol. Phys.* **1994**, *29*, 317.

[21] H. Peng, W. Chen, Y. Cheng, L. Hakuna, R. Strongin, B. Wang, *Sensors* **2012**, *12*, 15907.

Chapter 4

Development of Multi-functional Photo-triggered Fluorescent Prodrug for Imaging and Drug Release

4.1 Background

Despite the fact that nitrogen mustards such as mechlorethamine and chlorambcil are the earliest and perhaps most extensively studied of the DNA interstrand cross-linking agents, nowadays they still are the front line therapies for the treatment of many types of human cancers in clinics and provide an area of extremely intense and progressive investigation [1-3]. However, their applications are severely limited due to high systemic toxicity as a result of their poor selectivity between normal and cancer cells. One of the effective strategies to reduce toxicity towards normal cells is to transform inactive prodrugs that can be activated to release preferentially at the site of action in tumor cells. In this regard, significant efforts have been made on the development of stimuli, such as light or heat [4-13], hypoxia condition [14-25], oxidative stress[26-31], and other means[2, 32-36] to control release of the active DNA alkylating agents. Nevertheless, these methods cannot spatiotemporally monitor the release event in order to reach the optimal therapeutic effectiveness in high demanding personalized medicine.

The use of light as a remote-activation mechanism for drug delivery has received considerable attention as a result of its capacity of highly specific spatial and temporal control of drug release.[3] This feature renders the light-triggered theranostics particularly attractive in personalized medicine. Therefore, intensive efforts have been directed

towards the development of photo-triggered theranostic agents including DNA alkylators[37]. The studies in the field are mainly focused on the nanomaterial-based drug delivery systems (DDSs)[12, 38-42]. Despite impressive progress, to the best of our knowledge, a small molecule-based photo-triggered DDS enabling to simultaneously deliver and monitor drug release of DNA alkylating agents has not been reported [43-48] because unlike nanomaterial, it is formidably challenging to incorporate an imaging tag, a drug and a trigger into one small molecule. A new strategy that contributes to this subject should be of broad interest. Herein we wish to disclose the first example of photo-triggered fluorescent theranostic prodrug for controlled release and monitoring of DNA alkylating agent mechlorethamine.

4.2 Design Strategy

In the design of a new nitrogen mustard photo-triggered prodrug, three important criteria must be taken into consideration: (1) alleviate systemic toxicity and increase tumor selectivity; (2) provide precise control of drug release; (3) monitor drug release process using non-invasive, sensitive fluorescent imaging with desired 'off-on' signal. Therefore, a new prodrug **4-1** consisting of three essential components – a masked DNA cross-linking agent mechlorethamine, a 1-(2-nitrophenyl)ethyl (NPE) photo-trigger, and a coumarin fluorophore is designed (Scheme 4.1).

This prodrug is expected to act as an effective drug delivery system enabling concurrently both controlled release and fluorescent-based drug monitoring. It is conceivable that the toxicity of mechlorethamine would be significantly reduced by the positive charge developed on the nitrogen that strongly decreases the electron density of

mechlorethamine required for alkylation. Moreover, the strong electron-withdrawing moiety coupled with the second strong electron withdrawing NPE could effectively block internal charge transfer (ICT), thereby leading to the prodrug **4-1** initially nonfluorescent. However, upon photo-irradiation, the release of the active drug mechlorethamine accompanies a desired 'off-on' fluorescence signal by change from the 'pull-pull' to a 'push-pull' system. In addition, the coumarin fluorophore not only acts as a signal tag, but also as an antenna, greatly improve photolysis efficiency of NPE group by enhancing UV absorbance and transferring energy to NPE group. Finally, the positively charged prodrug **4-1** may also enhance the selectivity and binding affinity of negatively charged DNA.

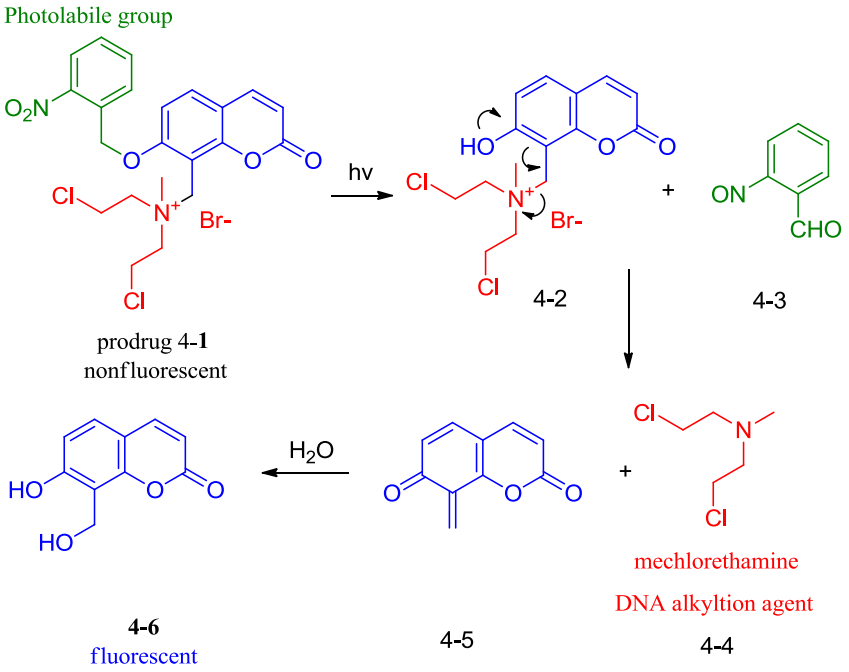

Scheme 4.1 Design of photo-triggered fluorescent prodrug for mechlorethamine.

4.3 Synthesis

The synthetic route for prodrug **4-1** is outlined in Scheme 4-2. Starting from 2-Methylresorcinol, 7-hydroxyl, 8-methyl coumarin 4-8 was made, which was then protected as coumarin acetate, followed by bromination with NBS, and hydrolysis to afford 7-hydroxyl-8-(hydroxymethyl) coumarin **4-11** in moderate yield. Under the mild basic condition, the photo sensitive group 1-(bromomethyl)-2-nitrobenzene was selectively coupled at the phenolic position to yield 8-(hydroxymethyl)-7-(2-nitrobenzyloxy)-coumarin **4-12**, which was then converted to **4-13** using tribromophosphine. Treatment of **4-13** with N-methyldiethanolamine yielded **4-14**, which was converted to target compound **4-1** using thionyl chloride.

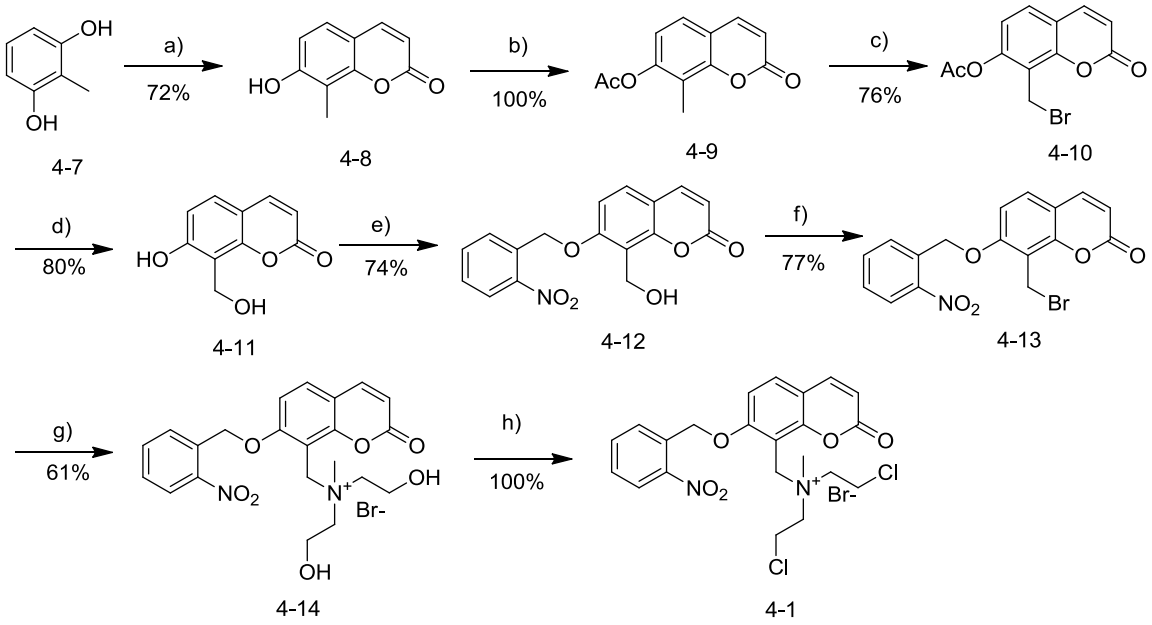

Scheme 4.2 Synthetic routes for prodrug 4-**1**. Reagents and conditions: (a). concentrated H_2SO_4, 2-hydroxysuccinic acid, MW (240W, 120℃), 4 min; (b). acetic anhydride, pyridine, rt, 12 h; (c). NBS, AIBN, CCl_4, reflux, 6 h; (d). $CaCO_3$, dioxane/H_2O=1/1, 50 ℃, 24 h; (e). 1-(bromomethyl)-2-nitrobenzene, K_2CO_3, MeCN, 50℃, in dark, 5h; (f). PBr_3, DCM, rt, in dark, 70 min; (g). 2,2'-(methylazanediyl)diethanol, dry MeCN, rt, in dark; (h). $SOCl_2$, rt, in dark, 3 d.

4.4 Photo-triggered Drug Release Studies

With the compound **4-1** in hand, firstly we performed photo-triggered drug release studies. According to the proposed mechanism (Scheme 4.1), both the active drug **4-4** and fluorescent product **4-6 will** be formed during the process. Compound **4-6** can be easily monitored and isolated for its strong fluorescence and stability in aqueous solution, while active drug **4-4** itself is not easily isolated and characterized due to its high reactivity and lack of UV-vis absorption. According to the previous report [49], we used diethyldithiocarbamate (DDT) to rapidly trap drug **4-4**, and monitor the UV absorption of the stable bisadduct **4-15** (Scheme 4.3). Comparing with the standard compound **4-15**, the presence of **4-4** was confirmed by RP-HPLC.

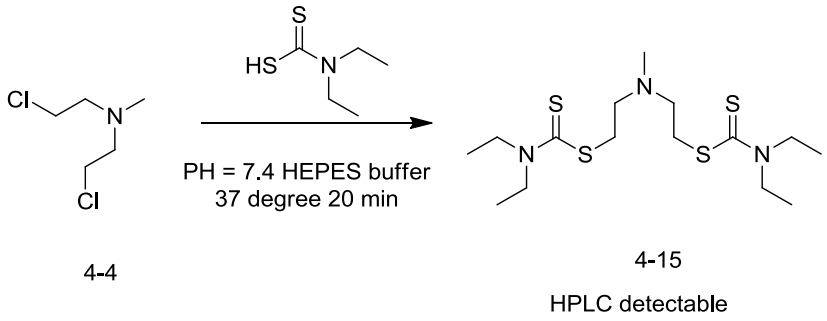

Scheme 4.3 Chemistry of detection of mechlorethamine

An aqueous solution containing 5 mM prodrug **4-1** was prepared and irradiated with a hand-held UV lamp (2 W, 365 nm). Time course study revealed complete disappearance of **4-1** in 90 min. A highly fluorescent presumed product was formed during the process, monitored by a fluorometer. The fluorescent molecule was isolated and characterized by ^{1}H and ^{13}C NMR and mass spectroscopy. Its structure was

determined to be compound **4-6**. Meanwhile, the irradiated solution was incubated with 27.5 mM DDC at 37°C for 20 min, HPLC analysis confirmed the presence of **4-4** by comparing with the standard peak of compound **4-15** at 20.3 min retention time under the same (RP) HPLC condition.

The above studies proved the proposed reaction mechanism and working hypothesis. Prodrug **4-1** was able to release and meanwhile monitor the release process by fluorescence.

4.5 Kinetic Studies

Next, we conducted the more detailed kinetic studies of the photolytic reaction of prodrug **4-1** with reversed-phase (RP) HPLC. The concentrations of prodrug **4-1**, photolytic products **4-15** and **4-4** were monitored. An aqueous solution of 2 mM prodrug **4-1** was irradiated under UV light (2 W, 365 nm) for different time courses. Then an aliquot sample was taken and injected to (RP) HPLC using water/acetonitrile mixture as mobile phase at a flow rate of 0.8 mL/min at λ_{max} 254 nm. We observed the decreasing of peak at 32.2 min accompanied with the concurrent appearance of new peak at 16.2 min. Peak at 32.2 min corresponded to the decomposition of prodrug **4-1** (Figure 4.1a), while the new peak resulted from the formation of photoproduct **4-6** (Figure 4.1b). The release of fluorescent product **4-6** was proportional to the time of UV irradiation.

(a)

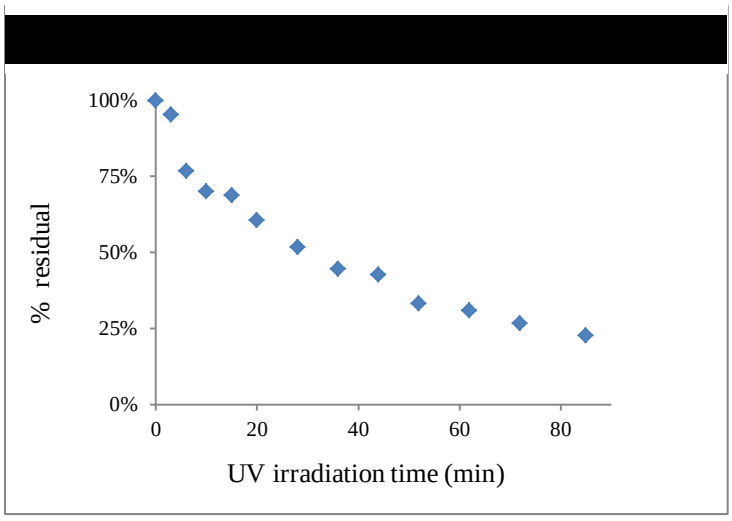
100%
75%
50%
25%
0%
% residual
0
20
40
60
80
UV irradiation time (min)

(b)

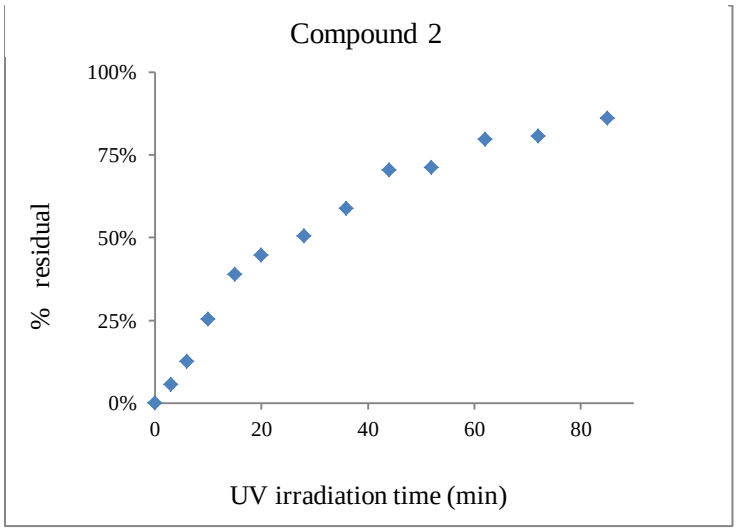
Compound 2
100%
75%
50%
25%
0%
% residual
0
20
40
60
80
UV irradiation time (min)

(c)

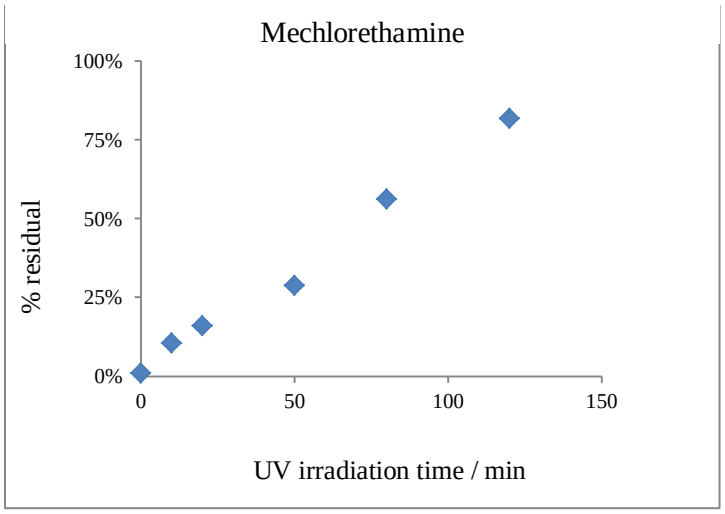

Figure 4.1. (a). Controlled decomposition of prodrug **4-1** in aqueous solution upon UV irradiation for designated time courses monitored by RP-HPLC. (b). Controlled release of fluorescent molecule compound **4-6** in aqueous solution upon UV irradiation for designated time courses monitored by RP-HPLC. (c). Controlled release of mechlorethamine **4-4** in aqueous solution upon UV irradiation for designated time courses monitored by RP-HPLC.

To quantify the amount of active drug **4-4** released from the photolytic reaction, DDT was used as a trapping agent. From the above reaction mixture, an aliquot sample was taken and incubated with 27.5 mM DDC for 20 min at 37°C to complete the trapping reaction. Then, it was injected into RP-HPLC, by monitoring the concentration of bisadduct **4-15** peak at 20.3 min, the amount of **4-4** can be calculated. Through path A: direct substitution reaction with prodrug **4-1**, there is roughly a constant concentration of **4-15** under all conditions for 20 min incubation time with DDC. The actual amount of bisadduct **4-15** released from the photolytic reaction (path B) can be obtained by subtracting **4-15** produced from path A from the total amount detected (Scheme 4.4). Using the standard curve of compound **4-15**, the conversion percentage was plotted

against time of UV irradiation. The amount of mechlorethamine released was proportional to the time of UV irradiation (Figure 4.1c).

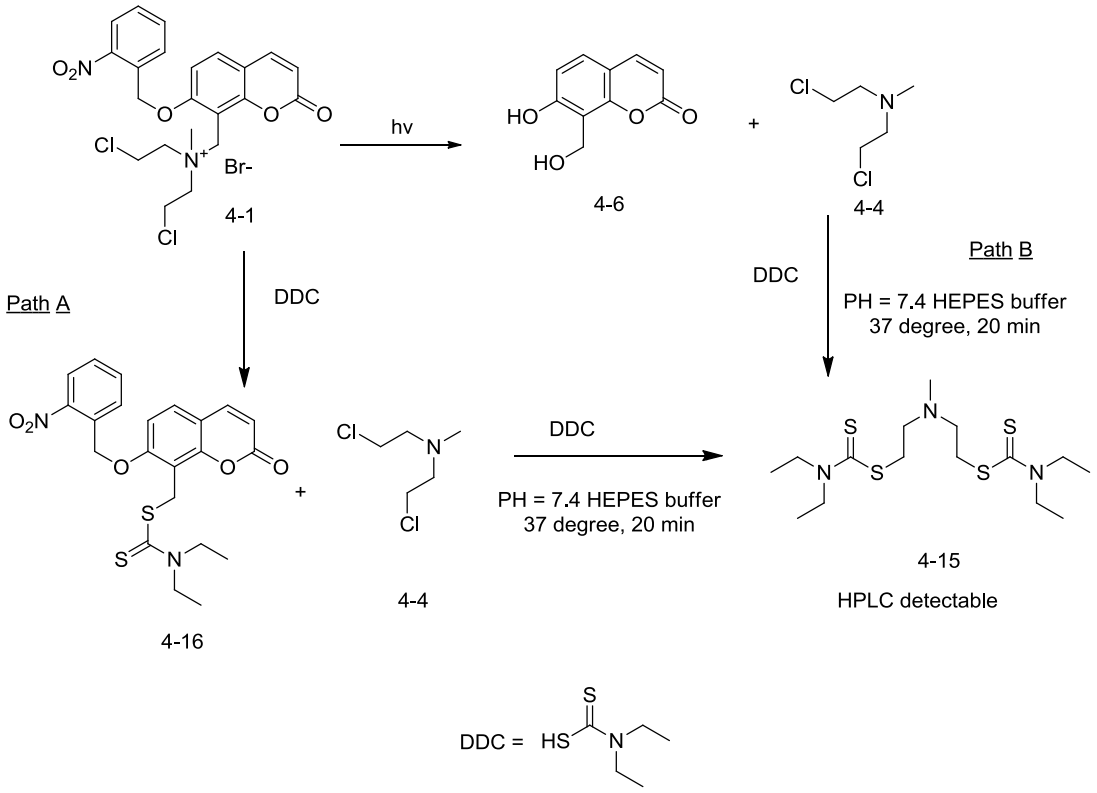

Scheme 4.4 Chemistry of detection of mechlorethamine release from prodrug 4-1 by: (path A) direct substitution with diethyldithiocarbamate (DDC) and (path B) photolytic fragmentation.

The above mentioned properties of prodrug **4-1** provided a way for the precise control of the progress of the photolysis reaction with different time courses of UV irradiation to release active drug **4-4** and fluorescent signaling molecule **4-6**.

4.6 Spectroscopic Properties

The spectroscopic properties of the photolytic reaction were investigated next. These experiments were performed in a pH 7.4 HEPES buffer. Both the UV absorption spectrum and fluorescence emission (λ_{ex} = 375 nm, λ_{ex} = 448 nm) were measured before and after treatment with UV light irradiation (365 nm). The absorption maximum of prodrug **4-1** is 324 nm (Figure 4.2). After exposure under UV for 15 min, a new absorption peak, a characteristic of compound **4-6**, at 364 nm appeared (Figure 4.2). Meanwhile, as expected, prodrug **4-1** was originally nonfluorescent due to the presence of the NPE group and the charged nitrogen moiety in the coumarin (Figure 4.1). The fluorescence intensity enhancement is proportional to the UV irradiation time (Figures 4.3a and 4.3b). Notably, maximal fluorescence emission was reached within 15 min UV irradiation with up to 152 folds. In contrast, no fluorescence intensity change was observed when prodrug **4-1** was exposed in a pH 7.4 HEPES buffer under ambient light, indicative of its high stability. Taken together, these findings provide support for the notion that the photo-controlled release system **4-1** only responses to photo- triggered cleavage. Moreover, the release event can be readily tracked by fluorescence.

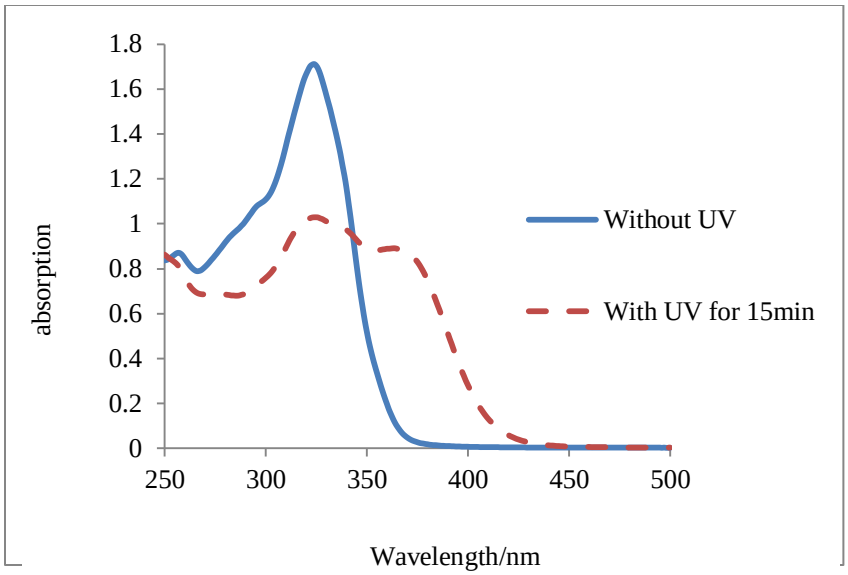

Figure 4.2. Photolytic activation of 0.1mM fluorescent prodrug **4-1** in pH=7.4 HEPES buffer, irradiated by a hand-held UV lamp (λ= 365nm). UV-vis spectra in the absence of UV and after 15 min UV exposure.

(a) (b)

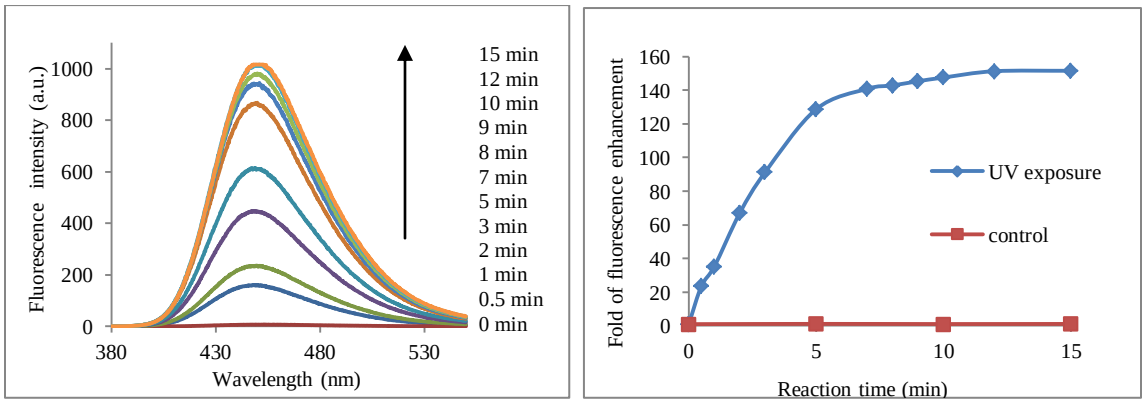

Figure 4.3. Photolytic activation of 0.1mM fluorescent prodrug **4-1** in pH=7.4 HEPES buffer, irradiated by a hand-held UV lamp (λ= 365nm) with different time courses. (a). Fluorescence spectra. (b). Fluorescence emission enhancement at 448 nm with different UV irradiation time.

4.7 DNA Cross-linking Activity Study

In the design of a prodrug system, the active parent drug must be released to ensure biological activity. It is expected that the UV uncaged bioactive mechlorethamine produced from prodrug **4-1** upon UV irradiation leads to the subsequent DNA intercross linking. Therefore, DNA cross linking activity studies were conducted. The experiments were conducted using linealized plasmid DNA by denaturing alkaline agarose gel electrophoresis as originally reported by Cech [50]. pBR322 plasmid DNA was linearized by *Eco*RI restriction endonulease digestion. DNA cross-linking experiment was carried out in a pH 7.4 Tris-HCl buffer. Due to the inherent toxicity of strong UV light and the possible UV induced cross link interference, a low-power UV light as light source was used. It was positioned 75 cm away from the reaction. After 1 h exposure to 365 nm UV irradiation, cross linking reactions were analyzed on denaturing alkaline agarose gel electrophoresis by the different mobility of ICL products versus single stranded DNA. 1kb DNA ladder was used as a molecular weight stardard (Figure 4.4, lane 1). Control reactions were performed with DNA in the absence of prodrug **4-1** treatment both in the dark (Figure 4.4, lane 2) and with 1 h UV exposure (Figure 4.4, lane 3). Results showed no noticeable cross-links formation in both cases which suggested that mild UV exposure for 1 h does not induce DNA cross-links formation. To exclude the possibility that the UV activated fragment **4-5** was responsible for DNA cross-links formation, control compound **4-14** was synthesized. According to the photoactivation mechanism, compound **4-14** was able to release the same fragment **4-5** as prodrug 4-1. Results indicated that both in the absence (Figure 4.4, lane 4) and presence of UV light (Figure 4.4, lane 5), control compound **4-14** did not induce noticeable cross-link prodructs. The same result was observed when DNA was treated with 1mM prodrug **4-1** in the absence

of UV light (Figure 4.4, lane 6). It indicated that prodrug **4-1** itself without UV exposure showed negligible activity in forming DNA cross-links. However, in the presence of prodrug **4-1** (1 mM) with exposure to UV light for 1 hour, efficient DNA cross-link was observed (Figure 4.4, lane 7), which is comparable to that of the active anticancer drug mechlorethamine (Figure 4.4, lane 8). These results show that prodrug **4-1** itself the lacks the cross link activity toward DNA, but can be activated by UV light to generate the activity by releasing the real drug mechlorethamine, and the other released fragment **4-5** was not responsible for DNA cross-links formation.

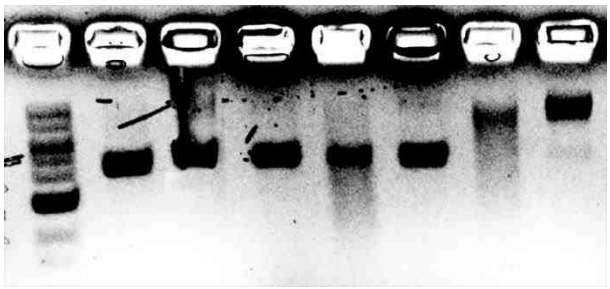

1 2 3 4 5 6 7 8

Figure 4.4. DNA cross-links formation with prodrug **4-1**/mechlorethamine with exposure to UV light (365 nm). Lane 1: 1 kb DNA ladder (molecular weight standard). Lane 2: 1 µg pBR322 in dark (negative control). Lane 3: 1 µg pBR322 with UV treatment for 1 hour. Lane 4: 1 µg pBR322 with treatment of 1mM control compound **4-14** in dark. Lane 5: 1 µg pBR322 with treatment of 1mM control compound **4-14** with 1 h UV exposure. Lane 6: 1 µg pBR322 with treatment of 1 mM prodrug **4-1** in dark. Lane 7: 1 µg pBR322 with treatment of 1 mM prodrug **4-1** with 1 h UV exposure. Lane 8: 1 µg pBR322 with treatment of 1 mM active drug mechlorethamine in dark.

4.8 Cell Viability Test

Before going into cellular tests, we firstly evaluated the stability and cell permeability of prodrug **4-1**. Concerning the fact that prodrug **4-1** is an electrophile, we tested its stability in a thiol rich cellular environment. As reported, GSH is present at very high levels in the cytosol, comprising about 90% of nonprotein sulfur with 1-2 mM concentrations in most of the cells [51]. An aqueous solution containing 5 mM prodrug **4-1** was incubated with 2.0 mM GSH for 6 hours at 37 ℃, DDC was incubated for 20 min to trap the released active drug **4-4**. An aliquot of solution was injected to RP-HPLC. We have not observed decomposition of prodrug **4-1** nor increased amount of compound **4-4**, which showed that prodrug **4-1** was very stable in a GSH rich cellular environment.

To evaluate the cell permeability of prodrug **4-1**, 0.8 mM prodrug **4-1** was incubated with HeLa cells for 2 hours, cell lysate was collected and injected into RP-HPLC, prodrug **4-1** peak was detected. It supported that prodrug **4-1** was cell permeable.

Having established that prodrug **4-1** is able to release active antineoplastic mechlorethamine and showed high potency in inducing DNA cross-links. We evaluated its ability in inhibiting cancer cell growth as well as its cytotoxicity towards normal cells. Cell viability was measured by using cell counting kit-8 (CCK-8). First of all, cytotoxicity of prodrug **4-1** was evaluated on normal skin cells (Hekn cell lines). As is shown in Figure 4.5, without UV exposure on Hekn cells, inactivated prodrug **4-1** showed negligible cytotoxicity towards normal skin cells. Even with a drug concentration of 0.8 mM, Hekn cell viability as high as 83.5% was observed. After 30 min UV exposure, activated prodrug **4-1** showed lower cell viability than inactivated prodrug under the same concentration, but also displays relatively low toxicity towards normal skin cells, although . Thus, prodrug **4-1** displays low systematic toxicity towards

normal cells both with and without UV activation. is low toxicity assures its potential for further study.

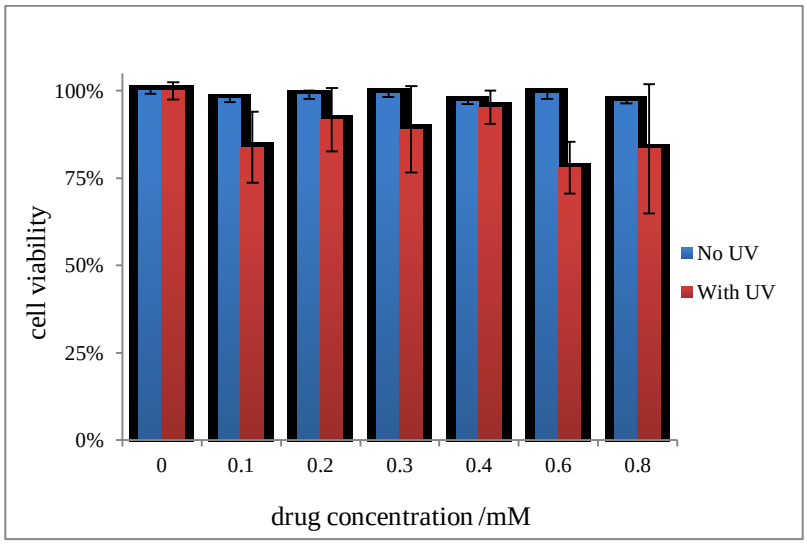

Figure 4.5 Cell viability assays of prodrug **4-1** on normal skin cells (Hekn cell lines). Prodrug **4-1** was incubated with the cells for 2 h followed by 30 min UV irradiation. The cell viability was measured after 24 h after incubation using cell counting kit-8 (CCK-8).

Next, cell viability was evaluated with prodrug **4-1** on cancer cells (HeLa cell lines). First of all, as is shown in Figure 4.6, prodrug **4-1** activated by 30 min UV irradiation showed significant greater potential in killing cancer cells than inactive prodrug **4-1** itself. With an increasing drug dosage, a larger amount of cancer cells (HeLa cells) was killed. Meanwhile, we have observed an impressive selectivity towards cancer cells. With a drug concentration of 0.8 mM, 27.8% cell viability on HeLa cells compared with 83.5% cell viability on Hekn cells. This might be explained by the ICL property of the inhibition mechanism. Cancer cells generally grow and divide at a much faster rate than normal cells. It is expected that much higher DNA replication and transcription activities

take place in cancer cells than those in normal cells, thus cell growth inhibition by intercross links formation is much more efficient towards cancer cells, accounting for the selectivity of the prodrug **4-1**.

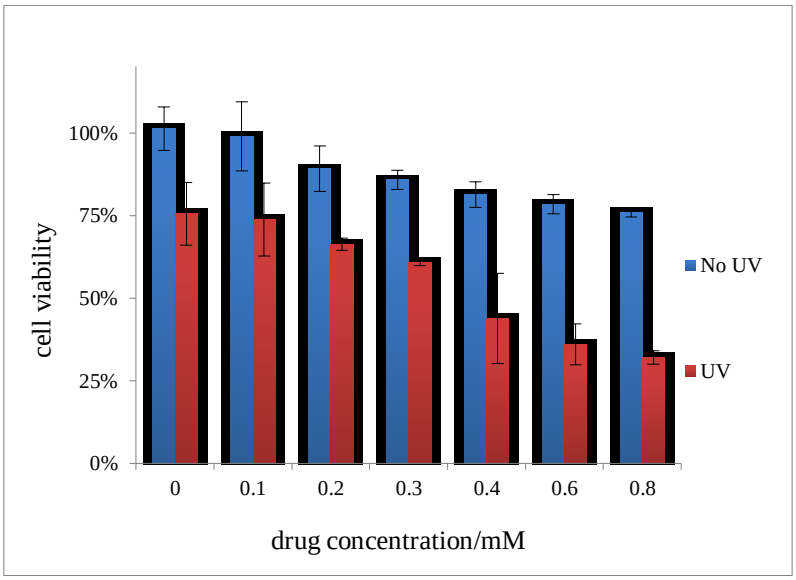

Figure 4.6 Cell viability assays of prodrug **4-1** on cancer cells (HeLa cell lines) Prodrug **4-1** was incubated with the cells for 2 h followed by 30 min UV irradiation. The cell viability was measured after 24 h after incubation using cell counting kit-8 (CCK-8).

During the drug release process, both mechlorethamine **4-4** and quinone methide type compound **4-5** were produced. As quinone methide was reported to exhibit DNA alkylating ability , we made control compound **4-14** to further investigate drug action mechanism. Compound **4-14** is different from prodrug **4-1** for it has the inactive 2,2'-(methylazanediyl)diethanol incorporated instead of the active drug mechlorethamine. As is shown in Figure 4.7, with dosage at 0.8 mM, control compound **4-14** exhibit weaker potential in killing cancer cells compared with prodrug **4-1** both in the presence and

absence of UV irradiation. Thus, it confirmed that the anticancer ability of prodrug **4-1** was mainly due to the release of mechlorethamine **4-4** instead of quinone methide type compound **4-5.**

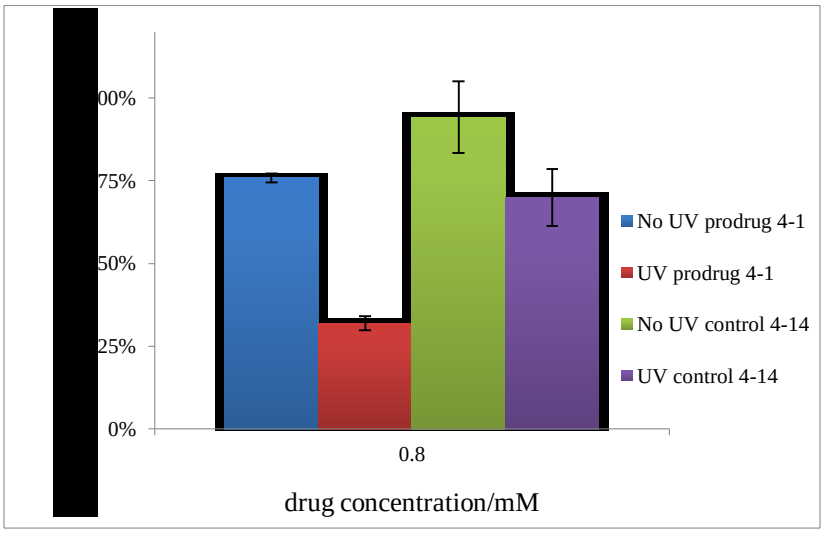

Figure 4.5. Cell viability assays of prodrug **4-1** and control compound **4-14** on cancer cells (HeLa cell lines) Prodrug **4-1** and control compound **4-14** were incubated with the cells for 2 h followed by 30 min UV irradiation. The cell viability was measured after 24 h incubation using cell counting kit-8 (CCK-8).

4.9 Fluorescence Imaging Study

Having demonstrated that the prodrug can release the active drug form, next we evaluate the second feature of the prodrug **4-1**. It is designed for fluorescent monitoring of photoactivated drug release in cells. Prodrug **4-1** was incubated with HeLa cells for 2 hours for cellular uptake, followed by 30 min UV exposure to release active drug **4-4** and the fluorescent signal molecule **4-6**. As is shown in Figure 4.6, HeLa cells exhibited strong fluorescence only with photoactivated prodrug (Figure 4.6 a). In the absence of

either prodrug **4-1** or UV light, no fluorescence was observed (Figure 4.6 b and 4.6 c). These results clearly showed that the prodrug **4-1** was cell permeable and the fluorescence signals reflected the process of UV activated drug release.

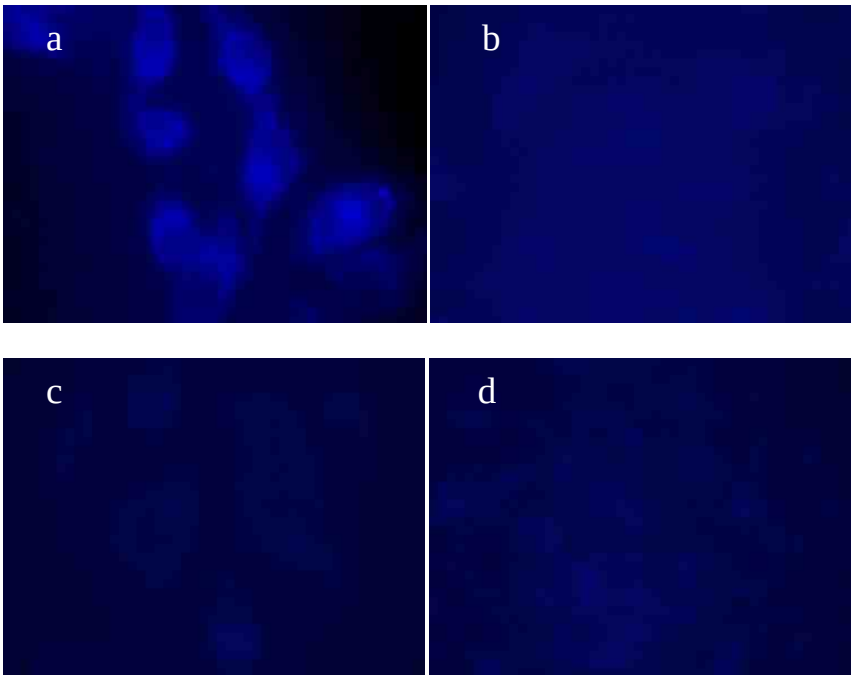

Figure 4.6. Fluorescence images of HeLa cells using an Olympus IX71 fluorescence microscope. (a) Fluorescence image of HeLa cells treated with prodrug **4-1** (350 μM) for 2 h followed by 30 min UV exposure; (b) Fluorescence image of HeLa cells treated with prodrug 4-**1** (350 μM) for 2 h in the absence of UV light, total incubation period of 2.5 h; (c) Fluorescence image of HeLa cells in the absence of prodrug **4-1** only with 30 min UV exposure. The total incubation time is 2.5 h; (d) Fluorescence image of HeLa cells in the absence of prodrug 4-**1** (350 μM) and without UV exposure.

To track the intracellular internalization and localization of prodrug **4-1**, we incubated it with HeLa cells at different times. The prodrug is cell permeable and nucleus

permeable (Figure 4.7). It was found that its distribution is time dependant and nucleus selective presumably due to its positive charged characteristic. The prodrug moves from cytoplasm to nuclei as incubation time prolongs. In a short incubation time (20 min), fluorescence was mainly observed in the cytoplasm upon UV irradiation, while 1 h, the signal was seen both in the cytoplasma and nuclei region. Longer incubation time (2 h) leads to stronger fluorescence in the nuclei region. The studies offer the important information of optimal time for the delivery of the drug at the desired site. Prodrug **4-1** is able to be monitored by convenient fluorescent tracking of drug localization in a spatiotemporal manner. Furthermore, the ability of controlled drug release into nuclei maximizes the DNA cross-linking efficiency.

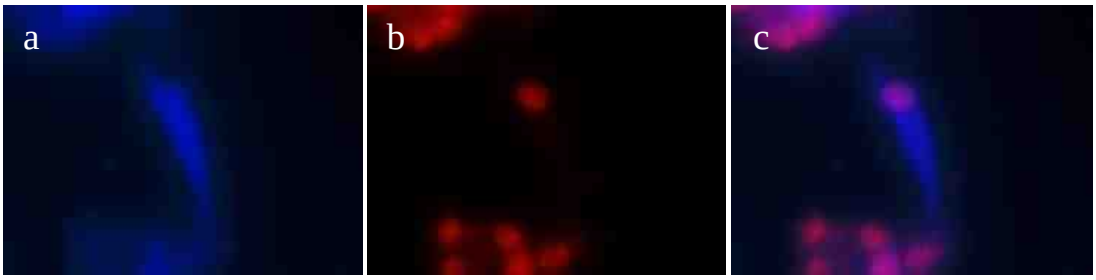

Figure 4.7. Fluorescence images of HeLa cells treated with 350 μM prodrug **4-1** followed by 30 min UV irradiation. HeLa cells were incubated with prodrug **4-1**, after 30 min UV irradiation, cells were fixed and stained with propidium iodide (red) for nuclei and prodrug **4-1** (blue) for the site of action. a) Fluorescence image of UV activated prodrug **4-1**; b) Fluorescence image of nuclei; c). Merged image of a and b.

4.10 Summary

In conclusion, we developed a novel dual functional photo-triggered fluorescent prodrug for anticancer drug releasing and monitoring. The release of the active DNA

alkylator mechlorethamine can be controlled with UV irradiation, accompanied with a maximum of 152 fold fluorescence increase. Moreover, we demonstrated that the photolytic product was able to induce effective DNA cross-linking activities which account for its anticancer activity. Prodrug **4-1** showed negligible cytotoxicity towards normal skin cells (Hekn cells) with and without UV activation. Nonetheless, the activated prodrug **4-1** exhibits potent anticancer activity towards cancer cells. Furthermore, importantly, the drug release progress can be conveniently monitored by the fluorescence enhancement in cells. Fluorescence imaging experiment showed that prodrug **4-1** is not only cell permeable but also nuclear permeable and selective. Therefore, these studies demonstrate that the prodrug could serve as a promising drug delivery system for spatiotemporal control release and monitoring of an anticancer drug to maximize the treatment efficacy in personalized medicine.

4.11 Experimental Section

General Information

All reactions were carried out in dried flasks. The reactions were monitored by TLC for completion. Commercially available reagents were used as received without further purification unless otherwise specified. Merck 60 silica gel was used for column chromatography, and Whatman silica gel plates with fluorescence F254 were used for thin-layer chromatography (TLC) analysis. ^{1}H and ^{13}C NMR spectra were recorded on Bruker Avance 500 or 300. Data for ^{1}H are reported as follows: chemical shift (ppm), and multiplicity (s = singlet, d = doublet, t = triplet, q = quartet, m = multiplet). Data for ^{13}C

NMR are reported as ppm. Mass Spectra were obtained from University of New Mexico Mass Spectral facility.

Synthesis of prodrug 4-1

Compound 4-1 was synthesized following the procedures in Scheme 4-2

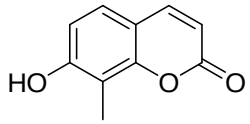

7-Hydroxy-8-methyl-2*H*-chromen-2-one (4-8)

A mixture of equimolar amount of 2-methylbenzene-1,3-diol (2.48 g, 20.0 mmol) and 2-hydroxysuccinic acid (2.48 g, 20.0 mmol) with 3.0 equiv. of concentrated sulfuric acid (5.88 g, 3.2 mL, 60 mmol) was exposed to mircrowave irradiation (240W, 120 °C) for 4 min. The reaction mixture was extracted with ethyl acetate and water. After solvent evaporation, the crude product was purified by silica gel column chromatography to give brown yellow solid as product (2.53 g, 72% yield). ^{1}H NMR (CD_3OD, 300 MHz): δ 7.75 (d, *J* = 9.3 Hz, 1H), 7.22 (d, *J* = 8.4 Hz, 1H), 6.75 (d, *J* = 8.4 Hz, 1H), 6.11 (d, *J* = 9.3 Hz, 1H), 2.20 (s, 3H).

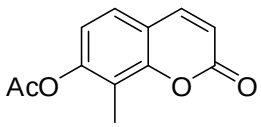

8-Methyl-2-oxo-2*H*-chromen-7-yl acetate (4-9)

7-Hydroxy-8-methyl-2*H*-chromen-2-one (1.76 g, 10 mmol) was dissolved in acetic anhydride (20.4 g, 200 mmol) and immersed in an ice water bath. After the addition of pyridine (948 mg, 12 mmol), the reaction mixture was stirred at rt for 12 h. Excess acetic anhydride was removed under reduced pressure. Residue was dissolved in dichloromethane, washed with saturated sodium bicarbonate, water, dried over sodium sulfate. The crude product was further purified by silica gel column chromatography to give (2.18 g, quantitative yield) white solids as product. ^{1}H NMR ($CDCl_3$, 300 MHz): δ 7.66 (d, *J* = 9.6 Hz, 1H), 7.31 (d, *J* = 8.4 Hz, 1H), 6.97 (d, *J* = 8.4 Hz, 1H), 6.35 (d, *J* = 9.6 Hz, 1H), 2.34 (s, 3H), 2.25 (s, 3H).

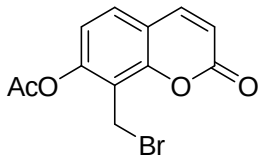

8-(Bromomethyl)-2-oxo-2H-chromen-7-yl acetate (4-10)

8-Methyl-2-oxo-2*H*-chromen-7-yl acetate (2.18 g, 10.0 mmol) was dissolved in 15 mL of carbon tetrachloride, then NBS (2.136 g, 12.0 mmol) was added to the reaction mixture followed by AIBN (49 mg, 0.2 mmol). The reaction mixture was stirred under reflux for 6 hours. After solvent removal under reduced pressure, the crude product was further purified by silica gel column chromatography to give light yellow solid as product (2.25 g, 76% yield). ^{1}H NMR ($CDCl_3$, 300 MHz): δ 7.67 (d, *J* = 9.6 Hz, 1H), 7.44 (d, *J* = 8.4 Hz, 1H), 7.08 (d, *J* = 8.4 Hz, 1H), 6.38 (d, *J* = 9.6 Hz, 1H), 4.63 (s, 2H), 2.40 (s, 3H). ^{13}C NMR ($CDCl_3$, 300 MHz): δ 168.17, 159.38, 152.20, 151.47, 142.95, 128.24, 119.28, 118.59, 116.69, 115.98, 20.83, 19.05.

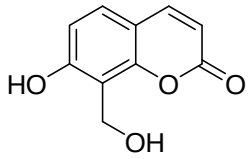

7-Hydroxy-8-(hydroxymethyl)-2*H*-chromen-2-one (4-11)

A mixture of calcium carbonate (2.6 g, 26 mmol) in 12 mL of water was added to a solution of 8-(bromomethyl)-2-oxo-2*H*-chromen-7-yl acetate (1.468 g, 5.0 mmol) in 12 mL of dioxane. The mixture was stirred at 50 °C for 24 h. Dioxane was removed under reduced pressure to give a white solid. After extraction using ethyl acetate and 2M HCl, the crude product was further purified by silica gel column chromatography to give white solids as product (936 mg, 80% yield). ^{1}H NMR (acetone-d_6, 300 MHz): δ 9.62 (s, 1H), 7.84 (d, J = 9.6 Hz, 1H), 7.43 (d, J = 8.7 Hz, 1H), 6.82 (d, J = 8.4 Hz, 1H), 6.15 (d, J = 9.6 Hz, 1H), 5.02 (s, 2H), 2.02 (d, J = 6.0 Hz, 1H). ^{13}C NMR (acetone-d_6, 300 MHz): δ 161.11, 160.85, 153.87, 145.08, 129.13, 114.57, 113.95, 112.62, 112.55, 56.05. ESI-MS: [M+H] calculated for $C_{10}H_9O_4$: 193.05; found: 193.05. m.p. : 158-160 °C.

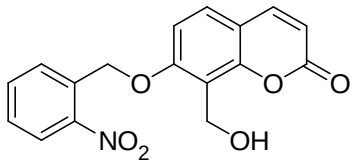

8-(Hydroxymethyl)-7-(2-nitrobenzyloxy)-2H-chromen-2-one (4-12).

Potassium carbonate (662 mg, 4.8 mmol) was dissolved in 25 mL of acetonitrile, followed by the addition of 7-hydroxy-8-(hydroxymethyl)-2*H*-chromen-2-one (936 mg, 4 mmol) and 1-(bromomethyl)-2-nitrobenzene (1046 mg, 4.8 mmol). The reaction mixture was stirred in dark at 50 °C for 5 h. After solvent removal under reduced pressure, the crude product was further purified by silica column chromatography to give white solids

as product (968 mg, 74% yield). ^{1}H NMR ($CDCl_3$, 300 MHz): δ 8.22 (d, *J* = 8.1 Hz, 1H), 7.90 (d, *J* = 7.8 Hz, 1H), 7.65 (m, 2H), 7.56 (m, 1H), 7.42 (d, *J* = 8.7 Hz, 1H), 6.94 (d, *J* = 8.7 Hz, 1H), 6.31 (d, *J* = 9.6 Hz, 1H), 5.64 (s, 2H), 5.07 (d, *J* = 6.0 Hz, 2H), 2.35 (t, *J* = 6.9 Hz, 1H). [M+H] calculated for $C_{17}H_{14}NO6$: 328.08; found: 328.08. m.p.: 212-214 °C.

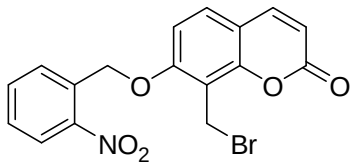

8 (8-(Bromomethyl)-7-(2-nitrobenzyloxy)-2H-chromen-2-one) (4-13):

A solution of tribromophosphine (643 mg, 226 μL, 2.4 mmol) in 2.0 mL of anhydrous dichloromethane was added dropwise to a solution of 8-(hydroxymethyl)-7-(2-nitrobenzyloxy)-2*H*-chromen-2-one (654 mg, 2 mmol) in 10 mL of anhydrous dichloromethane over 30 min with the temperature between -5 °C and -3 °C. The reaction mixture was stirred in dark at rt for 40 min. After the reaction is complete, it was washed with brine, concentrated and run column to give white solids as product (599 mg, 77% yield). ^{1}H NMR ($CDCl_3$, 300 MHz): δ 8.23 (d, *J* = 2.5 Hz, 1H), 8.04 (d, *J* = 7.8 Hz, 1H), 7.76 (d, *J* = 7.2 Hz, 1H), 7.65 (d, *J* = 9.6 Hz, 1H), 7.55 (d, *J* = 7.8 Hz, 1H), 7.43 (d, *J* = 8.7 Hz, 1H), 6.92 (d, *J* = 8.7 Hz, 1H), 6.32 (d, *J* = 9.6 Hz, 1H), 5.69 (s, 2H), 4.88 (s, 2H). ^{13}C NMR ($CDCl_3$, 300 MHz): δ 160.15, 158.64, 152.91, 146.71, 143.25, 134.50, 132.59, 129.23, 128.78, 128.32, 125.21, 114.58, 114.07, 113.51, 108.60, 67.57, 20.22. ESI-MS: [M+H] calculated for $C_{17}H_{13}BrNO5$: 390.00; found: 390.00. m.p.: 210-212 °C.

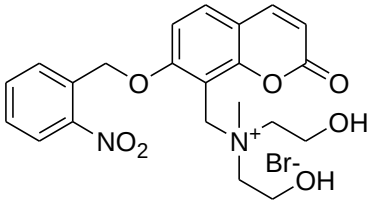

2-Hydroxy-*N*-(2-hydroxyethyl)-*N*-methyl-*N*-((7-(2-nitrobenzyloxy)-2-oxo-2*H*-chromen-8-yl)methyl)ethanaminium bromide (4-14)

A solution of 8-(bromomethyl)-7-(2-nitrobenzyloxy)-2*H*-chromen-2-one (389 mg, 1.0 mmol) and 2,2'-(methylazanediyl)diethanol (357 mg, 3.0 mmol) in 10 mL of anhydrous acetonitrile was stirred in dark at rt for 12 h. After filtration, white solids were obtained as product (309mg, 61% yield). ^{1}H NMR (DMSO-d_6, 300 MHz): δ 8.21 (d, J = 8.1 Hz, 1H), 8.07 (d, J = 9.6 Hz, 1H), 7.89 (d, J = 8.7 Hz, 1H), 7.81 (m, 2H), 7.68 (m, 1H), 7.29 (d, J = 9.0 Hz, 1H), 6.42 (d, J = 9.6 Hz, 1H), 5.71 (s, 1H), 5.25 (t, J = 4.8 Hz, 2H), 4.84 (s, 2H), 3.89 (m, 4H), 3.64 (m, 2H), 3.46 (m, 2H), 3.02 (s, 3H). ESI-MS: [M+H] calculated for $C_{22}H_{25}N_2O_7$: 429.17; found: 429.17. m.p.: 195-196 °C.

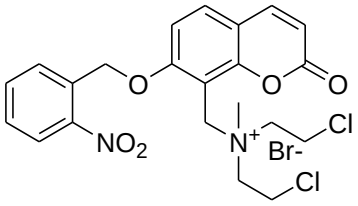

2-Chloro-*N*-(2-chloroethyl)-*N*-methyl-*N*-((7-(2-nitrobenzyloxy)-2-oxo-2*H*-chromen-8-yl)methyl)ethanaminium bromide (4-1)

2-Hydroxy-*N*-(2-hydroxyethyl)-*N*-methyl-*N*-((7-(2-nitrobenzyloxy)-2-oxo-2*H*-chromen-8-yl)methyl)ethanaminium bromide (254 mg, 0.5 mmol) was dissolved in 10 mL of thionyl chloride. The reaction mixture was stirred at rt for 3 d. After solvent evaporation under reduced pressure, white solid was obtained as product (272 mg, quantitative yield).

^{1}H NMR (DMSO-d_6, 300 MHz): δ 8.21 (d, J = 8.1 Hz, 1H), 8.08 (d, J = 9.3 Hz, 1H), 7.90 (d, J = 8.7 Hz, 1H), 7.78 (m, 2H), 7.67 (m, 1H), 7.28 (d, J = 8.7 Hz, 1H), 6.43 (d, J = 9.3 Hz, 1H), 5.74 (s, 2H), 4.88 (s, 2H), 4.17 (m, 4H), 3.86 (m, 4H), 3.15(s, 3H). ^{13}C NMR (DMSO-d_6, 300 MHz): 160.33, 158.95, 154.73, 147.23, 144.39, 134.32, 132.85, 131.31, 129.54, 129.45, 125.14, 113.56, 113.37, 109.98, 103.54, 68.21, 61.64, 55.03, 48.07, 36.51. ESI-MS: [M+H-Br] Calculated for $C_{22}H_{23}Cl_2N_2O_5$: 465.10, found 465.10. m.p.: 95-96 °C.

HPLC monitoring of drug release

(a)

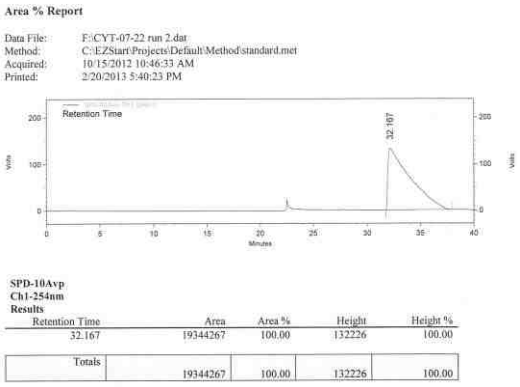

Area % Report

Data File: F:\CYT-07-22 run 2.dat
Method: C:\EZStart\Projects\Default\Method\standard.met
Acquired: 10/15/2012 10:46:33 AM
Printed: 2/20/2013 5:40:23 PM

SPD-10Avp
Ch1-254nm
Results

Retention Time	Area	Area %	Height	Height %
32.167	19344267	100.00	132226	100.00
Totals	19344267	100.00	132226	100.00

(b)

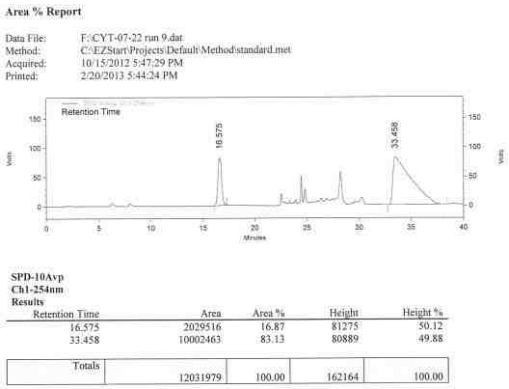

Area % Report

Data File: F:\CYT-07-22 run 9.dat
Method: C:\EZStart\Projects\Default\Method\standard.met
Acquired: 10/15/2012 5:47:29 PM
Printed: 2/20/2013 5:44:24 PM

SPD-10Avp
Ch1-254nm
Results

Retention Time	Area	Area %	Height	Height %
16.575	2029516	16.87	81275	50.12
33.458	10002463	83.13	80889	49.88
Totals	12031979	100.00	162164	100.00

(c)

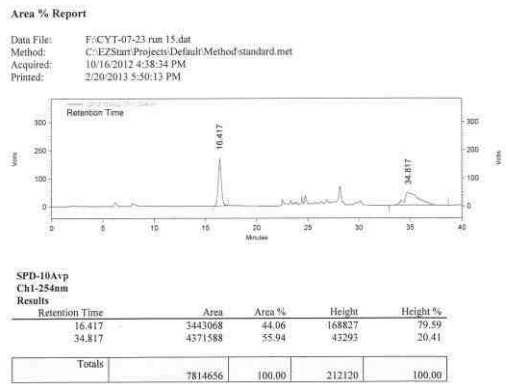

Area % Report

Data File: F:\CYT-07-23 run 15.dat
Method: C:\EZStart\Projects\Default\Method\standard.met
Acquired: 10/16/2012 4:38:34 PM
Printed: 2/20/2013 5:50:13 PM

SPD-10Avp
Ch1-254nm
Results

Retention Time	Area	Area %	Height	Height %
16.417	3443068	44.06	168827	79.59
34.817	4371588	55.94	43293	20.41
Totals	7814656	100.00	212120	100.00

Figure S1. HPLC monitoring of drug release of prodrug **4-1**. (a) 0 min; (b) 28 min; (c) 85 min. Photolytic activation of 0.1 mM fluorescent prodrug **4-1** in pH = 7.4 HEPES buffer, irradiated by a hand-held UV lamp (λ= 365 nm).

Prodrug **4-1** (2.0 mM) was dissolved in an aqueous solution of MeCN/H_2O (20:80), a hand-held UV lamp (365 nm, 2W) was positioned 10 cm away from the reaction vial as light source. After designated reaction time, an aliquot of 20 μL solution was taken and submitted to RP-HPLC to be analyzed by a 254 nm UV detector, the amount was integrated by the area under each peak, and calculated from the standard curves under the same HPLC condition.

HPLC condition: Eclipse XDB-C8 column, flow rate is 0.8 mL/min, 0-20 min: MeCN/H_2O (10:90), 20-40 min: MeCN/H_2O (30:70).

Protocol of study of UV irradiation reaction of prodrug 4-1

Prodrug **4-1** (13 mg) was dissolved in 239.2 μL of DMSO and 2152.8 μL of PBS buffer to make a solution of 10 mM. A hand-held UV lamp (365 nm, 2W) was positioned 10 cm away from the reaction vial as light source. Reaction was complete in 90 min, extracted with ethyl acetate and water, after solvent removal, the crude mixture was submitted to column chromatograph to obtain 1.5 mg white solids as product (isolated yield of 71%). ^{1}H NMR (acetone-d_6, 300 MHz): δ 9.62 (s, 1H), 7.84 (d, J = 9.6 Hz, 1H), 7.43 (d, J = 8.7 Hz, 1H), 6.82 (d, J = 8.4 Hz, 1H), 6.15 (d, J = 9.6 Hz, 1H), 5.02 (s, 2H), 2.02 (d, J = 6.0 Hz, 1H). ^{13}C NMR (acetone-d_6, 300 MHz): δ 161.11, 160.85, 153.87, 145.08, 129.13, 114.57, 113.95, 112.62, 112.55, 56.05. ESI-MS: [M+H] calculated for $C_{10}H_9O_4$: 193.05; found: 193.05.

Spectroscopic materials and methods

Millipore water was used to prepare all aqueous solutions. The pH was recorded by a Beckman ΦTM 240 pH meter. UV absorption spectra were recorded on a Shimadzu UV-1800 spectrophotometer. Fluorescence emission spectra were obtained on a Shimadzu RF-5301PC spectrofluorophotometer. Prodrug **4-1** in DMSO (10 mM) was prepared as the stock solution, 50 μL of the stock solution was added to 4.950 mL of 20 mM pH 7.4 HEPES buffer to make the final concentration of 0.1 mM. A hand-held UV lamp (365 nm, 2W) was positioned 10 cm away from the reaction vial as light source. Change in fluorescence emission (λ_{ex} = 375 nm, λ_{em} = 448 nm) and UV-vis spectra were measured at designated time interval.

Preparation of cell cultures

HeLa cell line was purchased from American Type Culture Collection. The cells were cultured in DMEM containing 10% FBS and 1% (v/v) antibiotic-antimycotic solution at 37 °C with 95% air/5% CO_2 in an incubator.

Human Epidermal Keratinocytes (HEKn) cells were obtained from Lifeline Cell Technology. The cells were cultured in DermaLife Basal Medium (DermaLife K Medium Complete Kit) at 37 °C with 95% air/5% CO_2 in an incubator.

Interstrad DNA cross-links formation study

General Procedure for Linearization of Plasmid pBR322 by EcoRI.

pBR322 Vector(New England Biolabs) (28µL, 28 µg) was incubated with EcoRI-HF(New England Biolabs) (20 µL),EcoR1 buffer (10 ×, 20 µL), and 132 µL of H_2O (sterile) for 3 h at 37 °C. NaOAc (20 µL, 3M) and ethanol (750 µL) were added, and the solution was cooled at -20 °C overnight. The mixture was centrifuged for 15 min at 16000 rpm, and the ethanol was decanted off. The remainder of the ethanol was evaporated off in vacuo at -20°C , and the remaining linearized DNA was suspended in 100 µLof sterile H2O. The amount of linearized pBR322 was quantitated by NANODROP 2000 spectrophotometer (Thermo Scientific).

Photoreaction of DNA with prodrug 4-1, control compound 4-14, or mechloethamine.

Solutions contained 1 µg linearized plasmid DNA in 0.15 M NaCl, 0.01 M Tris-HCl, and 0.001 M EDTA, pH 7.4. 10mM stock solution of prodrug **4-1** or control compound **4-14** or mechloethamine was added to a final concentration of 1mM, obtaining a final volume of 50 µL. The Interstrad DNA cross-link formation reactions were conducted 75 ± 5 cm away from UV light (30 W g30t8 bubble from General Electronic Company). After 1 hour incubation, the reaction solution was submitted to alkaline agarose gel electrophoresis.

General Protocol for Alkaline Agarose Gel Electrophoresis.

The agarose gels were prepared by adding 150 mL of a 50 mM NaCl / 2 mM EDTA (at pH = 8.0) to 1.8 g of agarose. The suspension was heated in a microwave oven until all of the agarose was dissolved(3 min). The gel was allowed to cool until 50°C and poured and

solidified for 1h at room temperature. The gel was soaked in an alkaline running buffer (25 mL of 2 N NaOH, 4 mL of 0.25 M EDTA in 1 L of H_2O). Agarose loading dye (New England Biolabs) (6 x, 10 µL) was added to the samples (50 µ L) , and the samples were loaded into the wells. The gel was run for 3 h at 200 mA/30 V. The gel was then neutralized for 45 min in a 1 M Tris pH = 7/1.5 M NaCl solution, which was refreshed every 15 min. The gel was subsequently stained in an ethidium bromide solution (100 µ L of a 10 mg/ mL ethidium bromide solution in 1 L of 1 M Tris /1.5 M NaCl buffer at pH = 7.5) for 1 h. Gels were visualized by UV and photographed using Gel Doc™ XR+ System(BIO-RAD).

Cell viability test

Cell viability was measured by using cell counting kit-8 (CCK-8), which quantitatively measures activities of dehydrogenases in cells. Cells (5×10^3 cells/well) were seeded into 96-well microtiter plates. Following treatment with prodrug 4-**1** and different reaction conditions (in the presence or absence of 365 nm UV light), 10 µL of CCK-8 solution was added to each well of the plate. The plate was placed into the incubator at 37 °C with 95% air/5% CO_2. After one hour incubation, the absorbance was measured at 450 nm in a Bio-Rad 3350 microplate reader. Cells without any treatment were used as 100% cell viability. The cell viability was calculated by using the formula: Cell viability = (Experimental absorbance value – culture medium absorbance value)/(without treatment absorbance value – culture medium absorbance value).

Fluorescence imaging of photoactivated prodrug 4-1

HeLa cells were plated onto polylysine-coated glass coverslips. After reaching 70% confluence, 350 μM prodrug was added to Hela cells, incubated for 2 h before 30 min UV exposure. Next, cells were washed thoroughly by DMEM. The coverslips were mounted on a glass slide. Images were acquired using an inverted microscope with a DAPI dichroic mirror.

Fluorescence subcellular imaging of photoactivated prodrug 4-1

HeLa cells were plated onto polylysine-coated glass coverslips. After reaching 70% confluence, cells were incubated with prodrug 4-1 for 30 min, followed by 30 min UV exposure. Cells were then washed 3 times with warmed DMEM medium, fixed with 4% paraformaldehyde for 15 min at room temperature (RT) and washed with PBS again. For counter staining, cells were permeabilized with 0.1% Triton-X100 for 10 min and rinsed with PBS again. Nuclei were labeled using propidium iodide (10 mg/mL) and cover glasses were mounted by AntifadeH mounting media. All slides were kept in dark until fluorescence images were acquired using an inverted microscope with a DAPI dichroic mirror for prodrug imaging and DSRED dichroic mirror for nuclei stain image.

4.12 References

[1] P. D. Lawley, *Bioessays* **1995**, *17*, 561.

[2] S. R. Rajski, R. M. Williams, *Chem. Rev.* **1998**, *98*, 2723.

[3] D. M. Noll, T. M. Mason, P. S. Miller, *Chem. Rev.* **2005**, *106*, 277.

[4] C. Alvarez-Lorenzo, L. Bromberg, A. Concheiro, *Photochem. Photobiol.* **2009**, *85*, 848.

[5] J. J. Tepe, R. M. Williams, *J. Am. Chem. Soc.* **1999**, *121*, 2951.

[6] P. Wang, R. Liu, X. Wu, H. Ma, X. Cao, P. Zhou, J. Zhang, X. Weng, X.-L. Zhang, J. Qi, X. Zhou, L. Weng, *J. Am. Chem. Soc.* **2003**, *125*, 1116.

[7] S. N. Richter, S. Maggi, S. C. Mels, M. Palumbo, M. Freccero, *J. Am. Chem. Soc.* **2004**, *126*, 13973.

[8] E. E. Weinert, R. Dondi, S. Colloredo-Melz, K. N. Frankenfield, C. H. Mitchell, M. Freccero, S. E. Rokita, *J. Am. Chem. Soc.* **2006**, *128*, 11940.

[9] I. S. Hong, H. Ding, M. M. Greenberg, *J. Am. Chem. Soc.* **2005**, *128*, 485.

[10] M. Di Antonio, F. Doria, S. N. Richter, C. Bertipaglia, M. Mella, C. Sissi, M. Palumbo, M. Freccero, *J. Am. Chem. Soc.* **2009**, *131*, 13132.

[11] D. Verga, M. Nadai, F. Doria, C. Percivalle, M. Di Antonio, M. Palumbo, S. N. Richter, M. Freccero, *J. Am. Chem. Soc.* **2010**, *132*, 14625.

[12] A. Jana, K. S. P. Devi, T. K. Maiti, N. D. P. Singh, *J. Am. Chem. Soc.* **2012**, *134*, 7656.

[13] R. Weinstain, E. Segal, R. Satchi-Fainaro, D. Shabat, *Chem. Commun.* **2010**, *46*, 553.

[14] Y. Chen, L. Hu, *Med. Res. Rev.* **2009**, *29*, 29.

[15] B. A. Teicher, A. C. Sartorelli, *J. Med. Chem.* **1980**, *23*, 955.

[16] R. A. McClelland, J. Roderick Fuller, N. Esther Seaman, A. Michael Rauth, R. Battistella, *Biochem. Pharmacol.* **1984**, *33*, 303.

[17] W. A. Denny, W. R. Wilson, *J. Med. Chem.* **1986**, *29*, 879.

[18] P. O'Neill, S. S. McNeil, T. C. Jenkins, *Biochem. Pharmacol.* **1987**, *36*, 1787.

[19] I. N. H. White, M. Suzanger, A. R. Mattocks, E. Bailey, P. B. Farmer, T. A. Connors, *Carcinogenesis* **1989**, *10*, 2113.

[20] K. E. O'Shea, M. A. Fox, *J. Am. Chem. Soc.* **1991**, *113*, 611.

[21] A. Firestone, R. T. Mulcahy, R. F. Borch, *J. Med. Chem.* **1991**, *34*, 2933.

[22] S. M. Hillier, J. C. Marquis, B. Zayas, J. S. Wishnok, R. G. Liberman, P. L. Skipper, S. R. Tannenbaum, J. M. Essigmann, R. G. Croy, *Mol. Cancer Ther.* **2006**, *5*, 977.

[23] R. S. Singleton, C. P. Guise, D. M. Ferry, S. M. Pullen, M. J. Dorie, J. M. Brown, A. V. Patterson, W. R. Wilson, *Cancer Res.* **2009**, *69*, 3884.

[24] C. P. Guise, M. R. Abbattista, S. R. Tipparaju, N. K. Lambie, J. Su, D. Li, W. R. Wilson, G. U. Dachs, A. V. Patterson, *Mol. Pharmacol.* **2012**, *81*, 31.

[25] M. Jameson, D. Rischin, M. Pegram, J. Gutheil, A. Patterson, W. Denny, W. Wilson, *Cancer Chemother. Pharmacol.* **2010**, *65*, 791.

[26] I. S. Hong, M. M. Greenberg, *J. Am. Chem. Soc.* **2005**, *127*, 10510.

[27] X. Weng, L. Ren, L. Weng, J. Huang, S. Zhu, X. Zhou, L. Weng, *Angew. Chem. Int. Ed.* **2007**, *46*, 8020.

[28] X. Peng, I. S. Hong, H. Li, M. M. Seidman, M. M. Greenberg, *J. Am. Chem. Soc.* **2008**, *130*, 10299.

[29] Y. Kuang, K. Balakrishnan, V. Gandhi, X. Peng, *J. Am. Chem. Soc.* **2011**, *133*, 19278.

[30] M. Op de Beeck, A. Madder, *J. Am. Chem. Soc.* **2010**, *133*, 796.

[31] S. Cao, Y. Wang, X. Peng, *Chem. Eur. J.* **2012**, *18*, 3850.

[32] Q. Zeng, S. E. Rokita, *J. Org. Chem.* **1996**, *61*, 9080.

[33] P. Pande, J. Shearer, J. Yang, W. A. Greenberg, S. E. Rokita, *J. Am. Chem. Soc.* **1999**, *121*, 6773.

[34] W. F. Veldhuyzen, Y.-F. Lam, S. E. Rokita, *Chem. Res. Toxicol.* **2001**, *14*, 1345.

[35] F. Kratz, I. A. Müller, C. Ryppa, A. Warnecke, *Chemmedchem* **2008**, *3*, 20.

[36] J. Wu, R. Huang, T. Wang, X. Zhao, W. Zhang, X. Weng, T. Tian, X. Zhou, *Org. Biomol. Chem.* **2013**, *11*, 2365.

[37] P. Rai, S. Mallidi, X. Zheng, R. Rahmanzadeh, Y. Mir, S. Elrington, A. Khurshid, T. Hasan, *Adv. Drug Delivery Rev.* **2010**, *62*, 1094.

[38] J. M. Bryson, K. M. Fichter, W.-J. Chu, J.-H. Lee, J. Li, L. A. Madsen, P. M. McLendon, T. M. Reineke, *Proc. Natl. Acad. Sci. U.S.A.* **2009**, *106*, 16913.

[39] Q. Lin, Q. Huang, C. Li, C. Bao, Z. Liu, F. Li, L. Zhu, *J. Am. Chem. Soc.* **2010**, *132*, 10645.

[40] Y.-P. Ho, K. W. Leong, *Nanoscale* **2010**, *2*, 60.

[41] S. Karthik, N. Puvvada, B. N. P. Kumar, S. Rajput, A. Pathak, M. Mandal, N. D. P. Singh, *ACS Appl. Mater. Interfaces* **2013**, *5*, 5232.

[42] Q. Lin, C. Bao, Y. Yang, Q. Liang, D. Zhang, S. Cheng, L. Zhu, *Adv. Mater.* **2013**, *25*, 1981.

[43] S. Santra, C. Kaittanis, O. J. Santiesteban, J. M. Perez, *J. Am. Chem. Soc.* **2011**, *133*, 16680.

[44] M. H. Lee, J. Y. Kim, J. H. Han, S. Bhuniya, J. L. Sessler, C. Kang, J. S. Kim, *J. Am. Chem. Soc.* **2012**, *134*, 12668.

[45] K. Ock, W. I. Jeon, E. O. Ganbold, M. Kim, J. Park, J. H. Seo, K. Cho, S.-W. Joo, S. Y. Lee, *Anal. Chem.* **2012**, *84*, 2172.

[46] O. Redy, D. Shabat, *J. Control. Release* **2012**, *164*, 276.

[47] J. Wu, R. Huang, C. Wang, W. Liu, J. Wang, X. Weng, T. Tian, X. Zhou, *Org. Biomol. Chem.* **2013**, *11*, 580.

[48] S. Maiti, N. Park, J. H. Han, H. M. Jeon, J. H. Lee, S. Bhuniya, C. Kang, J. S. Kim, *J. Am. Chem. Soc.* **2013**, *135*, 4567.

[49] M. Tercel, W. R. Wilson, W. A. Denny, *J. Med. Chem.* **1993**, *36*, 2578.

[50] T. R. Cech, *Biochemistry* **1981**, *20*, 1431.

[51] H. Peng, W. Chen, Y. Cheng, L. Hakuna, R. Strongin, B. Wang, *Sensors* **2012**, *12*, 1590.